NAVAL POSTGRADUATE SCHOOL
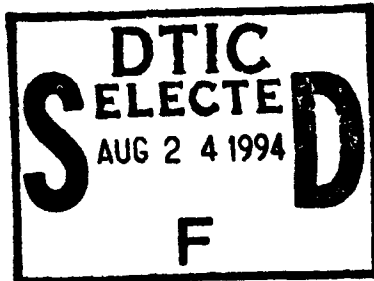## Monterey, California

AD-A283 654

94-26831

THESIS

PERFORMANCE EVALUATION OF GROUND BASED RADAR SYSTEMS

by

Stanley E. Grant

June 1994

Principal Advisor: Frederic H. Levien
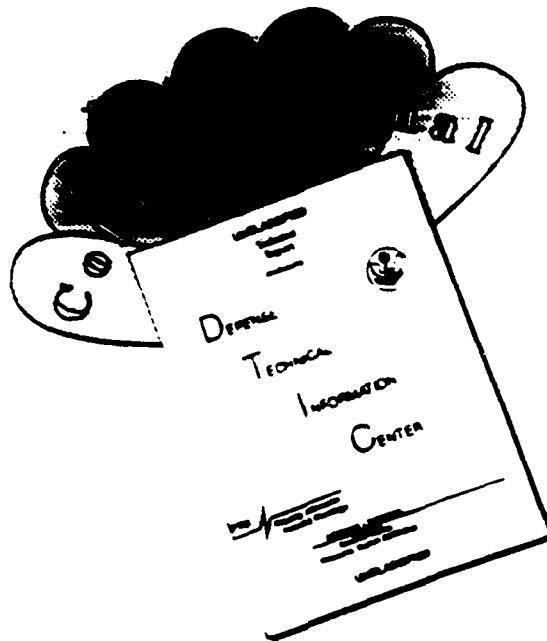
Approved for public release; distribution is unlimited.

94 8 23 030

DISCLAIMER NOTICE

THIS DOCUMENT IS BEST QUALITY AVAILABLE. THE COPY FURNISHED TO DTIC CONTAINED A SIGNIFICANT NUMBER OF COLOR PAGES WHICH DO NOT REPRODUCE LEGIBLY ON BLACK AND WHITE MICROFICHE.

REPORT DOCUMENTATION PAGE

1a Report Security Classification: Unclassified		1b Restrictive Markings		
2a Security Classification Authority		3 Distribution/Availability of Report		
2b Declassification/Downgrading Schedule		Approved for public release; distribution is unlimited.		
4 Performing Organization Report Number(s)		5 Monitoring Organization Report Number(s)		
6a Name of Performing Organization Naval Postgraduate School	6b Office Symbol *(if applicable)* 39	7a Name of Monitoring Organization Naval Postgraduate School		
6c Address *(city, state, and ZIP code)* Monterey CA 93943-5000		7b Address *(city, state, and ZIP code)* Monterey CA 93943-5000		
8a Name of Funding/Sponsoring Organization	6b Office Symbol *(if applicable)*	9 Procurement Instrument Identification Number		
Address *(city, state, and ZIP code)*		10 Source of Funding Numbers		
		Program Element No	Project No	Task No · Work Unit Accession No

11 Title *(include security classification)*   PERFORMANCE EVALUATION OF GROUND BASED RADAR SYSTEMS

12 Personal Author(s) Grant, Stanley E.

13a Type of Report Master's Thesis	13b Time Covered From To	14 Date of Report *(year, month, day)* June 1994	15 Page Count 122

16 Supplementary Notation The views expressed in this thesis are those of the author and do not reflect the official policy or position of the Department of Defense or the U.S. Government.

17 Cosati Codes			18 Subject Terms *(continue on reverse if necessary and identify by block number)*
Field	Group	Subgroup	Ground Based Sensors, Radar Systems, Terrain Effects, Atmospheric Effects

19 Abstract

19 Abstract *(continue on reverse if necessary and identify by block number)*

Ground based radar systems are a critical resource to the command, control and communications system. This thesis provides the tools and methods to better understand the actual performance of an operational ground based radar system. This thesis defines two measurable performance standards: 1) the baseline performance, which is based on the sensor's internal characteristics and 2) the theoretical performance, which considers not only the sensor's internal characteristics, but also the effects of the surrounding terrain and atmosphere on the sensor's performance. The baseline radar system performance, often used by operators, contractors, and radar modeling software to determine the expected system performance, is a simplistic and unrealistic means to predict actual radar system performance. The theoretical radar system performance is more complex; but, the results are much more indicative of the actual performance of an operational radar system. The AN/UPS-1 at the Naval Postgraduate School was used as the system under test to illustrate the baseline and theoretical radar system performance. The terrain effects are shown by performing a multipath study and producing coverage diagrams. The key variables used to construct the multipath study and coverage diagrams are discussed in detail. The atmospheric effects are illustrated by using the Integrated Refractive Effects Prediction System (IREPS) and the Engineer's Refractive Effects Prediction System (EREPS) software tools to produce Propagations Conditions Summaries and Coverage Displays. Atmospheric data (radiosonde), collected in May 1991 from the same location as the AN/UPS-1 system under test, was used with the IREPS and EREPS software to illustrate the impact of the atmosphere on the ground based radar system's performance. Any reasonably accurate prediction of ground based sensor system performance must consider the effects of the installed environment, as discussed in this thesis.

20 Distribution/Availability of Abstract X unclassified/unlimited __ same as report _·_ DTIC users	21 Abstract Security Classification Unclassified	
22a Name of Responsible Individual Frederic H. Levien	22b Telephone *(include Area Code)* (408) 656-2476	22c Office Symbol EC / LV

DD FORM 1473, 84 MAR   83 APR edition may be used until exhausted   security classification of this page

All other editions are obsolete   Unclassified

Performance Evaluation of
Ground Based Radar Systems

by

Stanley E. Grant
Captain, United States Air Force
B.S., Central Missouri State University, 1982
B.S., University of Missouri, 1984

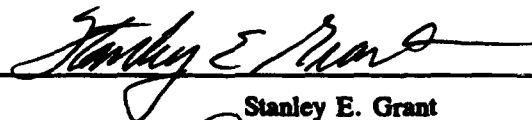Submitted in partial fulfillment
of the requirements for the degree of

MASTER OF SCIENCE IN SYSTEMS TECHNOLOGY
(Command, Control, and Communications)

from the

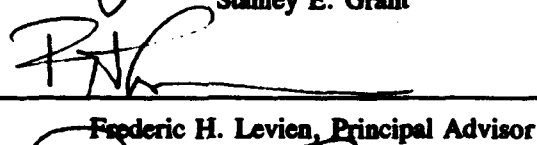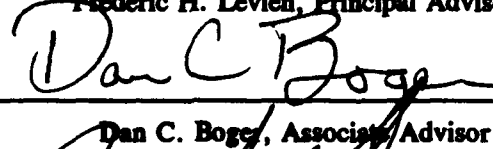NAVAL POSTGRADUATE SCHOOL
June 1994

Author: _____
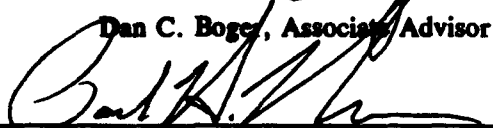Stanley E. Grant

Approved by: _____
Frederic H. Levien, Principal Advisor

_____
Dan C. Boger, Associate Advisor

_____
Paul H. Moose, Chairman
Command, Control and Communications Academic Group

ii

ABSTRACT

Ground based radar systems are a critical resource to the command, control and communications system. This thesis provides the tools and methods to better understand the actual performance of an operational ground based radar system. This thesis defines two measurable performance standards: 1) the baseline performance, which is based on the sensor's internal characteristics and 2) the theoretical performance, which considers not only the sensor's internal characteristics, but also the effects of the surrounding terrain and atmosphere on the sensor's performance. The baseline radar system performance, often used by operators, contractors, and radar modeling software to determine the expected system performance, is a simplistic and unrealistic means to predict actual radar system performance. The theoretical radar system performance is more complex; but, the results are much more indicative of the actual performance of an operational radar system. The AN/UPS-1 at the Naval Postgraduate School was used as the system under test to illustrate the baseline and theoretical radar system performance. The terrain effects are shown by performing a multipath study and producing coverage diagrams. The key variables used to construct the multipath study and coverage diagrams are discussed in detail. The atmospheric effects are illustrated by using the Integrated Refractive Effects Prediction System (IREPS) and the Engineer's Refractive Effects Prediction System (EREPS) software tools to produce Propagations Conditions Summaries and Coverage Displays. Atmospheric data (radiosonde), collected in May 1991 from the same location as the AN/UPS-1 system under test, was used with the IREPS and EREPS software to illustrate the impact of the atmosphere on the ground based radar system's performance. Any reasonably accurate prediction of ground based sensor system performance must consider the effects of the installed environment, as discussed in this thesis.

TABLE OF CONTENTS

LIST OF TABLES

LIST OF FIGURES

I. INTRODUCTION

A. BACKGROUND

The ground based radar system is a critical resource to the warfighter as a major component of the command and control system. The command and control system relies on the radar system to accurately locate targets in physical space in either two (range and azimuth) or three dimensions (range, azimuth, and height). It is important to note that the command and control system requires the accurate location of targets in terms of coordinates in physical space (i.e., grid location), not relative location in relation to another object (i.e., vector location). The mission of the radar system is to support this requirement established by the command and control system.

The mission of the radar system should be well defined and should include specific accuracy requirements for locating targets in physical space and the specific areas of radar coverage. Once these operational requirements are established the capabilities and limitations of the radar system should be validated and compared to the operational requirements to ensure compliance.

Unfortunately, operational mission requirements in terms of target location accuracy and specific areas of radar coverage are rarely well defined. Instead, the radar system's accuracy requirement and area of radar coverage are established by technical specifications. The technical specifications are obtained from a technical perspective that may be unrelated to the operational mission requirements. This approach to establishing

the radar system's mission may, or may not, fulfill the operational mission requirements. This backward approach to establishing the mission of the ground radar system must be corrected. Efforts must be made to tie the operational and technical perspectives together and clearly define the target location accuracy requirement, specific areas of radar coverage requirement, and the capabilities and limitations of the radar system.

The effort to establish a realistic operational mission requirement, and to define the radar system's capabilities and limitations, requires an understanding of the radar system's internal characteristics and the impact of the environment on the radar system. This thesis will analyze the radar system's internal characteristics and the impact of the environment on performance. Additionally, this thesis will present methods of determining the ground radar system's capabilities and limitations.

B. OBJECTIVES

The objective of this thesis is to detail methods that can be used to obtain a realistic prediction of a radar system's capabilities and limitations. This thesis will present two fundamental methods of predicting the radar system's capabilities and limitations, or performance, which are defined in this thesis as 1) baseline radar system performance and 2) theoretical radar system performance. The baseline radar system performance is based solely on the radar system's internal characteristics. The theoretical radar system performance is determined from the baseline radar system performance in addition to consideration of the effects on the radar system due to the installed environment.

2

Radar system performance and mission requirements are often inaccurately defined by only considering the basic internal radar system characteristics, or baseline radar system performance. The baseline radar system performance is often used because it is a quicker and easier method to predict the "real world" or actual radar system performance. Unfortunately, the baseline radar system performance is also an inherently inaccurate method of predicting actual radar system performance. This thesis will explore the inaccuracies inherent in predicting actual radar system performance based on baseline radar system performance.

The combined radar system characteristics and environmental factors analysis, or theoretical radar system performance, represents a "best estimate" prediction of actual radar system performance. This thesis will focus on the differences between the baseline performance and the theoretical performance obtained from analysis of key environmental factors. The problems associated with using only the baseline performance prediction will be shown by evaluating the impact of the environment on radar system performance. Additionally, this thesis will identify and explain the tools and techniques used to analyze the impact of the environment on the radar system.

To further the reader's understanding, examples will be provided which illustrate the points being made. The examples, where possible, will use the AN/UPS-1 radar system characteristics at the Naval Postgraduate School (NPS) as the system under test. The AN/UPS-1 radar is located in the radar lab on the fifth floor of Spanagel Hall, and the antenna is located on the roof of Spanagel Hall.

II. BASELINE RADAR SYSTEM PERFORMANCE

A. OVERVIEW

Baseline radar system performance is based solely on internal radar system parameters. The baseline performance is used by contractors, operators, mission planners, and radar modeling software. The baseline performance for this thesis will be obtained through the following radar range equation (RRE) (Eaves and Reedy, 1987 pg 182):

$$R_{max} = \left[\frac{P_t G_t G_r \lambda^2 \sigma}{(4\pi)^3 S_{min}} \right]^{\frac{1}{4}} \qquad (1)$$

P_t = transmitter signal power

G_t = transmitter antenna gain

G_r = receiver antenna gain

λ = wavelength of transmitted signal

σ = target RCS

S_{min} = receiver minimum detectable signal

R_{max} = maximum detection range.

The baseline performance will be obtained by solving equation 1 using the NPS AN/UPS-1 parameters. Equation 1, which excludes many internal system parameters as

4

well as external factors, is one of the more basic forms of the RRE. However, despite its inherent inaccuracy, this equation is often the only value used for radar performance.

B. SENSOR SYSTEM CHARACTERISTICS

In using the RRE for determining the baseline radar system performance, several key measured, or known, system parameters are used. The AN/UPS-1 basic transmitter and receiver parameters are listed in Table I. The antenna characteristics particular to the AN/UPS-1 at NPS are listed in Table II. The data listed in these tables are not a complete listing of all system parameters; however, the data is sufficiently complete to illustrate the type of information that is necessary to determine the baseline radar system performance. The data from these tables will be used in computing the baseline radar system performance with the following assumptions:

- The transmitter peak power output will be assumed to be operating at the maximum of 1400 kW.

- The receiver minimum discernable signal (MDS) and noise figure used to calculate the baseline performance and predict the theoretical performance will be -105 dBm and 9 dB respectively.

These assumptions are used because the transmitter peak power and MDS may vary with time (perhaps monthly) depending on the specific equipment. The actual, or measured, system parameters for the MDS and noise figure could be several dB higher or lower than these assumed values. Operational radar sites will often use the measured values in the RRE to provide the current "best estimate" of the baseline radar system performance.

5

TABLE I AN/UPS-1 PARAMETERS

Transmitter Frequency	1305 MHz
Pulse Width	4.2 μsec
PRF (Pulse Repetition Frequency)	267 Hz
Operational Range	275 nmi
IF (Intermediate Frequency)	.45 MHz
Peak Power	1400 kW max—1000 kW min
Avg Power (max)	1.6 kW
Minimum Discernable Signal	-105 dBm or greater
Noise Figure	9 dB or less

TABLE II AN/UPS-1 ANTENNA PARAMETERS

Type	Modified Parabolic	
Dimensions:		
Horizontal Aperture	16 feet ± 2 inches	
Vertical Aperture	4 feet 9 inches ± 2 inches	
Horizontal Beam Width	3.8 degrees	
Vertical Beam Width	10 degrees	
Side Lobe and Back Lobe dB Below Main Beam:	Side	Back
Azimuth	26 dB	30 dB
Elevation	20 dB	30 dB
Gain	27 dB	
Scan Rate	0 to 15 RPM	
Antenna Tilt	Adjustable from -2 to +5 degrees	

There are several types of antennas that can be used with the AN/UPS-1. The modified parabolic is the antenna type in use at the NPS. Therefore, the antenna beam pattern for the modified parabolic antenna will be used throughout this thesis. The antenna tilt, or elevation angle, is manually adjustable and is currently adjusted for +5 degrees. Elevation angles other than the +5 degree setting will be addressed in chapter III. The antenna will be assumed to have a rotation rate of 15 RPM.

C. BASELINE PERFORMANCE

The baseline performance for purposes of this example will be obtained by solving the RRE (equation 1) using the AN/UPS-1 system parameters detailed in Tables I and II and assuming a +6 dBsm (medium fighter size) radar cross section target. The RRE can be solved by inserting the values for each of the variables in the equation and solving for the maximum range. A simpler method would be to convert the variables from linear values to decibel values, add them, and then convert the summed value back to a linear value. This simpler method, illustrated in Table III, results in a summed decibel value of 210.7 dB m^4. This decibel value is then converted to the linear maximum detection range (100 nmi) as shown in equation 2. The resultant maximum detection range of 100 nmi, using the values listed in Table III, yields the baseline radar system performance that will be used throughout the remainder of this thesis.

7

TABLE III BASELINE PERFORMANCE

Symbol	Definition	Linear Value	Decibel Value
P_t	transmitter signal power	1400 kW	61.5 dBW
G_t	transmitter antenna gain	501.19	27 dB
G_r	receiver antenna gain	501.19	27 dB
λ^2	(wavelength)^2 of transmitted signal	.0528 square meters	- 12.8 dBsm
σ	target RCS	4 square meters	6 dBsm
$1/S_{min}$	receiver minimum detectable signal	$1/(3.1623 \times 10^{-14}$ W)	135 dBW (105 dBm)
$1/(4\pi)^3$		1/2000	- 33.0 dB
			210.7 dB m^4
R_{max}	maximum detection range		185 km (100 nmi)

$$R_{max} = \log^{-1}\left[\frac{210.7\,dBm^4}{40}\right] = 185.14\,km = 100\,nmi \qquad (2)$$

It should be noted that for small changes (less than 10 dB), a 1 dB change in the equation yields approximately a 5 nmi change in range. This method of approximating the change in range provides simple means of determining the effects of small changes in the MDS, noise figure, frequency, or radar cross section. For example, for a 4 dBsm increase in target RCS, the detection range would be approximately 120 nmi, an increase of 20 nmi.

III. THEORETICAL RADAR SYSTEM PERFORMANCE

A. OVERVIEW

The theoretical radar system performance is derived using the baseline radar system performance and the added significant effects on baseline performance due to the propagation environment in which the radar system operates. This includes the terrain features surrounding the sensor and the atmosphere through which the radar signal must travel. The major effects due to terrain that will be analyzed are multipath and screening. Screening effects, often referred to as terrain masking, are considered from a geometric perspective, i.e., the target is/is not within the line-of-sight of the radar system. The screening effects will be illustrated in this thesis by constructing Above Ground Level (AGL) and Radar Line-of-Sight (RLS) diagrams. The AGL diagram illustrates the predicted coverage when a aircraft is flying a terrain following profile. The RLS diagram, on the other hand, illustrates the predicted coverage when the aircraft is flying at a constant altitude.

Multipath effects, the effects due to reflections from the earth's surface and other relatively massive objects, alter the shape of the radar coverage envelope. The resulting radar coverage envelope is one of lobes and nulls. The lobes are areas of enhanced detection and the nulls are areas of degraded detection. The effects due to multipath will be analyzed in this thesis by the following procedure:

9

- Determine the vertical angle, or position, of the nulls and lobes relative to the earth's surface. The nulls and lobes develop in the radar coverage envelope due to reflections from specific and identifiable concentric circles on the surface of the earth called fresnel zones. The vertical angles of the nulls and lobes will be determined by performing a multipath study and plotting the results on an earth curvature diagram.

- Determine the specific area on the surface of the earth from whic : reflections will occur by identifying the fresnel zones.

- Determine if the roughness of the terrain within the fresnel zone is sufficient to disrupt the formation of the radar coverage envelope. The determination of surface roughness will be performed by defining and determining the roughness criterion.

The analysis of the impact of the atmosphere on the radar's performance will be performed by using two PC based software tools: Integrated Refractive Effects Prediction System (IREPS) and Engineer's Refractive Effects Prediction System (EREPS).

The IREPS will provide a summary of the current propagation conditions (propagation summary) and a vertical depiction of the predicted radar coverage envelope (Coverage Display). The IREPS products, propagation summary and coverage display, are derived from measured atmospheric data and radar system characteristics. The measured atmospheric data used to create these diagrams will be from radiosonde data collected at the NPS on the 7th and 10th of May 1991.

The EREPS program produces a coverage display similar to IREPS; however, the EREPS program considers additional radar system characteristics not considered by IREPS. Specific factors which may, or may not, be considered in both of these software tools will be presented in detail in their respective sections within this thesis.

B. PROPAGATION ENVIRONMENT

The propagation environment is comprised of two basic areas of interest: the terrain and the atmosphere. Each of these areas will have an impact on the performance of a sensor system. The significant propagation conditions affecting both terrain and atmospheric effects are: free-space, interference, diffraction, tropospheric scatter, and refraction.

- **Free-space**. Free-space is defined as a region whose properties are isotropic, homogeneous, and loss-free. In free-space the propagated wave spreads uniformly in all directions (Patterson, 1990, pg 17). Free-space calculations are the foundation of the calculations for baseline and theoretical performance predictions.

- **Interference**. There are various descriptions of this propagation condition: optical interference, surface reflection, multi-path, lobing and others. The condition is caused when the wave strikes a large, smooth, reflective surface such as the ocean. The wave is reflected at an angle equal to the angle of incidence. The result is constructive and destructive interference which adds and subtracts from the total energy delivered to the target. This adding and subtracting forms a pattern of lobes and nulls. The IREPS model does not consider various surface reflectivity or roughness and is designed specifically for the radar system looking over the ocean. Additionally, sea and land clutter are not considered (Patterson, 1990, pg 18).

- **Diffraction**. Diffraction occurs when the propagated wave curves around an object. Diffraction will occur beyond the radio horizon and is a function of frequency. The lower frequencies are affected to a greater degree than the higher frequencies. At radar frequencies the wavelength is small when compared to the earth's dimensions and little energy is diffracted (Patterson, 1990, pg 21).

- **Tropospheric Scatter**. At ranges far beyond the horizon, the propagation loss is dominated by troposcatter. Propagation in the troposcatter region is the result of scattering by small inhomogeneities within the atmosphere's refractive structure. Tropospheric scatter is considered by EREPS and IREPS (Patterson, 1990, pg 21).

- **Refraction**. Refraction refers to the property of a medium which causes an electromagnetic wave to bend as the wave enters or leaves the medium. A measure of the amount of refraction is the index of refraction (Patterson, 1990, pg 5). Refraction must be considered to determine the amount of bending that will occur

and the resulting impact on screening and multipath. The bending of the radar wave will change the radiation pattern, or radar coverage, and the specific area on the surface of the earth radiated by the radar.

1. Terrain Analysis

The terrain surrounding the radar system significantly affects the performance of the sensor. The major effects due to the terrain are caused by either reflections or screening. The reflections from the earth's surface affect the radar system's performance by adding to, or subtracting from, the direct wave reaching the target. The result produces a periodic lobing effect in elevation. These lobes (or regions of enhanced coverage) occur where the phase of the reflected signal causes addition in phase with the primary signal, and nulls where it causes cancellation (180° out of phase) (Barton, 1991, pg 2-11). The analysis of the terrain effects due to reflections will be performed by fresnel zone analysis and a multipath study. The fresnel zone analysis provides a method of identifying the area where the radar wave will reflect off the earth's surface. The multipath study will predict the location of the lobes and nulls within the vertical area of coverage. The effects on the radar system due to screening will be evaluated by Above Ground Level (AGL) diagrams and Radar Line-of-Sight (RLS) coverage diagrams. However, prior to performing the detailed terrain analysis the contributions of refraction to terrain effects must be discussed in more detail.

a. Refraction.

The normal value for the index of refraction (n), defined below in equation 3, near the surface of the earth varies between 1.00025 and 1.0004. Due to this

12

very small variance in the range of the index of refraction (which is difficult to work with) refractivity (N) is defined and used in its place as shown in equation 4. This concept of refractivity is a much more convenient measure of refraction (Patterson, 1990, pg 6).

$$n=\frac{c}{v} \qquad (3)$$

$$N=(n-1)\,10^6=\frac{77.6\,(p)}{T}+\frac{e\,(3.73x10^5)}{T^2} \qquad (4)$$

n = index of refraction

c = speed of light in meters/second

v = velocity of the wave in the medium of interest in meters/second

N = refractivity

p = atmosphere's barometric pressure in millibars

T = atmosphere's absolute temperature in degrees Kelvin

e = partial pressure of water vapor in millibars.

The result of solving equation 4, for the normal conditions of the index of refraction mentioned above, are values of refractivity (N) ranging from 250 to 400. The contributions of atmospheric barometric pressure, temperature and humidity determine refractivity and therefore the amount and direction of bending of the radar waves. The amount and direction of the bending of the wave will affect the terrain analysis as well as the propagation through the atmosphere, which will be discussed in

greater detail in section 2 (Atmospheric Analysis). From the terrain analysis perspective the objective is to determine where the radar wave will strike the earth's surface. This is determined by the effective earth radius factor, or K-factor, which is derived from refractivity. The K-factor is the means to determine the contribution of atmospheric effects on the terrain analysis.

b. K-Factor.

Within the earth's atmosphere the velocity of the radar wave is less than that of free space and the index of refraction normally decreases with increasing altitude. This results in the propagating wave being bent downward from a straight line. Since it is more convenient to compute refractive effects in terms of waves traveling in straight lines, the actual earth's radius is not used when evaluating the radar wave's propagation path. Instead, a term called the effective earth's radius is substituted which has the effect of converting the curved radar propagation path into straight lines. The effective earth radius factor, K, is defined as the factor that is multiplied by the actual earth radius, a, to give the effective earth radius a_e (a_e = Ka). The K-factor is computed through the following equation (Patterson, 1990, pg 7):

$$K = \frac{1}{(1.0 + (10^{-6})(a)(\frac{dN}{dZ}))} \tag{5}$$

a = mean earth's radius (6.371 x 10^6 meters)

N = refractivity

Z = altitude

14

dN/dZ = - 0.039 N-units per meter (for standard conditions).

Using the standard value for dN/dZ, and solving equation 5, yields a K-factor of 1.33 (or four thirds). The K-factor is used extensively in all facets of radar performance analysis. The K-factor can either be calculated or it can be retrieved from data bases from various sources. There are several questions that must be answered when obtaining the K-factor from a data base:

- The data is normally taken from fixed sites around the world and the site's data are averaged to provide a vicinity average. Is this vicinity average a good approximation for my location?

- The K-factor is provided as a quarterly average, seasonal average, and annual average. Which is appropriate to my needs?

- Is the data base reliable?

The average annual K-factor used in this thesis for the NPS area is 1.348. This K-factor was obtained from the 84th RADES (Radar Evaluation Squadron) at Hill AFB, UT. The following table was provided by the RADES for the averaged K-factors from the Vandenburg AFB and Oakland, California, radiosonde sites:

TABLE IV K-FACTORS FOR NPS AREA

Months	K-factors
December - February	1.333
March - May	1.338
June - August	1.364
September - November	1.353
Annual	1.348

Provided by 84 RADES (Letter 24 January 1994)

The K-factors listed in Table IV are the annual and three-month average K-factors for the NPS area. The three-month averaged values do not vary significantly from one another due to the moderate change in weather conditions throughout the year in the NPS area; however, daily K-factor values, if calculated, may vary to a greater degree.

The Electromagnetic Compatibility Analysis Center (ECAC) was consulted (Connor, 1994) and SDS program (provided with the EREPS software) was run to confirm the K-factors provided by the RADES. The ECAC data, supported the RADES values; however, the SDS program provided considerably different values for the NPS K-factors. If the K-factors provided by the SDS program were used instead of the K-factors provided by the RADES, the placement of the nulls and lobes would be exactly opposite, in other words, the nulls would be substituted for lobes and the lobes would be replaced by nulls. Due to the significant difference in K-factors, the details of how the SDS program, the RADES, and ECAC determine the K-factors were investigated. The following paragraphs highlight these details and the reasons the K-

factors provided by the RADES, listed in Table IV, were used in this thesis instead of the SDS K-factors.

The RADES and ECAC both use the GTE Sylvania data base which was obtained from a large-scale analysis of approximately 3 million worldwide radiosonde soundings during a 5 year period, from 1966 to 1969 and 1973 to 1974 (Patterson, 1988, pg 68). It is used for radar sites propagating over land or over the ocean. The SDS meteorological data base is derived from the Radiosonde Data Analysis II and DUCT 63 data bases. The data is subdivided from the 648 world Marsden Squares into 293 Marsden Squares primarily to support maritime missions. The results of querying the SDS data base for this thesis are the Marsden Square map (Figure 1) and the accompanying Annual Surface Duct Summary (Figure 2).

The Marsden Square map is the means to select the Marsden Square in which the radar site of interest is located. For example, the NPS site is located at 36° 35' 39" N and 121° 52' 32" W, this location was selected by placing the crosshair in the Marsden Square that contains these coordinates. This is shown on Figure 1 by the 37 N and 122 W label at the bottom of the figure. Once this selection is made the Annual Surface Duct Summary (Figure 2) appears on the computer screen.

The Annual Surface Duct Summary data can be sorted by any particular radiosonde station or the composite average from all stations in that particular Marsden Square can be used. For the NPS site, two radiosonde stations data were available,
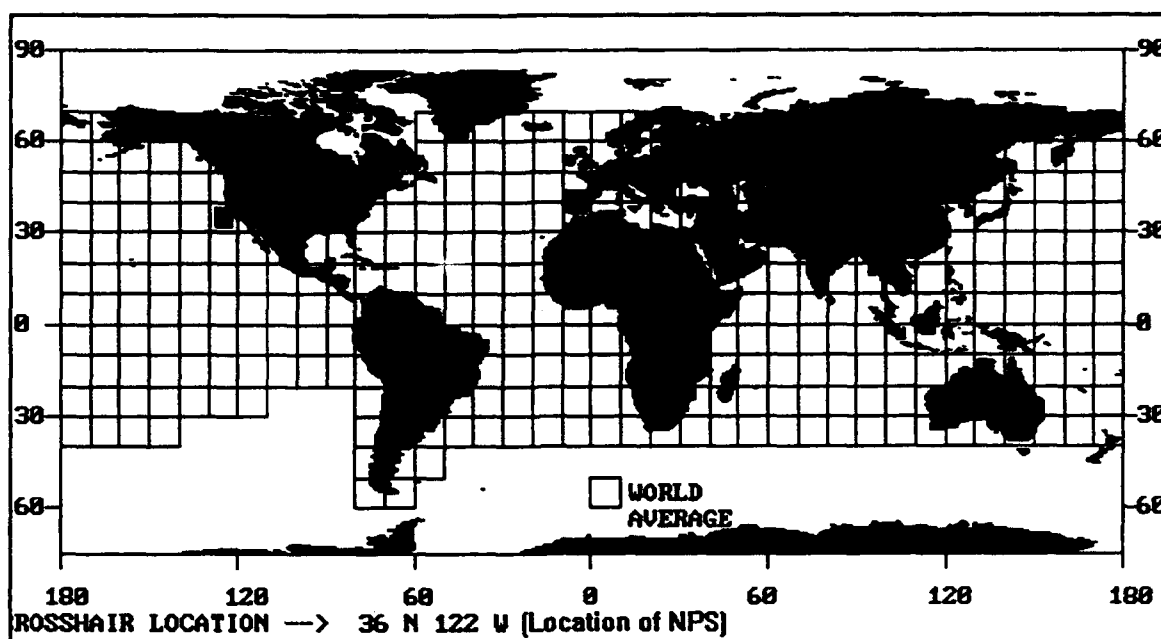
Figure 1 SDS Marsden Squares
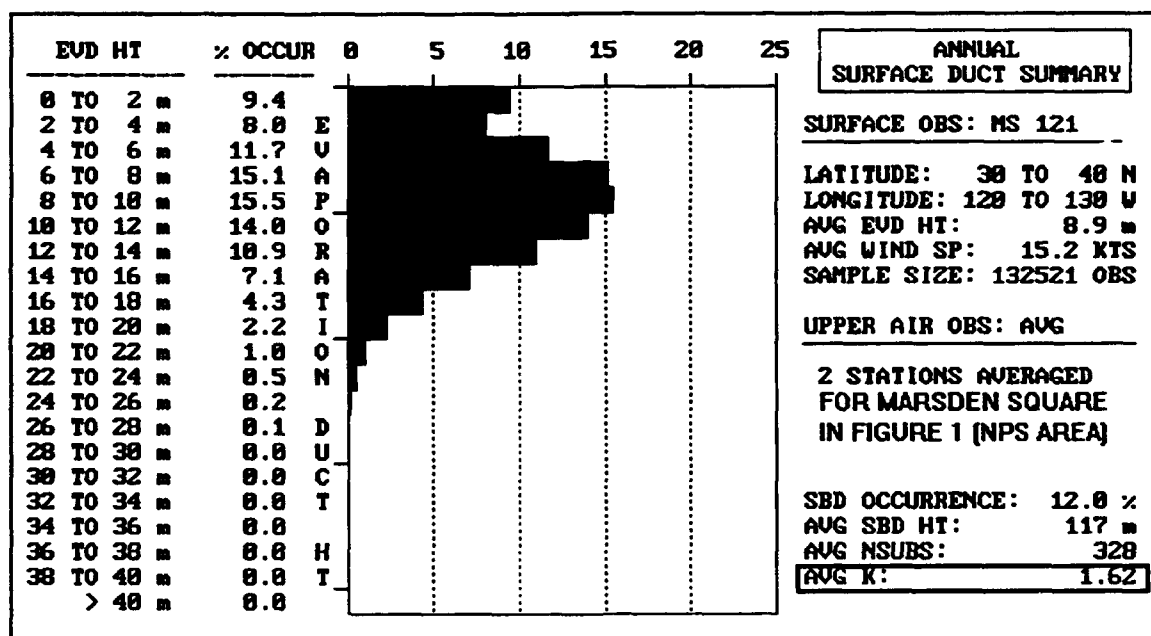
Figure 2 Annual Duct Summary (NPS Area)

18

Oakland, California, and Vandenburg AFB, California. The composite average for these two sites was used to produce Figure 2. The atmospheric data, which will be used in greater detail in the Atmospheric Analysis section, provided in Figure 2 is the percentage of occurrences (sorted by height) of elevated ducts, average elevated and surface-based duct heights (AVG SBD HT), average refractivity (AVG NSUBS), and the average annual K-factor.

The average annual K-factor, obtained from the SDS program, for the NPS area noted in Figure 2 is 1.62. The 1.62 K-factor, as mentioned earlier, is inconsistent with the value obtained from the RADES and ECAC. After consulting the RADES, ECAC, and the NPS Meteorology Department (Davidson, 1994) the SDS 1.62 K-factor was determined to be incorrect for the NPS area. Therefore, the K-factor of 1.348 obtained from the RADES will be used throughout the remainder of this thesis. Having illustrated the issues involved in determining K-factor values and having determined the correct K-factor, i.e., the amount of bending of the radar wave we would expect in the NPS area, we will now consider the terrain the radar wave will reflect from. This will be accomplished by calculating the fresnel zones for the AN/UPS-1 at NPS.

c.   *Fresnel Zone Theory.*

Huygens' principle (Angelokos and Everhart, 1968) states that each element of a primary wave front acts as a new source of radiation, sending out a secondary wave front; each element in the secondary wave front then re-radiates. The re-radiation of the waves continues indefinitely (Hund, 1952). This principle provides

19

the basis for the ever-expanding wavefront which results in electromagnetic energy taking multiple paths between the transmitter and receiver. The majority of the signal arriving at the receiver is from the direct path. However, power from other portions of the signal which have taken an indirect path, arrive simultaneously with the direct wave (see Figure 3). These indirect waves can contribute constructively or destructively to the direct path.
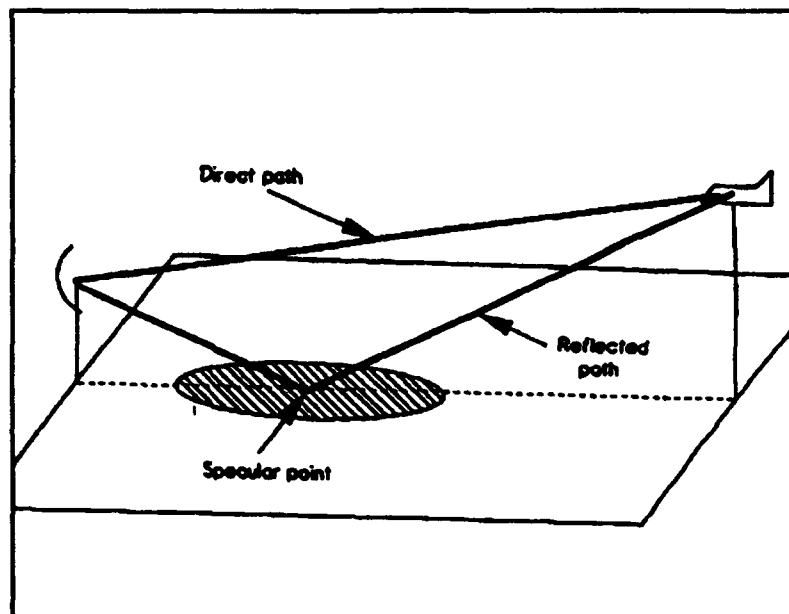
Figure 3 Direct and Reflected Path

A study of fresnel zone theory provides the means to determine the content of the resultant signal. Fresnel zone theory is applied in two fundamental ways: in terms of concentric circles around the direct wave (diffraction) and concentric circles around a point of reflection (reflection).

The fresnel zones are made up of concentric circles about the direct path and the indirect path. These concentric circles are areas in which the signal received from

20

the direct path has a phase shift when compared to the signal arriving from the indirect path due to the difference in path length. The first fresnel zone contains paths up to 1/2 wavelength longer; the second fresnel zone has paths up to two 1/2 wavelengths, or a full wavelength longer; the third fresnel zone has paths up to three 1/2 wavelengths longer and so on. Since each zone is 180 degrees out of phase with the previous, the resultant signal upon arrival at the receiver is either constructive or destructive, i.e., each odd numbered zone is constructive and each even numbered zone is destructive (assuming 180 degree phase shift due to reflection has occurred). The area of each of the zones is approximately equal, that is, each contains the same amount of energy. Since the area is nearly the same for each zone, the contributions at the target from any two adjacent zones will tend to cancel. However, due to the difference in path lengths, losses do occur and the result is that the first fresnel zone contains approximately 1/4 of the total transmitted energy. Additionally, the energy arriving at the target from all zones is about half that from the first zone (Air Force Communication Command, 1986, pg 5-79).

Figure 4 illustrates the fresnel zones; note that the cross section shows that the fresnel zones give the appearance of a series of concentric circles. Each successively higher order fresnel zone has a slightly larger radius, referred to as the fresnel zone radius. The value of any fresnel zone radius varies along the path. It reaches its largest value at the midpoint of the path and decreases symmetrically toward either end (Berry, 1990, pg 69). Once the fresnel zones are defined, the obstruction losses (negligible for radar systems) and reflection characteristics can be determined.

21
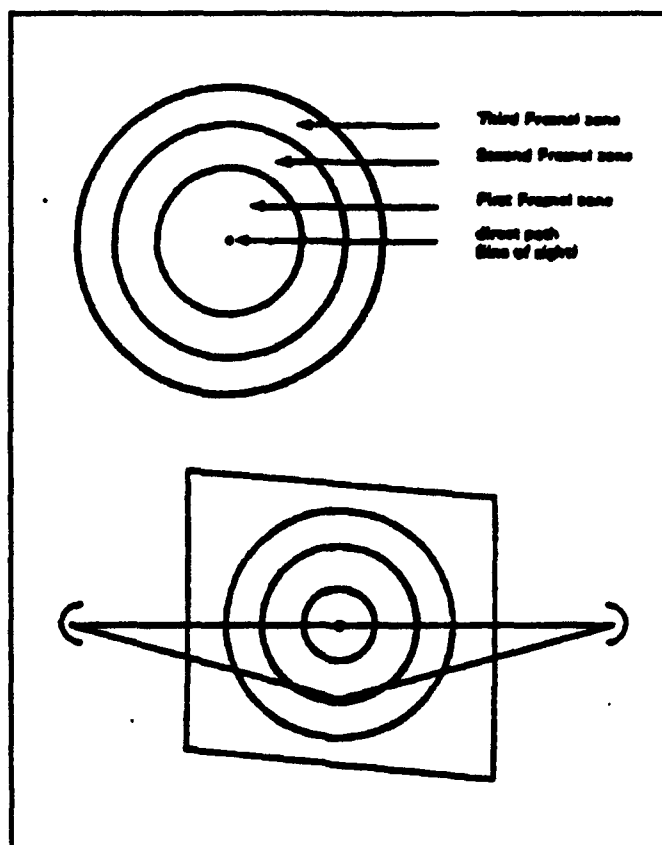
Figure 4 Fresnel Zones

    (1)   Obstruction. Obstruction losses are considered for the direct wave to the target. When 0.6 or greater of the first fresnel zone (or slightly more than half of the area illustrated in Figure 4) of the direct wave is clear, obstruction losses are considered negligible. However, when less than 0.6 clearance (fresnel zone blockages) the losses are no longer considered negligible and can be calculated. Obstruction losses are normally computed for communications circuits because the communication circuit is ground-to-ground where partial obstruction is likely (Freeman, 1991, pg 219). However, obstruction losses are not normally computed for ground radar systems because the radar system is normally ground-to-air. Additionally, at radar frequencies (normally

22

higher than ground communications frequencies) the wavelength is small when compared to the earth's dimensions and little energy is lost due to obstruction (Patterson, 1990, pg 21). Therefore, for this thesis the obstruction losses for the radar system will be considered negligible. The primary consideration is not losses but screening or blockage of the area of interest. The screening effect due to terrain in the area of interest assumes no radar detection will occur. The effects of screening, and the AGL and RLS diagrams, which provide the analysis for the impact due to screening, will be covered in greater detail in sections e, f, and g (pages 41-52).

(2)   *Reflection.* The ability to reflect radio waves is very useful in some applications and a hinderance in others. Waves that are reflected undergo approximately a 180 degree phase shift from the phase of the incident wave. Furthermore, the difference in the path length introduces an additional phase shift. The additional phase shift due to path length and the 180 degree phase shift due to the reflection can either aid or oppose the direct signal at the receiver. The grazing angle, the type of terrain (either smooth or rough), terrain composition (conductivity and dielectric constant), and the polarization of the wave will determine the amount of energy that will be reflected (Angelokos and Everhart, 1968). The energy reflected from a smooth moist earth, a thin layer of air lying just above the earth, or a calm body of water will be greater than energy reflected from rough, rocky terrain.

When there is more than 0.6 fresnel zone clearance on a path, the received signal strength can be more or less than the free-space value, depending upon the relative strength and phase of the reflected signal that reaches the receive antenna.

23

Reflected waves can interfere with the direct wave to a point of no reception or can cause an increase in signal strengths; therefore, this alteration in the free-space radiation pattern caused by reflections from terrain in the vicinity of the transmission source must be considered when predicting radar performance. Reflective multipath fading is caused by signal reflections occurring in even-numbered fresnel zones. The extent of these earth-surface effects depend on the effective antenna height, surface roughness, and terrain features. The signal can vary greatly because the ground reflections may arrive at the receiver in a manner that will either aid or oppose the direct wave. This effect (multipath) creates a vertical pattern of nulls and lobes. A null is an area of reduced signal and a lobe is an area of increased signal. Figure 5 (Barton, 1988, pg 296) illustrates the effects of lobing on the radar coverage. The figure is a vertical dissection of the radar coverage envelope on a height versus range overlay. The range is plotted on a downward curve to illustrate the effects of the earth's curvature. The vertical elevation angle is annotated on the right to provide a perspective of vertical scale. The vertical radar coverage antenna beam pattern excluding the effects of multipath are shown by the free-space coverage line. The effects due to multipath are shown by the lobes (enhanced coverage) and the nulls (degraded coverage).

When the signal from the reflective surface is from the first fresnel zone the signal undergoes two 180 degree phase shifts. The first phase shift occurs due to the path difference from the direct signal versus the reflected signal. The second phase shift is attributed to reflection. The result then is the energy from the first fresnel zone will increase the total received signal strength. The amount of increase will depend

24
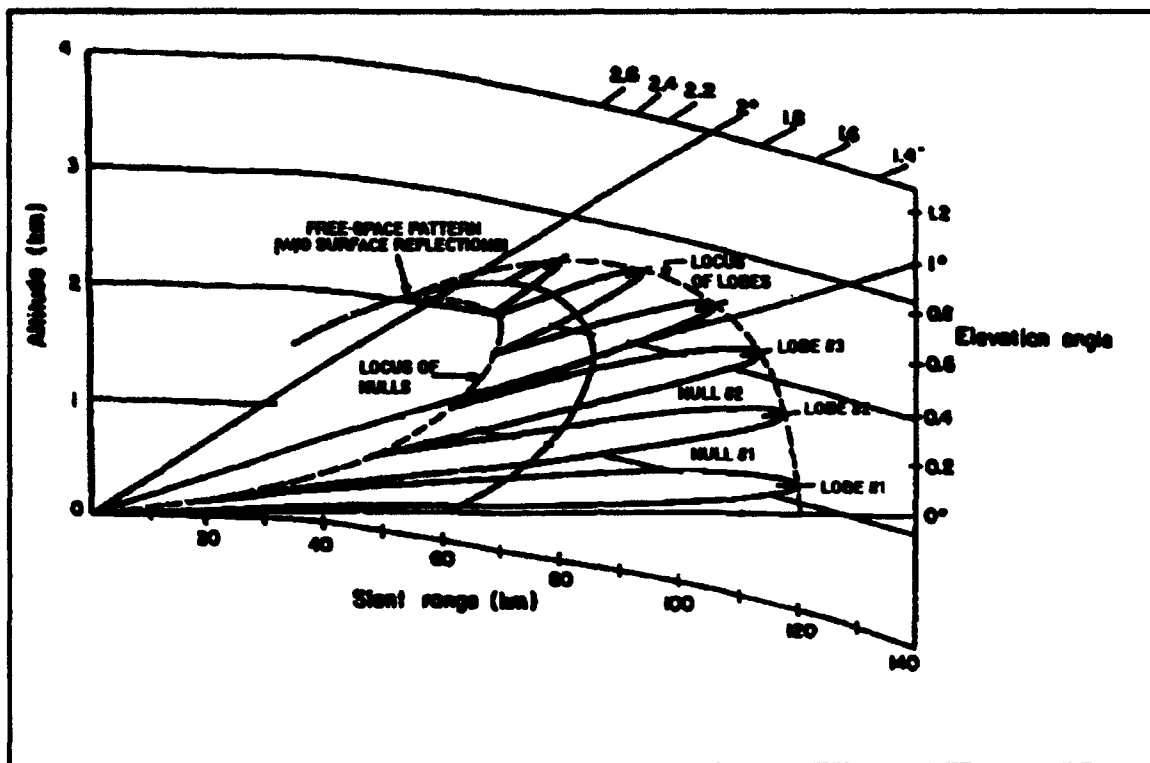
Figure 5 Radar Coverage With Lobing

upon the type of reflection, surface. Theoretically the maximum signal strength for a single reflection gain is 6 dB more than the free space condition (Air Force Communication Command, 1986, pg 5-79). The reflection from the second fresnel zone is 180 degrees out of phase from the direct signal and therefore reduces the received energy. The amount of degradation is again dependent upon the composition and roughness of the reflective surface but could be as much as 35 to 40 dB.

Most radar modeling software, such as IREPS and EREPS, assumes a smooth reflective surface. However, the smoothness, or roughness, of the terrain can be determined and then used to determine the effect on radar performance. A surface is defined as smooth if the height of surface irregularities, Δh (Figure 6), at the reflection

25

point produces a net signal phase difference of less than 45 degrees (or one-eighth wave length) between the waves reflected from the peaks and the waves reflected from the troughs of the irregular surface. This condition is satisfied when the terrain peak-to-trough height difference, Δh, is less than a critical height difference Δh_c, where Δh_c is related to the grazing angle, ψ, as follows (FAA ORDER 6340.15, May 1983):

$$\Delta h_c = \left(\frac{\lambda}{(8)\,(2)\,\sin\psi} \right) \qquad\qquad (6)$$

Δh_c = critical height difference in feet

ψ = grazing angle in degrees

λ = wavelength of radar signal in feet.

Figure 6   Terrain Roughness

The reflective surface in front of the radar is considered rough if $\Delta h > \Delta h_c$ as defined by the roughness criterion equation (equation 6) and Figure 6. As the roughness criterion and Figure 6 illustrate, surface roughness is a function of frequency, grazing angle, as well as the surface irregularities (Δh) in front of the radar. Figure 7 is a visual representation of the application of the roughness criterion equation

26

for two frequencies: 1300 and 1030 MHz. For example, for a 1300 MHz radar (approximately the frequency of the NPS radar) and a grazing angle (horizontal scale) of 4 degrees, the critical height (vertical scale) would be 0.4 feet. Therefore, if the trough-to-peak change in the terrain in front of the radar was less than 0.4 feet the surface would be considered smooth. The roughness criterion defined in equation 6, and illustrated in Figure 7, shall be applied to the NPS radar site in subsection b (Multipath Study).
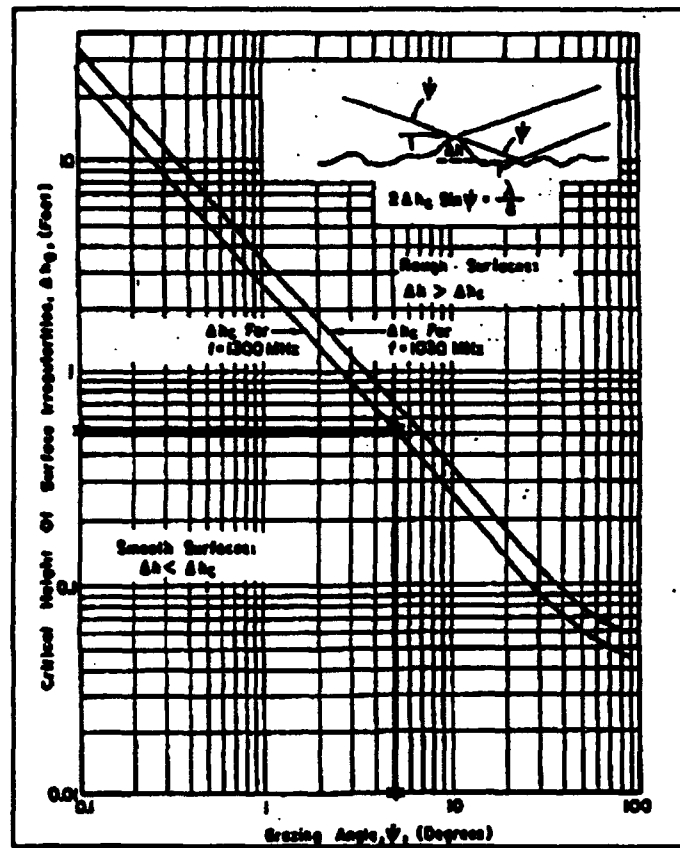
Figure 7 Roughness Criterion

(3)   Fresnel Zone Geometry. The roughness of the terrain, or surface of the earth, where the reflections occur can be determined through equation 6 as discussed in the previous section. The question should be asked "To what area of terrain should the roughness criterion be applied to ?". The area of specific terrain that the roughness criterion should be applied is found by defining the fresnel zones. The range limits R_L of the fresnel zones, illustrated in Figure 8, can be calculated by solving equation 7 (FAA ORDER 6340.15, 1983, pg 105):

$$R_L = \left[\frac{1}{2n} + \frac{1}{n^2} \pm \frac{\sqrt{1+n}}{n^2} \right] \frac{8h_a^2}{\lambda} \tag{7}$$

R_L = fresnel zone range limits in feet (near and far point relative to the radar site)

n = fresnel zone (1= first lobe, 2=first null, 3=second lobe, 4=second null, ...)

λ = wavelength of radar signal in feet

h_a = height of antenna in feet.

Solving equation 7 for R_L highlights the terrain of interest, i.e., the area in front of the radar from which ground reflections will occur that will degrade or enhance the direct wave. Since the fresnel zone is circular, only the near and far points of the fresnel zones are calculated. As illustrated in Figure 8, the first near and far points (n=1) define the area on the surface of the earth for the first fresnel zone that results in the formation of the first lobe in the radar coverage envelope. Likewise, the

28

THIRD NULL

SECOND NULL

FIRST NULL

LOBE #3

LOBE #2

LOBE #1

Near Fresnel Points

Far Fresnel Points

Second Fresnel Zone

First Fresnel Zone

Note: "Near" and "Far" refer to distance from radar antenna.
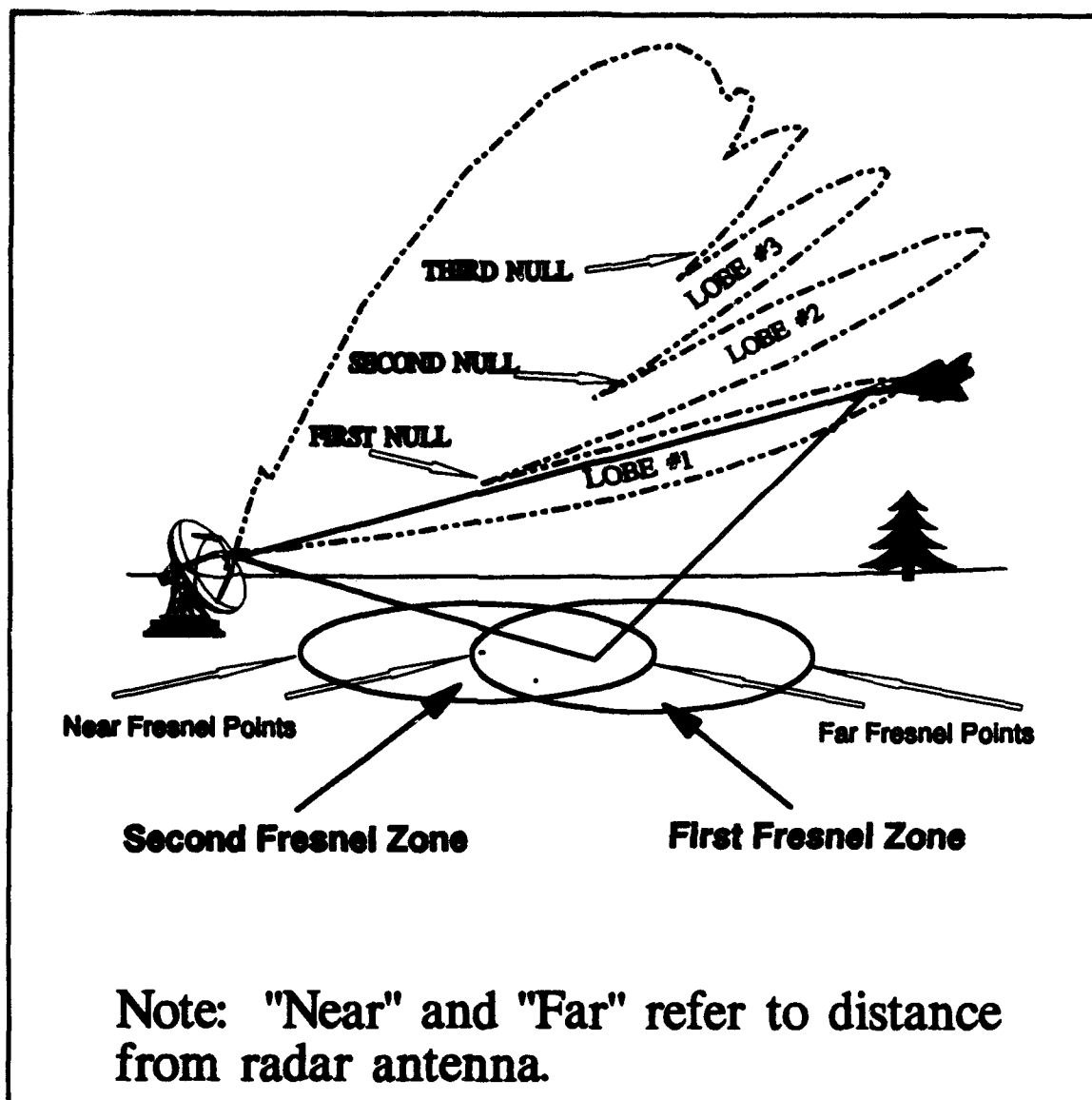
Figure 8   Fresnel Zone (Near and Far Points)

second near and far points (n=2) define the area for the second fresnel zone and the first

null in the radar coverage envelope.

The ground reflections from the fresnel zones are greatest when the

reflecting surface is smooth, and are decreased when the reflecting surface is uneven.

Uneven land areas, trees, grass, rough sea, etc., may absorb or scatter a large portion of the reflected energy, thus nullifying any effect of reflected signal upon the direct wave. On the other hand, large smooth areas such as a calm sea, a flooded field, or a relatively flat desert, or snow covered area, can cause a relatively large reflected signal (FAA ORDER 6340.15, 1983). The determination of the position of the nulls and the application of the fresnel zones and roughness criterion for the NPS radar will be performed in the Multipath Study section.

d. *Multipath Study.*

The multipath study for this thesis is performed to evaluate the impact due to energy radiated from the radar striking the surface of the earth and reflected towards the target. The study will consist of determining the position of the nulls, the application of fresnel zone and roughness criterion theory outlined in the previous section, and analyzing the effects of antenna tilt on multipath for the AN/UPS-1 at NPS.

The position of the null angles is a function of the antenna height, frequency, and null (or lobe) of interest. The angles of the nulls and lobes can be approximated by using the following equation (FAA ORDER 6340.15, 1983, pg 81):

$$\theta = \frac{14098n}{h_a f} \qquad (8)$$

θ = angle of nulls and lobes

n = 2, 4, 6...(for nulls) 1, 3, 5 ... (for lobes)

30

h_a = antenna height in feet

f = frequency in MHz.

Once the angles of the nulls are approximated by solving equation 8, the angle of the nulls can then be plotted on earth curvature backgrounds such as the lobing study (Figure 9). Figure 9 is a plot of the position of first 7 nulls, and the position of the first 6 lobes since they occur between the nulls, for the AN/UPS-1 at NPS. The AN/UPS-1 radar antenna (with a elevation of 158 ft) is positioned at the point of origin on the plot. A -2.00 degree screening angle was assumed (i.e., actual screening from surrounding terrain was not considered) to provide the lower null angle positions. The null angles are plotted on a earth curvature background using the average annual K-factor of 1.35. The raw data (provided by the 84 RADES at Hill AFB) (Estebo, 1994) used to plot the nulls on Figure 9 are listed in Appendix A. The height of the antenna above the reflecting surface determines the number of nulls and lobes that will occur and the angles at which they will occur as seen in equation 8. For antennas at lower elevations, the number of nulls would be less than antennas at higher elevations. Consequently, for a high-sited radar (such as at NPS at 158 ft) the lobe structure becomes very fine. When the lobing structure is fine the results are as shown in Figure 9. The nulls occur very frequently resulting in obtaining, and losing, track on a target very rapidly, assuming the null is deep enough to lose track. For example, again assuming the null is deep enough to lose track, if an aircraft were flying at a constant altitude of 20,000 ft, Figure 9 indicates by the position of the first null and lobe that detection would begin just inside

31

ELEVATION ANGLE IN DEGREES

Lines are
NULL Angles

RANGE IN NAUTICAL MILES

Example:

Aircraft at 20,000 ft

Point A null on horizon lower portion of first lobe (detection begins)

Area between points A and B first lobe (detection for width of lobe)

Point B first null between lobes (no detection for width of null)

Area between points B and C second lobe (detection for width of lobe)

Point C second null between lobes (no detection for width of null)

Process continues

Figure 9 Predicted Null Angle Positions for AN/UPS-1 at the NPS

190 nmi (Point A). Similarly, detection would continue until the aircraft approached the second null at 170 nmi (Point B) at which time the radar would lose track. The radar would then again track the aircraft just inside 170 nmi and lose track again as the aircraft approached 157 nmi (Point C). This shows that a 20 to 10 nmi interval between detections would be expected for the NPS radar system. The results of changing the antenna height are illustrated in Appendix B. Appendix B shows that the radiation pattern for a lower antenna height is characterized by fewer lobes at higher elevation angles and greater spacing between the lobes. The consequent reduction in low-angle coverage is in addition to that imposed by changing the radar line-of-sight. Lowering the height of the antenna raises the radar line-of-sight and results in a reduction in range coverage at the lower altitudes. Therefore, if the detection of target aircraft at low angles is critical to meeting operational requirements, the sacrifice in low-angle coverage that results from decreasing the antenna height must be carefully considered.

The null angle positions predicted for the AN/UPS-1 at NPS are fairly close together as noted above; however, the depth of each of the nulls will depend upon the roughness of the terrain in each fresnel zone. Therefore, each fresnel zone for the NPS radar system must be calculated to determine the roughness of the terrain within the zone as discussed in the previous section. Solving for the position of the near and far points for the fresnel zones (illustrated in Figure 8) for the first three nulls, using equation 7 ($h_a = 158$ ft, $\lambda = .7543$ ft, and $n = 2, 4, 6$) results in the range limits shown in Table V. As shown in Table V, the fresnel zones can extend several miles from the radar site. For the AN/UPS-1 at NPS the fresnel zone near point for the first null is

33

2.92 nmi and the far point is nearly 41 nmi from the radar antenna. For the NPS radar the composite of the first three fresnel zones for the first three nulls extend from 1.64 nmi (closest near point) to 40.66 nmi (furthest far point) from the radar site. This composite area defines the area of reflection that will contribute to the formation of the first three nulls.

TABLE V   FRESNEL ZONES FOR AN/UPS-1

Fresnel Zones Range Limits (R_L) Computed by solving equation 7 (ha=158 ft, λ=0.7543)					
Null #	n	Near Point (ft)	Far Point (ft)	Near Point (nmi)	Far Point (nmi)
1	2	17,740	247,036	2.92	40.66
2	4	12,643	86,714	2.08	14.27
3	6	9,962	48,984	1.63	8.06

The data presented in Table V can also displayed graphically to illustrate the effects of antenna height on distance to reflection points. Figure 10 illustrates the effects for a fixed frequency of 1300 MHz up to an antenna height of 100 ft. For example, the near point for the first fresnel zone, for a antenna height of 50 ft (vertical scale), would be approximately 2000 ft from the radar. Similarly, the far point would be approximately 25,000 ft from the radar. The far point of the fresnel zone for the first null, for an antenna 100 ft in height, depicted in the figure extends to 100,000 ft from the radar site. The change in antenna height is shown to significantly increase the distance to the fresnel zone far point, and therefore, shift the area on the surface of the

34

earth where reflections will occur.
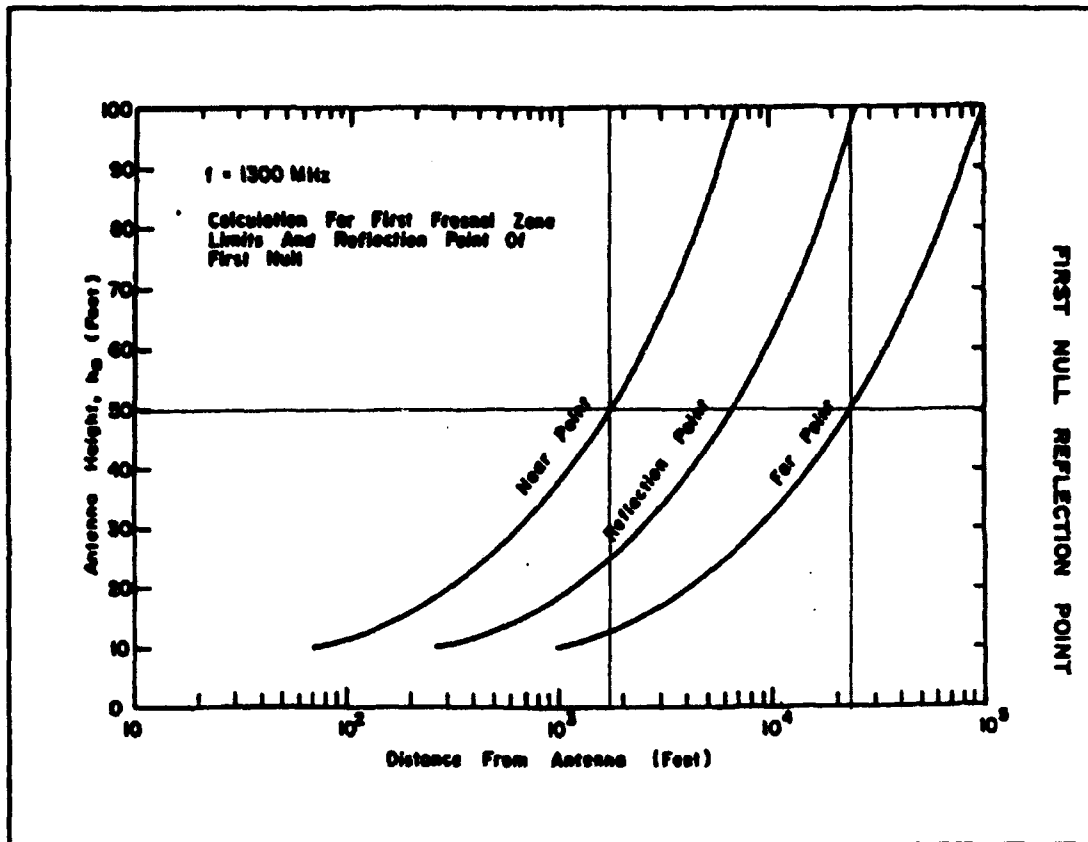
Figure 10 First Fresnel Zone Limits

The amount of terrain roughness, within the fresnel zone described above, that could impact the depth of the nulls can be calculated by solving equation 9 as shown:

$$\Delta h_c = \frac{\frac{\lambda}{8}}{2\sin\psi} \tag{9}$$

35

λ = wavelength = 0.7543 ft (for AN/UPS-1)

ψ = grazing angle in degrees

Δh_c = critical height in feet.

To solve equation 9, first, the grazing angle for the near and far fresnel point must be found. This is done by solving the right triangles formed with a antenna height of 158 ft and a range of 9,962 ft (near point) and 247,036 ft (far point). The angles associated with those dimensions yields the grazing angles of 0.9087 and 0.0366 respectively. Applying these grazing angles to the roughness criterion equation yields the following:

$$\Delta h_c = \frac{0.0943 ft}{2 \sin(.9087)} = 2.97 ft \qquad (10)$$

$$\Delta h_c = \frac{0.0943 ft}{2 \sin(.0366)} = 73.72 ft \qquad (11)$$

The critical height (Δh_c) for the fresnel near point is 2.97 ft and the critical height for the fresnel far point is 73.72 ft. This illustrates that the amount of terrain change before the terrain is considered rough is greatly increased as the grazing angle is decreased and the further the reflection occurs from the radar site. The results also show that for the NPS radar site, and for bearings seaward, 3 foot waves in

36

Monterey bay (approximately 1.6 nmi from NPS) will impact radar performance. If radar reflections occur in the Monterey bay with less than 3 foot waves the surface roughness would be considered smooth and the depth of the null (third and higher) would be greater. If the null depth is greater, radar detection will be reduced at the null angles. Therefore, assuming less than 3 foot waves in the bay (i.e., smooth reflective surface), and for the third null as solved above, the detection would be degraded at the null angle for the third null. The third null angle is +0.25 degrees as noted in Figure 9; therefore, detection at this angle over the water would be degraded. The degraded, or enhanced, performance discussed thus far has been due to terrain surrounding the radar. However, degraded and enhanced performance can also be due to position, or tilt angle, of the radar antenna.

Antenna tilt, the vertical angle at which the radar antenna is pointing, will also determine the depth of nulls, range of the lobes, and consequently overall radar performance. The AN/UPS-1 antenna tilt at NPS is currently set at +5.0 degrees but is manually adjustable from -2.0 to +5.0 degrees. The radar coverage will change due to tilt as shown in Figure 11 (Connor, 1994). Figure 11 is the free-space (multipath effects are not considered) vertical coverage for an average target at 100 nmi for various antenna tilt angles. It should be noted that the detection range on the radar horizon decreases as the antenna elevation is increased from zero-degrees to five-degrees tilt, when no effects from surface reflections are considered. When multipath effects are considered the radar coverage is altered considerably.
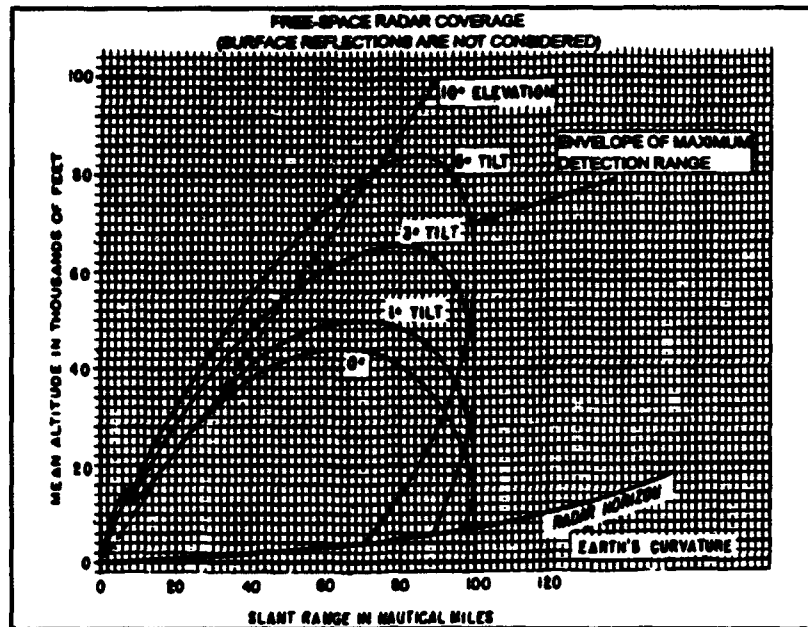
Figure 11 AN/UPS-1 Free-Space Radar Coverage vs Antenna Tilt Angle(surface reflections are not considered)

Figure 12 (Connor, 1994) is an illustration of the AN/UPS-1 antenna at a +5 degree tilt (the tilt at NPS). Figure 12 shows the predicted coverage for the +5 degree tilt at lower elevation angles (below 10 degrees) is significantly enhanced, or significantly degraded, when compared to the free-space coverage. For example, for an aircraft at a constant altitude of 20,000 ft (vertical scale) detection will occur at 120 nmi (horizontal scale) from the radar. However, if the free-space detection envelope is used the detection would occur at approximately 84 nmi. Therefore, when considering the effects of multipath the range of the radar for an aircraft at 20,000 ft is increased by 36 nmi. The effect of multipath for higher elevation angles in reduced to the point of no significant impact, or change in expected range, on the fifth null.
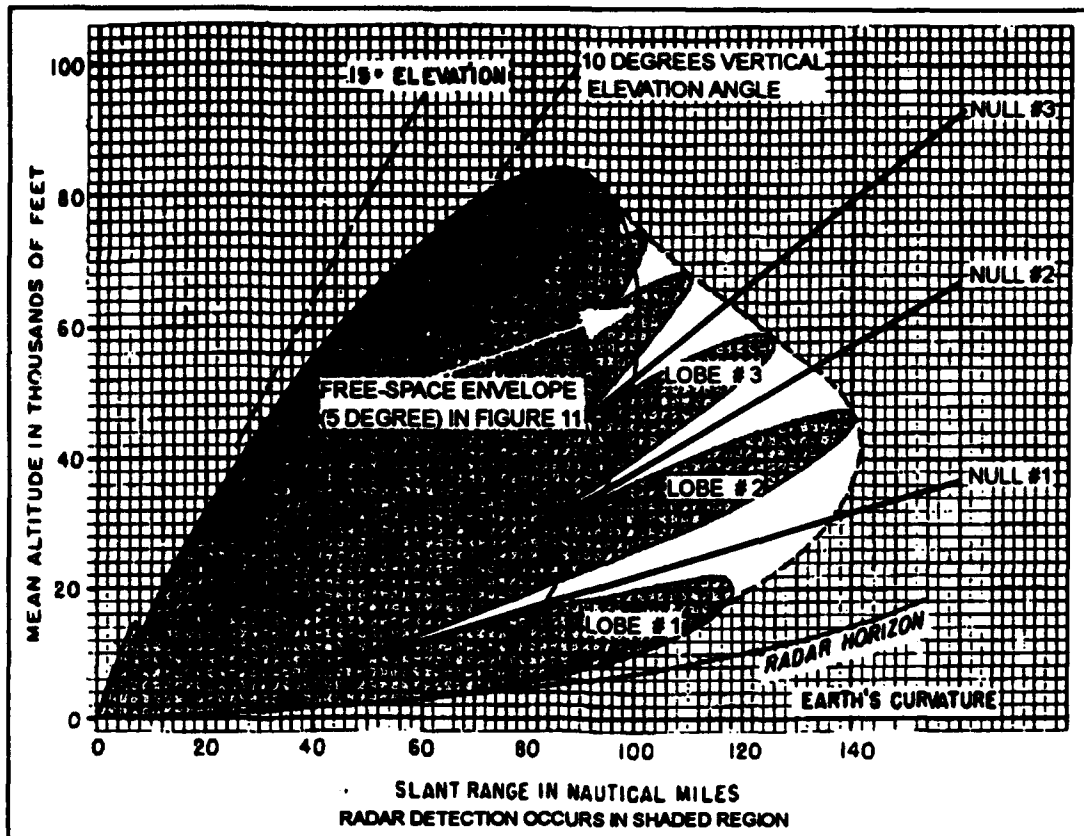
Figure 12 AN/UPS-1 Radar Coverage with 5° Antenna Tilt (shows effects of surface reflection)

As the antenna tilt is lowered, multipath becomes more pronounced. This is because more of the radar signal is radiated toward the earth's surface as the antenna is pointed downward. Figure 13 (Connor, 1994) depicts the impact of reducing the antenna tilt by two degrees, i.e., setting the AN/UPS-1 antenna at a tilt of 3 degrees. As noted in Figure 11 the free-space coverage is different between the 5 and 3 degrees tilt. When multipath effects are considered, as well as the tilt angle, the coverage is drastically different. As the antenna tilt is reduced the depth of the nulls, and the
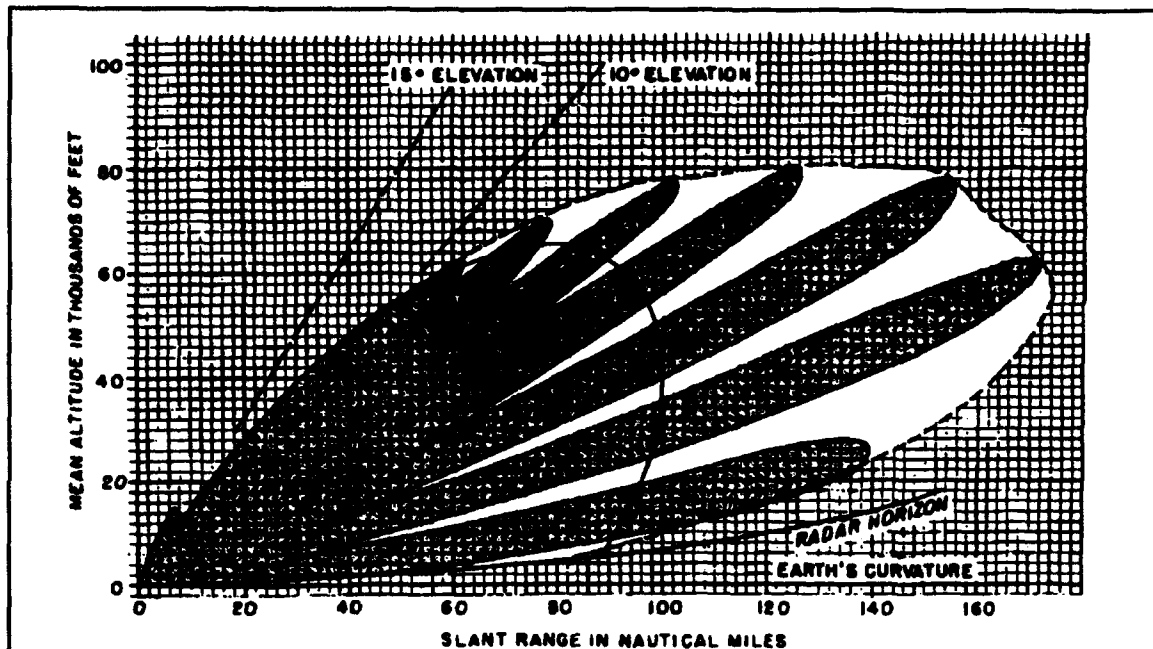
Figure 13 AN/UPS-1 Vertical Coverage Pattern (3° Tilt)

enhancement of the lobes, is considerably increased. For example, Figure 13 shows at 60,000 ft the detection range, due to the multipath, increased from the free-space detection range of 94 nmi to 170 nmi. As observed on Figure 12 the detection range for an aircraft flying at a constant altitude of 60,000 ft the detection range for a 5 degree tilt would be about 126 nmi. Comparing this to the detection range for the same aircraft altitude for the 3 degree tilt, shown in Figure 13, we see the detection range is increased to 170 nmi. The change in antenna tilt results in a significant improvement in detection at that altitude. These figures (Figures 11, 12, and 13) are based on a smooth reflective surface within the fresnel zones and antenna heights of 15 feet (nominal deployed antenna height for AN/UPS-1). The antenna height at the NPS is 158 ft; therefore, the vertical radar coverage envelope would be not be the same. However, these figures are included in this thesis to illustrate the effects of various tilt angles and multipath on radar

40

coverage.

e. Screening.

The effects of screening (also known as terrain masking) on radar coverage can significantly impact performance. Screening is caused by terrain features that block the radar signal from an area, or region, of airspace that would otherwise be illuminated by the radar. Screening is a geometric problem: if the earth is smooth, the curvature of the earth causes the screening (Figure 14), and if there are hills or mountains, then screening is increased and radar coverage is reduced. The geometric considerations for screening is the height of the radar antenna, height of any screening object, and the distance to the screening object. The signal path from the radar antenna to the upper limit of a screening object is called the radar line-of-sight (RLS). The RLS establishes the maximum theoretical range obtainable at a given altitude. This range is generally measured along the RLS to the intersection with the altitude curve of interest as shown in Figure 15. From the screening limitations shown in Figure 15, the AGL and RLS diagrams are derived.
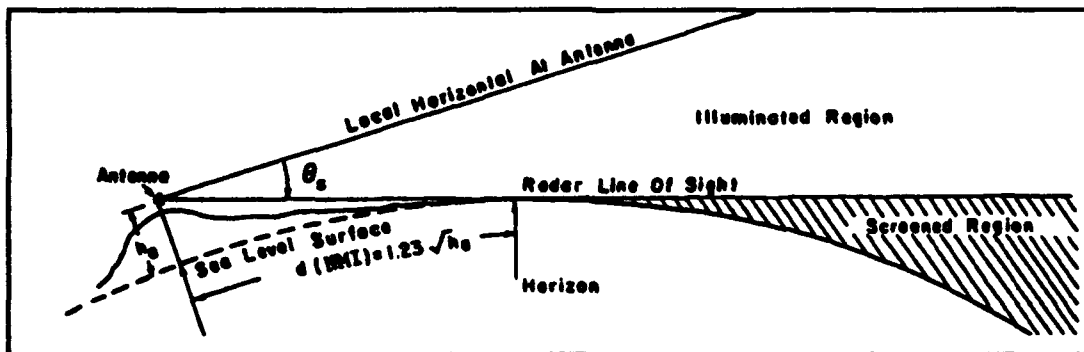
Figure 14 Curved Earth Screening

41
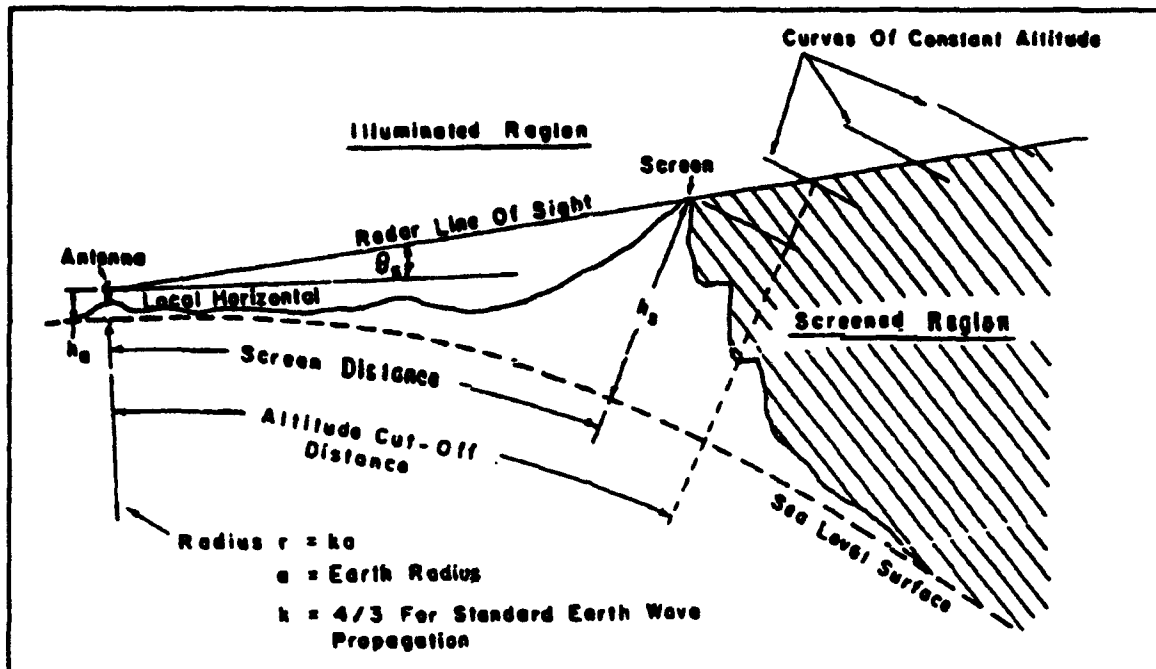
Figure 15 Radar Line-of-Sight

f. Above-Ground-Level Diagrams.

Figures 16-19 are AGL diagrams for the AN/UPS-1 at NPS for target or aircraft altitudes of 500, 1000, 2000, and 5000 ft AGL. When an aircraft is flying at lower altitudes the altitude is normally reported in feet Above-Ground-Level; therefore, the AGL diagram is constructed to predict coverage for the lower flying and terrain following aircraft. The shaded regions on the AGL diagrams provide a visual representation of the predicted areas of radar coverage and are derived from Digitized Terrain Elevation Data (DTED) provided by the Defense Mapping Agency. The digitized terrain features are used to provide a digitized map with the obstacle screening information illustrated in Figure 15. Areas where radar coverage is limited as the aircraft flies over lower terrain features are shown in the AGL diagrams by the

42

unshaded/blank areas between two shaded regions. For example, as shown on the 500 ft AGL diagram (Figure 16), between 10 to 50 degrees and 25 to 50 nmi (range rings are 25 nmi), an aircraft inbound to the radar would momentarily be visible (shaded region) to the radar as it flew above the higher terrain due to screening. The inbound aircraft would not be visible to the radar (blank area) again until it was within 25 nmi (first range ring) of the radar. Figures 16 - 19 also depict the effect as the aircraft altitude is increased. If the shaded regions are compared from one diagram to the other, the following should be noted:

- The detection regions increase as the altitudes are increased.

- The detection regions include more of the valley areas (blank areas between shaded regions) as the altitudes increase.

- Screening inland is significant and remains a limiting factor for detection as the altitudes are increased.

- At the azimuths between 310° and 327° the limitation is the earth curvature. This is noted because of the appearance of the shaded region being truncated, or ending abruptly.

The 5,000 ft AGL diagram illustrates the impact of the mountainous terrain surrounding the NPS. The limitations due to screening reduces the radar detection to only 25 nmi from 100° to 290° azimuths and to only 50 nmi from 55° to 300°. The azimuths of 310° to 328° are the only azimuths limited by the curvature of the earth and not impacted by the screening due to the mountainous terrain surrounding the NPS. This limitation applies to only 18° out of the entire 360° of coverage for a detection range of 100 nmi. These severe limitations due to screening would be

indicative of picking a very poor location to place a radar system. However, the NPS radar system is a educational/non-operational system and good siting was not a consideration when determining the location for the radar. These diagrams also illustrate the severity of the impact which the location, or installed environment, can have on radar system performance. This severe impact must be considered when determining the capabilities and limitations of a radar system.
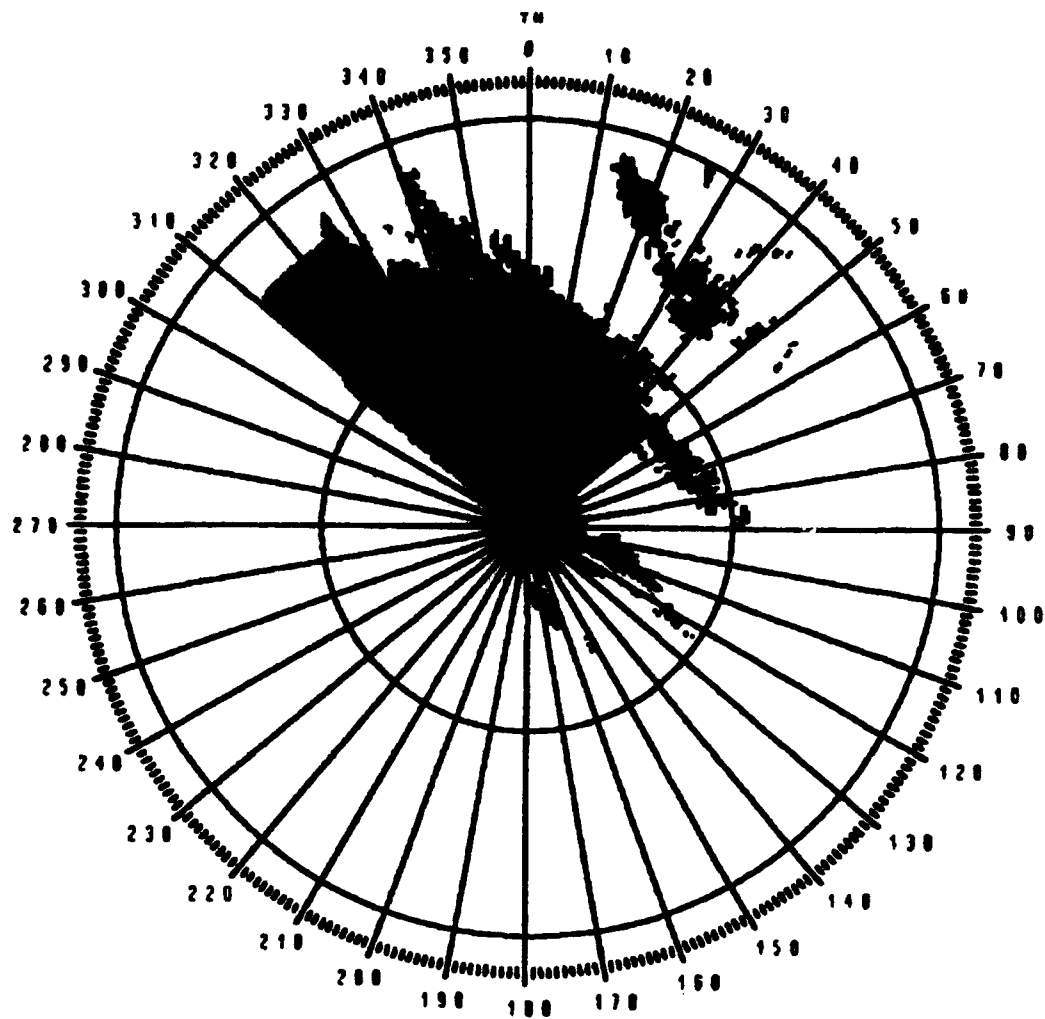
500 ft Above Ground Level (AGL) Diagram

Shading Indicates Areas of Radar Coverage When Aircraft Altitude is 500 ft AGL

Location: Naval Postgraduate School
Equipment: AN/UPS-1
Focal Point Elevation: 158 ft

Range Ring Interval: 25 nmi
K-Factor: 1.348

Figure 16 Above Ground Level Coverage Diagram (500 ft)
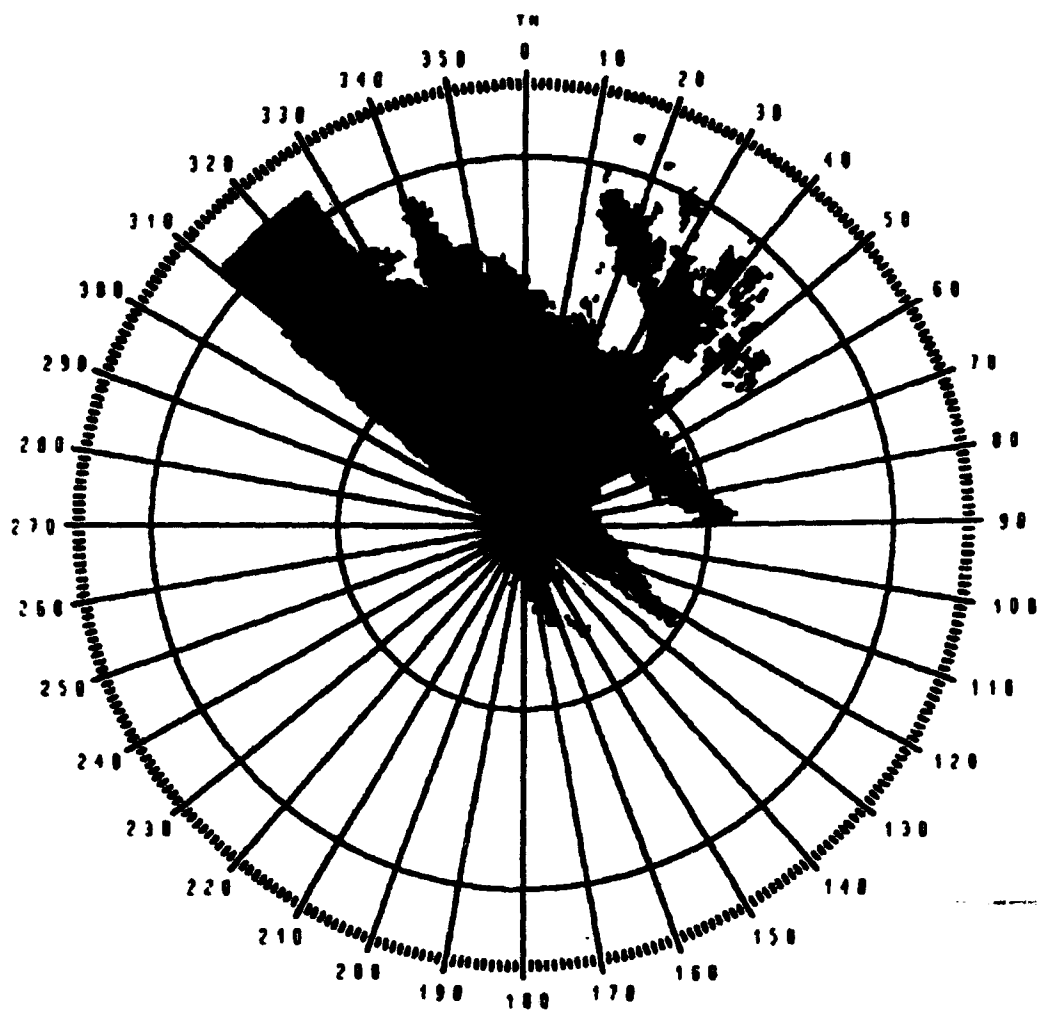
1000 ft Above Ground Level (AGL) Diagram

Shading Indicates Areas of Radar Coverage When Aircraft Altitude is 1000 ft AGL

Location: Naval Postgraduate School
Equipment: AN/UPS-1
Focal Point Elevation: 158 ft

Range Ring Interval: 25 nmi
K-Factor: 1.348

Figure 17 Above Ground Level Coverage Diagram (1000 ft)

2000 ft Above Ground Level (AGL) Diagram

Shading Indicates Areas of Radar Coverage When Aircraft Altitude is 2000 ft AGL

Location: Naval Postgraduate School   Range Ring Interval: 25 nmi
Equipment: AN/UPS-1   K-Factor: 1.348
Focal Point Elevation: 158 ft
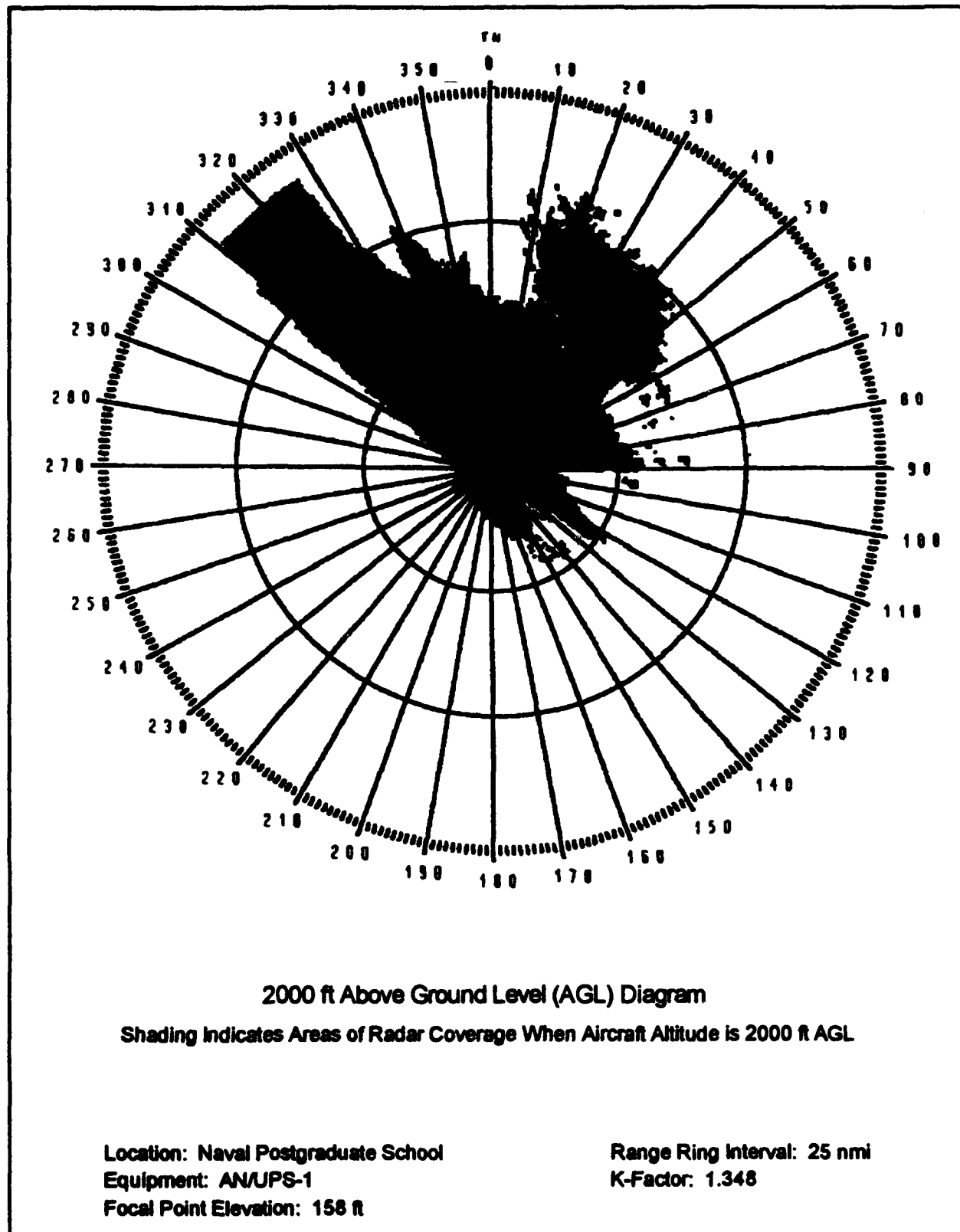
Figure 18 Above Ground Level Coverage Diagram (2000 ft)

5000 ft Above Ground Level (AGL) Diagram

Shading Indicates Areas of Radar Coverage When Aircraft Altitude is 5000 ft AGL

Location: Naval Postgraduate School   Range Ring Interval: 25 nmi
Equipment: AN/UPS-1   K-Factor: 1.348
Focal Point Elevation: 158 ft
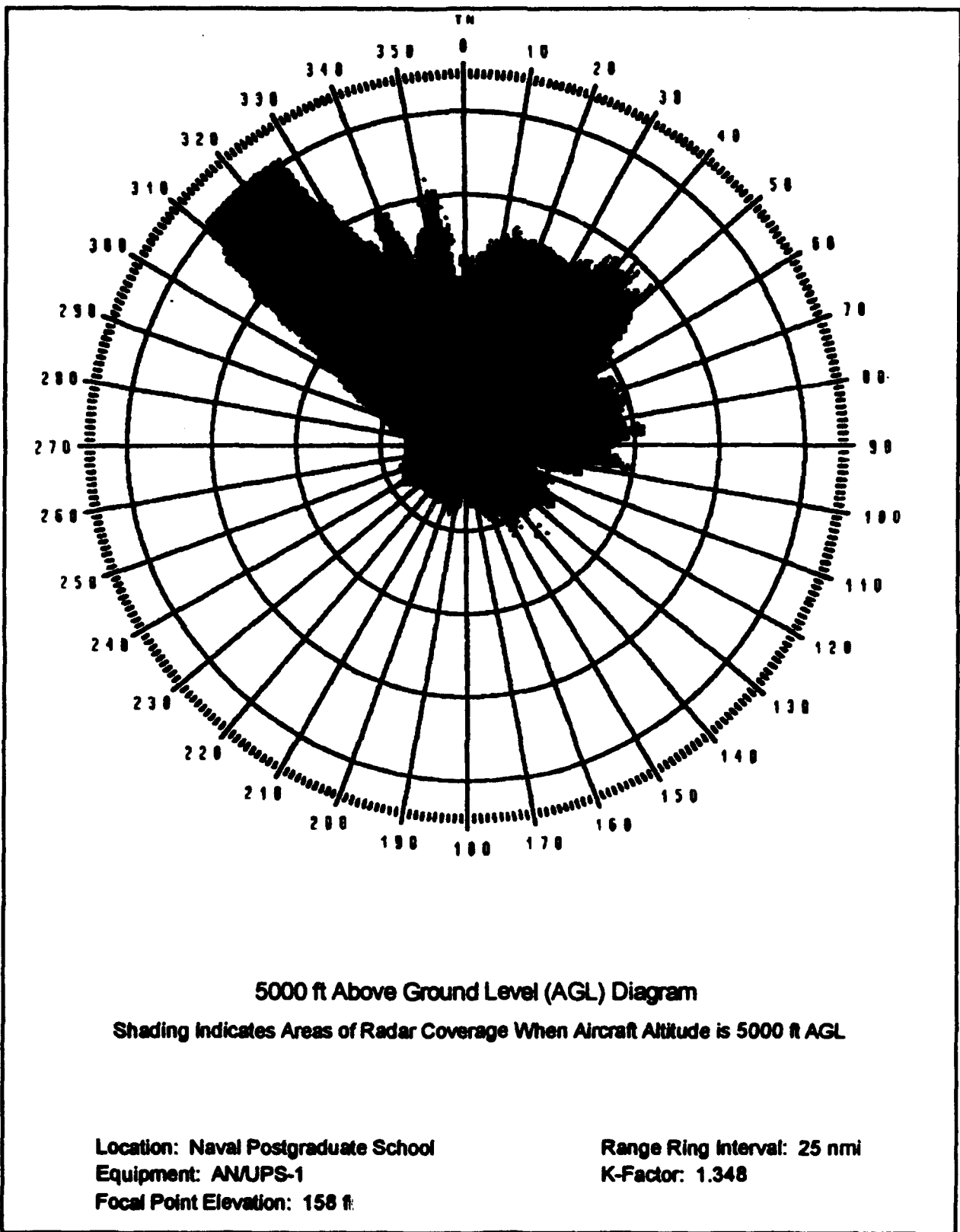
Figure 19 Above Ground Level Coverage Diagram (5000 ft)

g. Radar Line-Of-Sight Diagrams.

The Radar Line-of-Sight (RLS) diagrams (Figures 20 and 21), like the AGL diagrams, predict those areas where an aircraft can be detected. However, the RLS diagrams illustrate those areas of detection based on aircraft flying at higher, and constant (MSL), altitudes not terrain following (AGL). However, to include overlap in predicted coverage for the AGL and RLS diagrams the 5,000 ft altitude is included in both types of diagrams. The curves of constant altitude shown in Figure 15 are the side view representation of the various altitude rings depicted in the top view RLS diagrams. It should be noted that the figures are different, however, in that the RLS diagrams illustrates the illuminated, or detection, region with shading while Figure 15 depicted the non-detection regions by shading. The RLS, as did the AGL, diagrams show the effects of mountainous terrain which severely restricts radar coverage in nearly all azimuths at the NPS. The same restrictive coverage seen on the AGL diagrams from 50 to 310 degrees can also be seen on the RLS diagrams. The only area that is restricted by the earth's curvature is from 310 to 330 degrees. Figure 20 illustrates the predicted radar coverage for altitudes of 5, 15, and 25 thousand feet MSL. Figure 21 illustrates the predic d radar coverage for altitudes of 10, 20, and 30 thousand feet MSL. As expected, the figures show that when the aircraft flies at higher altitudes the NPS's radar coverage is improved. For example, on Figure 20, the radar horizon for an aircraft at 5,000 ft at 320 degrees is 100 nmi; however, at 25,000 ft at the same azimuth the predicted radar range is slightly better than 200 nmi. Figures 16-21, when taken as a group, provide the user with the radar coverage for the airspace surrounding the NPS.

49

TARGET ALTITUDES (ft MSL):

■ 5,000   ▦ 15,000   ▧ 25,000

EQUIPMENT: AN/UPS-1	RANGE RING INTERVAL: 50 NMI
LOCATION: NAVAL POSTGRADUATE SCHOOL	FOCAL PT ELEVATION: 157 FT
MONTEREY, CA	K-FACTOR: 1.348
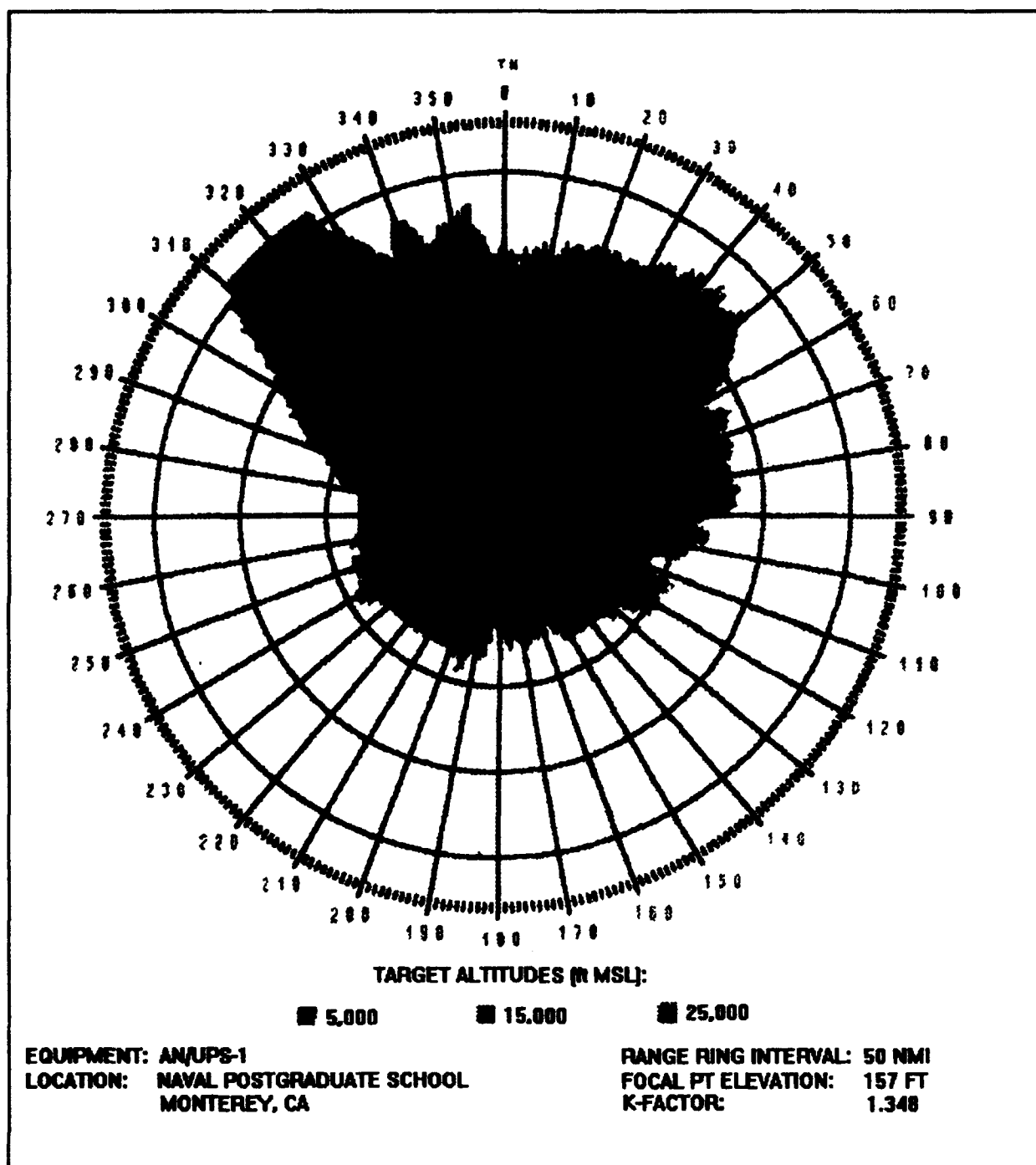
Figure 20 Radar Line-of-Sight (RLS) Coverage Diagram (5, 15, and 25 thousand feet)

TARGET ALTITUDES (ft MSL) :

■ 10,000   ■ 20,000   ■ 30,000

EQUIPMENT : AN/UPS-1
LOCATION : NAVAL POSTGRADUATE SCHOOL
MONTEREY, CA

RANGE RING INTERVAL: 50 NMI
FOCAL PT ELEV: 157 FT
K-FACTOR: 1.348
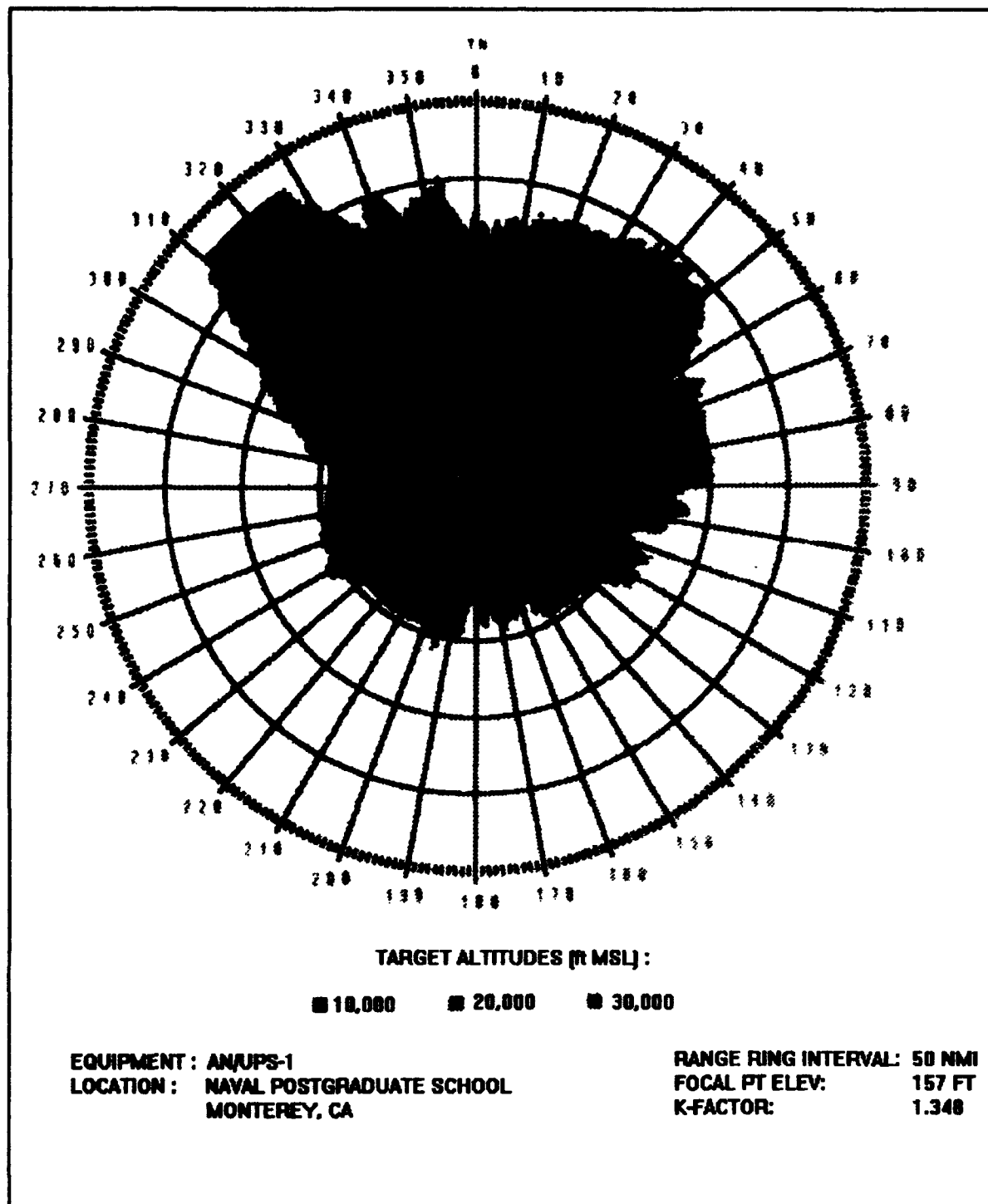
Figure 21 Radar Line-of-Sight (RLS) Coverage Diagram (10, 20, and 30 thousand feet)

2. Atmospheric Analysis

The atmosphere can cause the radar wave to be dispersed, attenuated, refracted and retarded (Kingsley, 1992, pg 173). The effects of the atmosphere cause the greatest day-to-day variability in the ground radar system's performance. The computer programs currently used to model and evaluate the effects of the atmosphere on radar propagation are the Integrated Refractive Effects Prediction System (IREPS) and Engineer's Refractive Effects Prediction System (EREPS). Both programs were written by personnel assigned to the Naval Ocean Systems Center in San Diego, CA and will be discussed in detail in the sections that follow. These programs, IREPS and EREPS, will be used to predict the effects of the atmosphere on the AN/UPS-1 at the NPS. In order to understand the analysis performed by IREPS and EREPS, the environmental factors must be understood; therefore, the standard and non-standard environments will be discussed. The IREPS analysis tools for predicting radar system performance are: 1) the Propagation Conditions Summary and 2) the Coverage Display.

a. *Integrated Refractive Effects Prediction System.*

In free space, an electromagnetic wave will travel in a straight line because the index of refraction is the same everywhere (Patterson, 1988, pg 15). In 1925, the International Commission for Aeronavigation defined the "international standard atmosphere." This hypothetical atmosphere had an arbitrarily selected set of characteristics reflecting an average condition of the real atmosphere. Non-standard variations in temperature in the lower atmosphere causes the propagated wave to become

distorted. The distortion can result in reduced or increased detection ranges and it can also result in holes in coverage. The objective of IREPS is to provide a near-real-time assessment of the effects of the lower atmosphere on a wide variety of EM systems. The inputs to the model measurements of on-scene data of the lower atmosphere are collected by either balloon-borne radiosonde, aircraft-borne microwave refractometer, or near-surface measurements (Hitney and Richter, 1975, pg 376). Additionally, data on the particular sensor being modeled will be input, in this case data from the radar at NPS. Once all inputs are provided the outputs are in the form of easy-to-interpret displays that can be used to develop a basic understanding of the radar capabilities and limitations.

The IREPS program will model the sensor propagation resulting from standard or non-standard propagation conditions (Patterson, 1988, pg 14). Generalities of anticipated weather can be determined from climatological data. Due to variations, and their effects on radar performance, specific weather/radiosonde information should be obtained from either the sources listed in the previous paragraph or the user's weather support unit. The major atmospheric area of interest for IREPS is the troposphere which extends from the earth's surface to 8 kilometers above the earth at polar latitudes or 18 kilometers at equatorial latitudes.

The effects from the atmosphere that impact radar performance are mainly through the processes of refraction, reflection, absorption, and scattering of radiated energy. The effects of refraction and reflection from the ionosphere and the effects of atmospheric absorption are negligible at the frequencies between 0.1 to 20 GHz; therefore, these effects are not considered by IREPS. There are four basic

atmospheric conditions which are of interest, and they are normal, subrefraction, superrefraction, and trapping.

- Normal propagation conditions. The bending or refraction of electromagnetic energy as it passes through the air occurs because of the structure of the troposphere. Since the density of the troposphere decreases with altitude, the top of an electromagnetic wave transmitted at low elevation angles travels faster than the bottom of the wave. During normal conditions, refractivity predictably decreases as altitude increases. The result is a downward bending of the wave front.

- Subrefraction. Subrefraction occurs when air at higher altitudes is more dense than the air below it. The resulting propagation path will curve upward with reference to a straight line and upward relative to the earth's surface. Radar ranges and clutter are significantly reduced.

- Superrefraction. Radar signal path curves downward more sharply than "normal" refraction but not as much as the curvature of the earth. Radar detection ranges, clutter and echo intensity will increase, resulting in higher false target data counts. Search performance, especially against small targets, may be degraded if clutter increases significantly.

- Trapping or Ducting. The propagation path curves sharply downward, equal to or greater than the earth's curvature. Radar ranges can be greatly extended or holes in coverage may occur. In addition, ground clutter may increase significantly. Search performance may be degraded due to increased false target rates.

From 7-10 May 1991, a survey was conducted using six shore stations and one "at-sea" platform to determine the degree of refractive changes caused by the lower tropospheric variability along the California coast. The survey consisted of radiosonde (vertical profile of the troposphere in terms of barometric pressure, temperature, and relative humidity) data collections and various other tests. One of the stations taking part in the survey was the Naval Postgraduate School. The radiosonde data collected at the NPS site was obtained and will be used in this thesis to perform the atmospheric analysis. Table IV contains the 7 May 1991 NPS radiosonde data entered

TABLE VI IREPS ENVIRONMENTAL DATA LIST

```
IREPS PC-2.00                                              PAGE 1 OF 2
                   **** ENVIRONMENTAL DATA LIST ****

LOCATION: NPS                        EVAPORATION DUCT PARAMETERS:
DATE/TIME: 7 MAY 91 23:27 GMT          SEA TEMPERATURE= 11.7 deg C
TRUE WIND SPEED=  4.1 m/sec            AIR TEMPERATURE= 18.5 deg C
SURFACE PRESSURE= 1012.5 MB          RELATIVE HUMIDITY=  68.0 PERCENT
RADIOSONDE LAUNCH HEIGHT=   9.1 M    EVAPORATION DUCT HEIGHT=   9.5 M


      PRESS  TEMP   RH   DEW PT
LEVEL (MB)   (C)   (%)  DEP(C)  METERS  N UNITS  N/KM  M UNITS  CONDITION
  1   969.1  16.0  84.0   2.7   302.5   328.3    -14.5  388.3   NORMAL
  2   967.1  15.9  84.0   2.7   400.1   327.5     19.9  390.3   SUB
  3   966.5  15.8  85.0   2.5   405.3   327.8   -114.2  391.4   TRAP
  4   958.0  15.7  53.0   9.5   480.5   299.7    -13.4  375.1   NORMAL
  5   892.0  16.3  41.0  13.4  1087.2   273.0    -13.3  443.6   NORMAL
  6   871.0  15.7  30.0  14.4  1201.8   264.5    -18.6  465.7   NORMAL
  7   870.5  15.6  30.0  14.4  1294.4   264.1    -22.6  467.3   NORMAL
  8   861.8  15.6  33.0  16.3  1379.6   257.8    -25.3  474.3   SUPER
  9   851.6  15.4  26.0  19.5  1480.5   249.4     -8.2  481.8   NORMAL
 10   850.3  15.4  26.0  19.5  1493.5   249.1     14.8  483.5   SUB
 11   834.7  14.7  42.0  12.9  1650.2   256.7     -9.0  515.7   NORMAL
```

into IREPS to illustrate the type of data obtained from the radiosonde launch.

The complete listing of the raw radiosonde data collected on 7 May 1991 is contained in Appendix C. Additionally, all of the radiosonde data collected during this time period was plotted and included as Appendix D. The plots are in altitude versus temperature and temperature dew point. The IREPS program will only accept 28 entries in the environmental data list. Therefore, the 200+ raw radiosonde data points shown in Appendix C for the 7 May 1991 and 10 May 1991 had to be reduced by the author. This was done by selecting "significant levels" based on deviations in humidity of 3

percent and in temperature of 0.5° C while preserving regions of strong gradient in either humidity or temperature. The reduced data was then entered into the IREPS environmental data base. The two data listings (7 and 10 May) were selected based on the plots contained in Appendix D. The selection was made to provide one data set of fairly "normal" conditions and another that contained a surface based duct to illustrate different atmospheric conditions. Once the environmental data list and the radar parameters have been entered into the IREPS program various analyses can be performed to determine the theoretical radar system performance. The atmospheric analysis in this thesis will be performed using the Propagation Conditions Summary and the Coverage Display.

(1)   *Propagation Conditions Summary.* Figures 22 and 23 are the Propagation Condition Summaries based on data collected from radiosonde launch data (discussed above) from the NPS on 7 and 10 May 1991. The Propagation Conditions Summary is a plot of altitude versus refractivity (discussed in section B.1.a Refraction). It provides a visual representation of the existing refractive conditions for the time and location of the environmental data entered. The vertical column to the right of the plot shown in Figure 22, uses a black bar to indicate the presence and the vertical extent, or height, of any ducts. Additionally, a text summary of conditions in plain-language of the expected effects for the three categories of propagation (surface-to-surface, surface-to-air, and air-to-air) are also shown to the left on Figure 22.

The propagation summary for the 7 May data (Figure 22) shows the presence of a duct at approximately 270 meters to 480 meters. While the plot

56
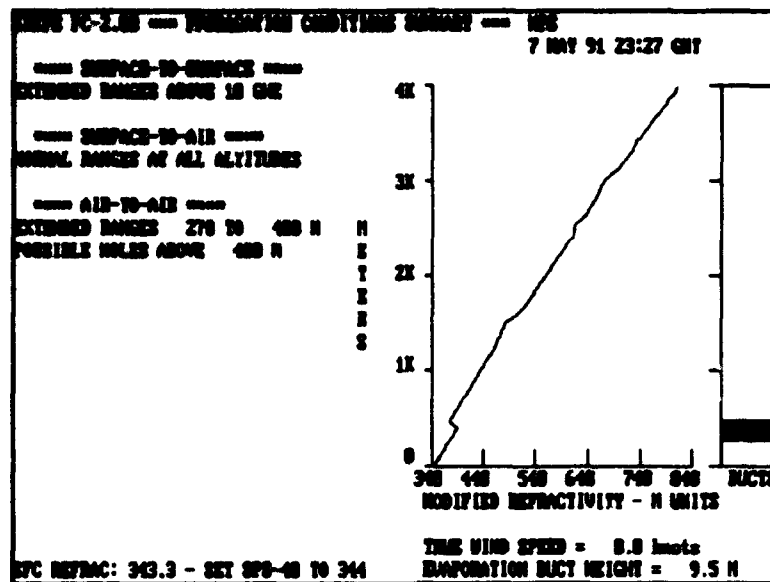
Figure 22 Propagation Summary (7 May)
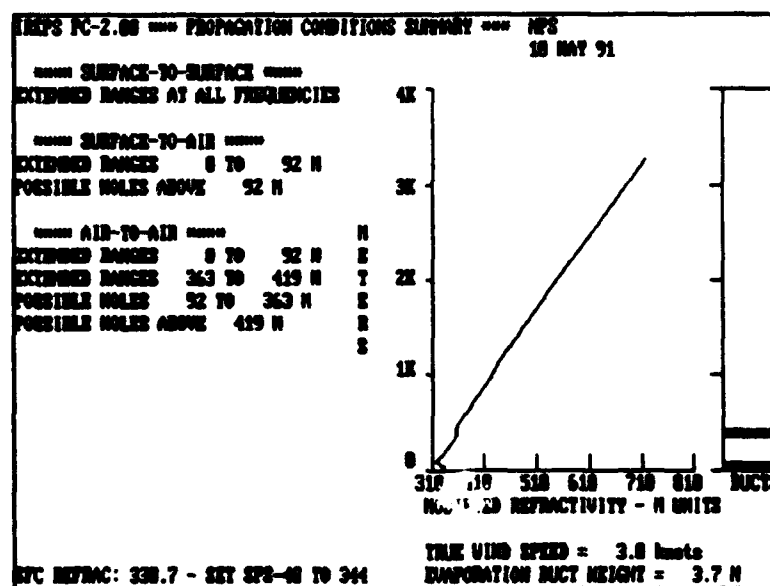
Figure 23 Propagation Summary (10 May)

57

illustrates the location of the duct, the approximate location can also be obtained from the air-to-air extended ranges text on the left side of the figure. From the text on the left of the figure we can note that the position and extent of this duct is expected to cause surface-to-surface radar ranges to be extended if the frequency of the radar is above 10 GHz. The surface-to-air radar coverage is expected to be normal and the air-to-air coverage is expected to have extended ranges at 270 to 480 meters with possible holes in coverage above 480 meters. Therefore, the impact of these conditions on the AN/UPS-1 system's performance is negligible according to the surface-to-surface and surface-to-air predictions noted on Figure 22.

The position and extent of the ducts for the 10 May data (Figure 23), on the other hand, are different and yield significantly different results. There are two ducts shown and they are positioned from 0 (surface-based) to 92 meters and from 363 to 419 meters. As shown on the left of Figure 23, the surface based duct is causing the surface-to-surface radar coverage to be extended at all frequencies and the surface-to-air coverage is expected to be extended from the surface to 92 meters with possible holes in coverage above 92 and 419 meters. These predictions (extended ranges and possible holes) of radar coverage represent a significant impact in to the performance of the AN/UPS-1 radar at NPS on the 10th of May. The 7 and 10 May radiosonde data, summarized and illustrated in the Propagation Conditions Summary, is then used to create the Coverage Displays which are side view depictions of the NPS radar coverage.

(2)   Coverage Display.   The Coverage Displays, Figures 24 and 25, are two dimensional side views of the predicted radar coverage overlaid on a height versus range scale.   The primary use of the Coverage Display is for long range air-search radars, surface-based or airborne, and surface-search radars when employed against low-flying air targets (Patterson, 1988, pg 92).   The color coded shading on the coverage diagram is very useful in describing the actual target detection regions based on various detection ranges.   The color coded detection ranges, correspond to variances in free-space detection ranges (25, 50, 75, and 100 nmi), are based on changes in the variables in the radar range equation (equation 1) such as radar cross-section, antenna gain, or transmitter power.

The Coverage Displays were created by inputing the 7 and 10 May radiosonde data, used to produce the Propagation Conditions Summaries, and the AN/UPS-1 radar system parameters.   The AN/UPS-1 radar system parameters (Tables I and II) that were entered into the IREPS program are displayed on the right of the diagrams (Figures 24 and 25).   The Coverage Displays are produced with selectable height and range limits; the author selected the height and range limits of 30,000 ft and 150 nmi respectively.   The color coded free-space ranges were chosen for purposes of this thesis, such as, the 100 nmi free-space detection range coincides with the baseline performance of Chapter II.

Figure 25 illustrates the effects discussed for the 10 May Propagation Conditions Summary.   The figure shows the extended range (the 100 nmi free-space range extends beyond the maximum range) at low altitudes as predicted by the

59
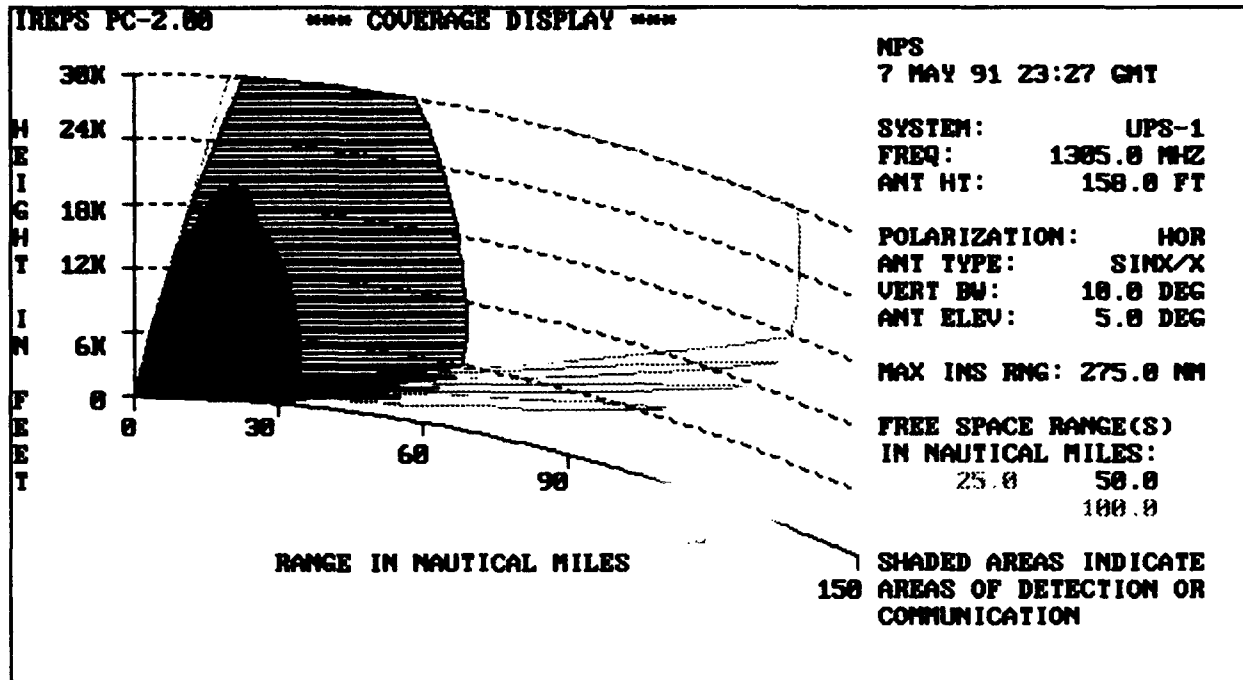
Figure 24 IREPS Coverage Display (7 May 1991)
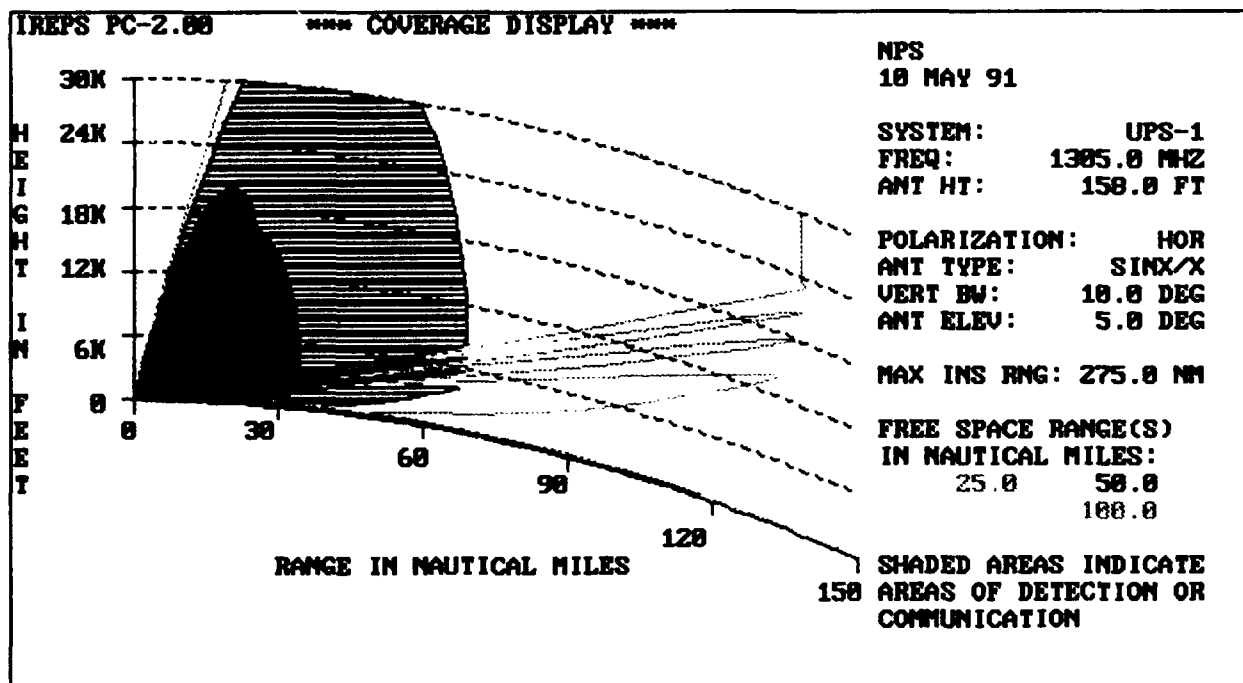
Figure 25 IREPS Coverage Display (10 May 1991)

Propagation Conditions Summary. Additionally, the possible "holes" are shown by thewidening of the nulls producing broader areas of non-detection. The effect not discussed by the Propagation Conditions Summary and shown on the figure is the bending of the lobes upward. The positions have changed entirely; the first lobe is where the second used to be and the first null is where the third lobe appeared in Figure 25. The lobes are also extended. Looking at the 100nmi free-space range, the first lobe in Figure 24 extends to approximately 110 nmi while in Figure 25 the first lobe extends to 135 nmi. The extended ranges, repositioning of the nulls and lobes, changing the width of lobes and nulls, and the low-level detection to maximum range all result in a decidedly different coverage in Figure 25 than was depicted in Figure 24. The differences in these figures illustrate the necessity for accurate and timely atmospheric data if accurate theoretical coverage predictions are to be made. While the atmospheric data that was used to create these diagrams were collected two days apart, the change from "normal" to anomalous propagation may be separated by a few hours and may have more of an impact on radar performance than has been presented here. Additionally, the Coverage Diagrams produced by the IREPS program are produced using only the basic radar system data listed on the right side of the diagram. The EREPS program, on the other hand, uses more precise/indepth radar system characteristics, but is only capable of utilizing averaged atmospheric data rather than actual radiosonde data as used by IREPS. Therefore, EREPS produces an averaged estimate of theoretical radar system coverage.

61

b. Engineer's Refractive Effects Prediction System.

The EREPS program will produce a two dimensional view of radar coverage similar to the Coverage Display produced by IREPS. The radar system characteristics that are entered into the EREPS program are much more detailed than the characteristics entered into the IREPS program. The detailed radar system characteristics allow the user to vary radar system parameters and observe the effects on the predicted radar coverage. The detailed radar system characteristics used to produce the EREPS coverage displays (Figures 26-29) are the AN/UPS-1 radar system characteristics obtained from Tables I and II. The detailed radar system characteristics input into EREPS are shown on the right side of the figures (same as the IREPS diagram).

Figures 26 and 27 are the predicted radar coverage during "normal" propagation conditions but with different antenna heights. Figure 26 illustrates the predicted radar coverage if the AN/UPS-1 system's antenna is located 158 feet above the reflective surface (such as the NPS system). Figure 27 illustrates the predicted radar coverage if the AN/UPS-1 system's antenna is at its nominally deployed height of 15 feet. The figures show the significant difference in radar coverage if the antenna height is changed. The high-sited radar system as discussed earlier in this thesis will produce fine grained lobing compared to the low-sited radar system. While the detection range for both systems is approximately 90 nmi, for an inbound aircraft at 11,000 ft, the aircraft on the high-sited (Figure 26) radar's display will appear and disappear from scan-to-scan. The radar will then maintain constant detection when the inbound aircraft is approximately 76 nmi from the radar. The aircraft detection for the low-sited radar, on

FREQ	MHz	1385
POLARIZATION		HOR
RADR HT	ft	158
ANT TYPE		SINX/X
VER BW	deg	10
ELEV ANG	deg	5
PK POW	kW	1400
P WIDTH	us	4.2
ANT GN	dBi	27
SYS LOSS	dB	8
REC NF	dB	9
HOR BW	deg	3.0
PRF	Hz	267
SCAN RT	rpm	15
RCS	sqm	.4
PD		0.5
PFA		1.0E-8
SW CASE		0-STDY
FS RANGE	nmi	63.0
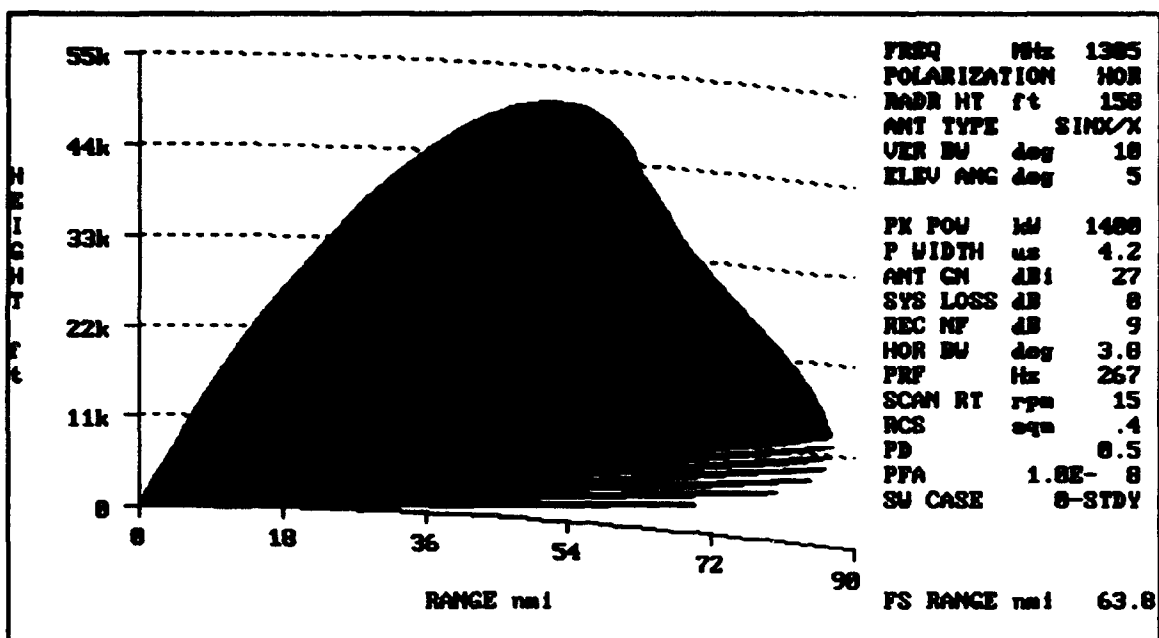
Figure 26 EREPS Coverage Display ("normal" propagation conditions and antenna height of 158 ft)

FREQ	MHz	1385
POLARIZATION		HOR
RADR HT	ft	15
ANT TYPE		SINX/X
VER BW	deg	10
ELEV ANG	deg	5
PK POW	kW	1400
P WIDTH	us	4.2
ANT GN	dBi	27
SYS LOSS	dB	8
REC NF	dB	9
HOR BW	deg	3.0
PRF	Hz	267
SCAN RT	rpm	15
RCS	sqm	.4
PD		0.5
PFA		1.0E-8
SW CASE		0-STDY
FS RANGE	nmi	63.0
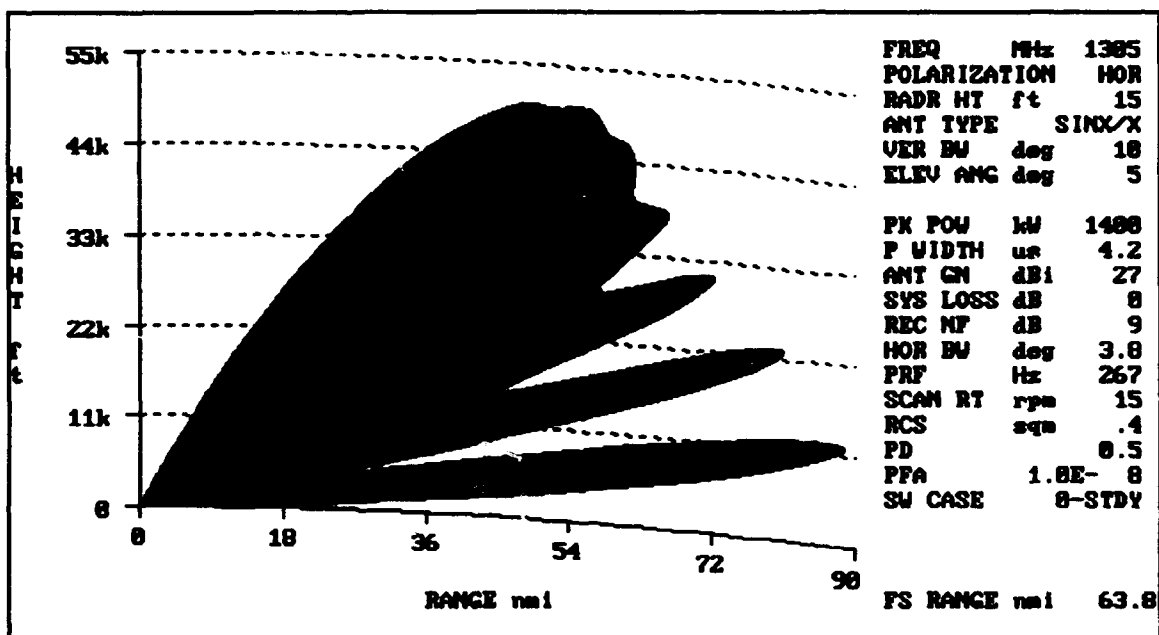
Figure 27 EREPS Coverage Display ("normal" propagation conditions and antenna height of 15 ft)

63

the other hand, will disappear for several scans. This can be seen on Figure 27; for an inbound aircraft at 11,000 ft, the first null starts at 72 nmi and ends at approximately 50 nmi. This represents a 22 nmi gap in radar coverage. Constant detection doesn't occur until the aircraft has closed to 50 nmi from the radar. Figures 26 and 27 demonstrate the significant effect antenna height has on radar coverage during "normal" propagation conditions. Figures 28 and 29 contain the same radar characteristics as the previous figures; however, the propagation conditions are no longer "normal". A surface based duct condition exists to illustrate the effects of the atmosphere.

Figures 28 and 29 illustrate the effects of a surface based duct given two different antenna heights. The antenna heights will affect the thickness of the extended range duct. Figure 28 (antenna height of 158 ft) shows low-level detection is possible out to 150 nmi for altitudes up to 2,000 ft. Figure 29 (antenna height of 15 ft) shows low-level detection is possible to slightly beyond 120 nmi, but the altitude is approximately 1,000 ft which is significantly less than Figure 28. Additionally, comparing the predicted coverage for the low-sited radars with and without a surface based duct (Figures 27 and 29), it is notable that the 90 nmi detection range for an inbound aircraft at 11,000 ft in Figure 27 has been reduced to approximately 52 nmi in Figure 29. This significant reduction in range (38 nmi) is attributed only to a change in the atmospheric conditions. In addition to the significant impact on detection ranges, the presence of a surface based duct can degrade radar performance in many other ways (not addressed in this thesis) such as an increase in clutter, errors in radar height reporting, and increased vulnerability to jamming at lower altitudes.
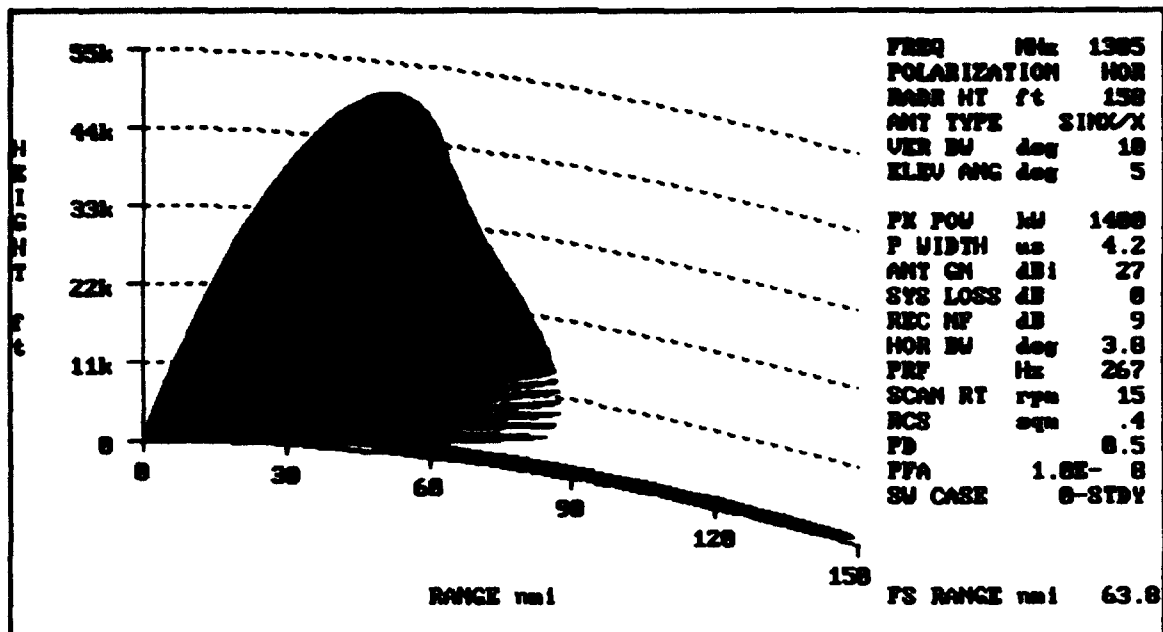
Figure 28 EREPS Coverage Display (surface based duct propagation conditions and antenna height of 158 ft)
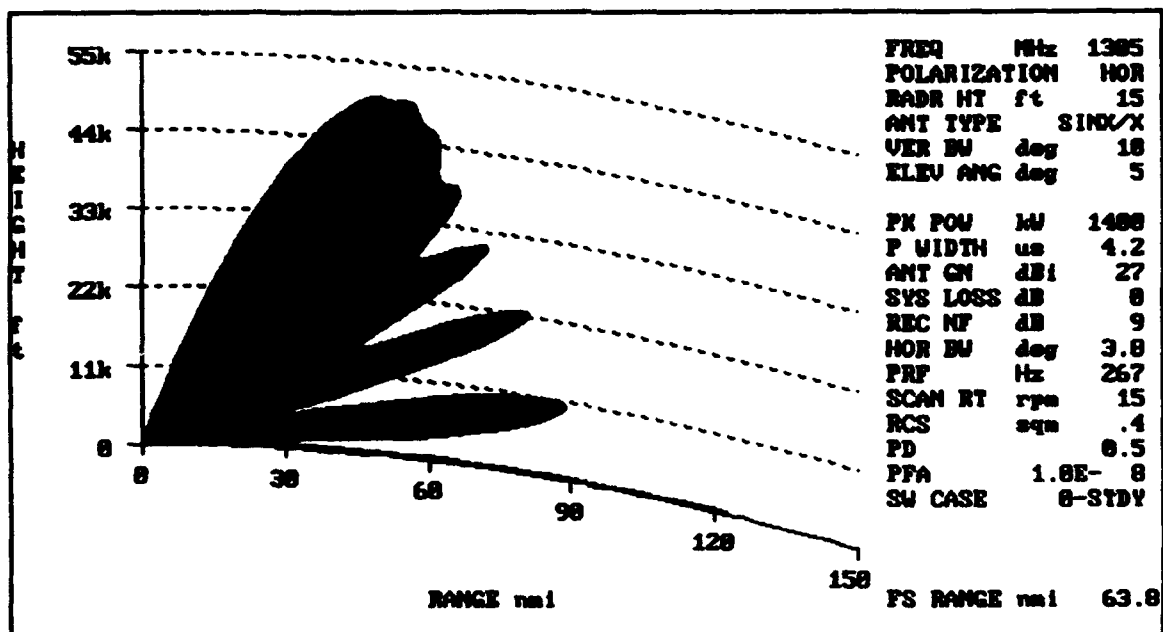
Figure 29 EREPS Coverage Display (surface based duct propagation conditions and antenna height of 15 ft)

As mentioned above, the environment in which the radar operates can significantly alter radar performance. Appendix E provides a "real world" example of the effects of the installed environment on the radar's performance. Appendix E contains reproductions of photographs of a section of a PPI (Planned Position Indicator, i.e., radar display). The Appendix illustrates the significant effects of the installed environment on radar performance.

IV. SUMMARY AND CONCLUSIONS

The ground based radar system's performance is often modeled by contractors, operators, mission planners, and radar modeling software in terms of the radar system's baseline performance. This thesis has shown the baseline performance, based solely on the radar system's internal characteristics, is a simplistic and inaccurate estimate of the capabilities and limitations of the radar system. To serve as an example of how the baseline performance can be calculated, the baseline performance was calculated for the AN/UPS-1 at the NPS. From this example, the baseline performance for the radar system at NPS was determined to be 100 nmi for a 6 dBsm target. This 100 nmi detection range for the baseline performance served as a reference for comparison with the theoretical performance.

The theoretical radar system performance ("best estimate" of actual radar performance), as discussed in Chapter III, can only be determined by considering the effects due to the surrounding terrain and the atmosphere through which the propagating radar wave travels. The effects of the terrain on the radar propagation was shown to be significantly altered by several key variables:

- K-Factor. The K-factor is the amount the radar wave bends as it propagates. The amount of bending will determine the distance, and path, the propagated wave will travel before it strikes the surface of the earth or the target.

- Fresnel Zones. The fresnel zones are the areas on the surface of the earth where reflections from the radar will occur. The reflections from the odd numbered

fresnel zones will create the lobes in the radar coverage envelope. The reflections from the even numbered fresnel zones will create the nulls in the radar coverage envelope.

- **Roughness Criterion.** The roughness of the surface of the earth within the defined fresnel zone will determine the depth of the nulls, or the enhancement of the lobes, within the radar coverage envelope. The determination of the amount of deviation necessary for the area to be considered rough is a function of grazing angle, radar frequency, and change in terrain height. If the surface is considered rough the depth of the nulls, or the enhancement of the lobe, will be reduced.

- **Screening.** The radar will not detect targets in areas masked by terrain, or screened. The AGL diagrams were used to determine the screened areas, and those areas where detection will occur, for a terrain following aircraft. The RLS diagrams were used to determine the screened areas, and areas of detection, for a aircraft flying at a constant altitude.

- **Antenna Height.** The antenna height will determine the number of lobes and nulls, the distance between the lobes and nulls (i.e., fine grain lobing is indicative of high sited radars), and the general shape of the radar coverage envelope. The extent of low-level radar coverage is determined by the height of the radar antenna.

- **Antenna Tilt.** The antenna tilt angle will impact the depth of the nulls, amount of improved range in the lobes, and the general shape of the radar coverage envelope. Antenna tilt will also determine the extent of low-level radar coverage.

The terrain effects due to these variables were demonstrated by applying them to the AN/UPS-1 at NPS. The effects of the terrain were shown to significantly degrade the predicted performance of the radar at NPS.

The effects due to the atmosphere were then considered and analyzed for the AN/UPS-1 at NPS. Actual atmospheric radiosonde data from the NPS location was used with the IREPS and EREPS programs to illustrate the methods, and impact, of the atmosphere on radar performance. The effect of the atmosphere on radar propagation can vary day-to-day as illustrated by the variance from the 7 May 1991 to 10 May 1991 radiosonde data and coverage displays. The impact of the atmosphere was illustrated

68

with the NPS data and siting parameters. The impact of atmospheric and terrain factors on radar performance will provide a greater understanding of the capabilities and limitations of the ground based radar system. This understanding will enhance the ability of the warfighter in determining the expected area of coverage for the ground radar system and thus how it effects the mission.

The understanding of the capabilities and limitations of the radar system enables the radar users to understand the anomalies in the radar's performance. For instance, if a surface-based duct existed, extended low-level detections and possible increased ground clutter would be expected. When reduced radar detections occur due to changes in the atmosphere, the operator would understand and expect these anomalies and therefore not consider the degradation as a hardware or maintenance problem. Additionally, if the radar is experiencing degraded performance due to surface reflections the cause of the degraded performance can be identified. Once the particular cause of degraded performance is identified, corrective actions may be feasible, for example smoothing or roughening the terrain from where specific reflections occur. Understanding the capabilities and limitations of the radar system will significantly affect the operation and maintenance of a radar system. Taking a different perspective, understanding the capabilities and limitation of the enemy's radar system provides the attacker an advantage.

The understanding of the theoretical performance of a radar system can significantly alter the positioning of attack and ECM aircraft. Prediction of the theoretical performance of the radar system will enable the attacker to optimally position

attack or ECM aircraft based on current atmospheric conditions. For example, Figure 30 (Patterson, 1988, pg 92) illustrates the optimum positioning of attack and ECM aircraft given "normal" propagation conditions. The "standard" procedure, as illustrated, for attack aircraft in penetrating an enemy's defenses is to fly low to remain beneath the radar coverage (i.e., screened or terrain masked). The optimum azimuth for this procedure can be determined by using the information contained in the AGL and RLS diagrams. Additionally, the optimum position, using the "standard" procedure, for ECM aircraft would be to position the ECM aircraft at higher altitudes within the range of the jamming capabilities of the jammer. These assumptions are valid only during "normal" or non-ducting conditions. For surface-based ducting conditions however, the enemy is given a greater detection range capability for targets flying within the duct than for a target at higher altitudes. Knowledge of the existence and height of a surface-based duct would enable the attack aircraft to select the optimum altitude for penetration. Figure 31 (Patterson, 1988, pg 93) shows the optimum placement for attack and ECM aircraft when a surface-based duct is present. The placement of the attack and ECM aircraft can be significantly different when a surface-based duct is present as shown by comparing Figures 30 and 31.

The optimum placement of the ECM aircraft is done to maximize the effectiveness of its jammers. By positioning the ECM aircraft in a radar lobe, or within the surface based duct, its jamming effects will be significantly enhanced and its standoff range will be greatly extended. The enhanced jamming effects and increased standoff range are
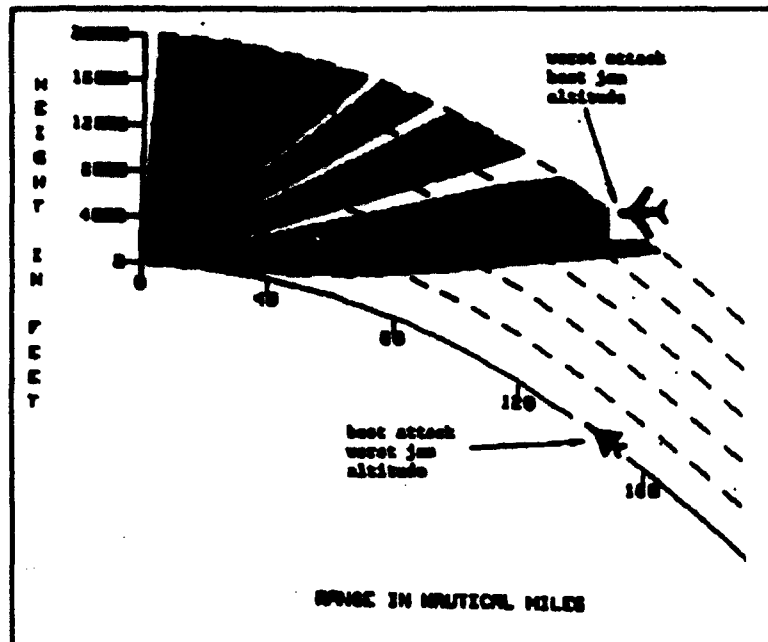
Figure 30 Optimum Position of Attack and ECM Aircraft ("normal" propagation conditions)
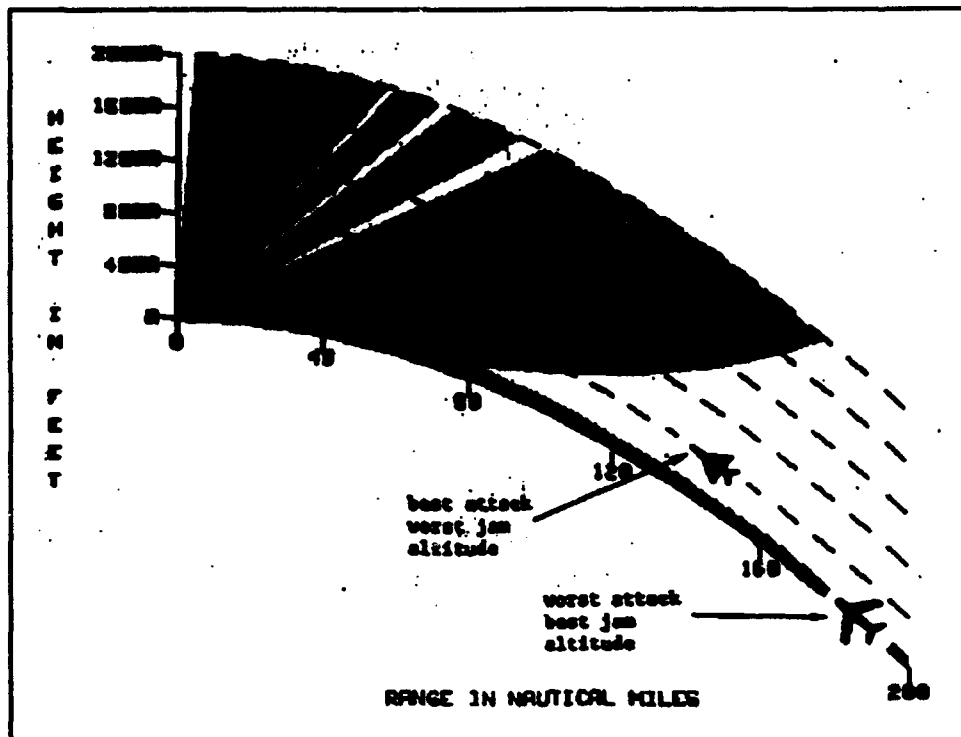
Figure 31 Optimum Position of Attack and ECM Aircraft (surface based duct present)

71

demonstrated in Figure 32 (Patterson, 1988, pg 95). The figure is a reproduction of two

photos taken of a radar's scope while being jammed by a EA-6B flying above, and in,

a surface-based duct. The figure shows the significantly enhanced jamming (multiple

strobes at various azimuths) capability of the EA-6B flying in the surface-based duct.

EA-6B POSITIONED 26 NMI FROM RADAR   EA-6B POSITIONED 55 NMI FROM THE RADAR
ABOVE THE SURFACE-BASED DUCT AT 13,000 FT   INSIDE THE SURFACE-BASED DUCT AT 500 FT
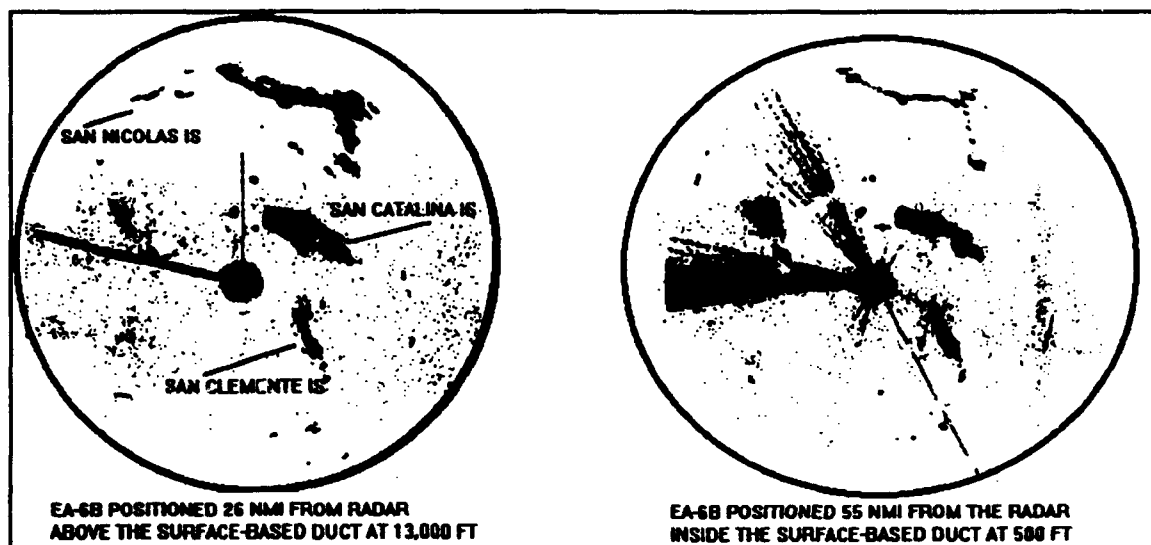
Figure 32 Photographs of Radar Scope with EA-6B Jamming

As demonstrated in this thesis, the actual radar performance can be significantly

altered due to its installed environment. The baseline radar system performance is often

not an adequate prediction of radar performance. The theoretical radar system approach

should be taken to determine the capabilities and limitations of the ground based sensor.

The effects from the terrain and atmosphere on the radar coverage are major concerns

and must be included in any realistic determination of radar performance. From an air-

defense perspective the areas of non-coverage, or radar system limitations, should be

72

understood and compensated for by either additional resources or procedures. From the attacker's perspective, knowledge of the capabilities and limitations of the enemy's radar system may be of vital importance to determining the optimum position of the attacking aircraft.

LIST OF REFERENCES

Department of Transportation Federal Aviation Administration Primary/Secondary En Route Radar Siting Handbook, FAA ORDER 6340.15, May 1983.

Freeman, R. L. , Telecommunication Transmission Handbook, 3rd ed., 1991

Eaves, J. L. and Reedy, E. K., Principles of Modern Radar, Van Nostrand Reinhold, 1987.

Barton, D. K., Modern Radar System Analysis, Artech House Inc., 1988.

Radio Corporation of America, Technical Manual for Radar Set AN/UPS-1 and AN/UPS-1A, Department of the Navy, Bureau of Ships, 1 July 1963.

Kingsley, S. P. and Quegan, S., Understanding Radar Systems, McGraw-Hill Book Company, 1992.

Herbert V. Hitney and Juergen H. Richter, Atmospheric Effects on Radar Target Identification and Imaging, Proceedings of the NATO Advanced Study Institute held in Goslar/Harz, F.R.G., September 22- October 3, 1975.

Patterson, W. L., Effective Use of the Electromagnetic Products of TESS and IREPS, Technical Document 1369, Naval Ocean Systems Center, October 1988.

Patterson, W. L., Engineer's Refractive Effects Prediction System (EREPS) Revision 2.0, Technical Document 1342, Naval Ocean Systems Center, February 1990.

Berry, J. B., Radiowave Propagation for Communications System Engineering, George Washington University, 1990.

Angelokos, D. J., and Everhart, T. E., Microwave Communications, McGraw-Hill Book Company, 1968.

Air Force Communications Command, Evaluation of AM/SSBSC Systems, AFCC Systems Evaluation School, March 1986.

Connor, J., Electromagnetic Compatibility Analysis Center, Annapolis MD, 3 March 1994 Facsimile.

Davidson, K., Naval Postgraduate School Meteorology Department, Interview 2 February 1994.

Estebo, G. , 84th RADES Hill AFB UT, 2 February 1994 Facsimile.

APPENDIX A

RAW NULL POSITION DATA
(Obtained from 84 RADES letter 24 January 1994)

Lobing Study

Site Name: NPS, CA

Focal Point Elevation: 158   ft
Reflective Surface Elevation: 1.00   ft
Radar Frequency: 1305.0 MHz
K-Factor: 1.350
Average Screening Angle: -2.0000 degrees

The 1st null forms immediately above the horizon
and intersects 6000 ft at 111.19 nm

Lobe No.		Reflective Dist NM	Gamma Radians	Degrees								
LOBE	1	8.85	-0.000306	-0.017537	; theoret. rng at	6000	ft	is	95.88	nm
NULL	2	6.63	0.001273	0.072959	; theoret. rng at	6000	ft	is	88.73	nm
LOBE	2	5.26	0.002662	0.152538	; theoret. rng at	6000	ft	is	82.90	nm
NULL	3	4.32	0.003971	0.227497	; theoret. rng at	6000	ft	is	77.81	nm
LOBE	3	3.65	0.005237	0.300030	; theoret. rng at	6000	ft	is	73.23	nm
NULL	4	3.15	0.006477	0.371125	; theoret. rng at	5000	ft	is	69.06	nm
LOBE	4	2.76	0.007702	0.441299	; theoret. rng at	6000	ft	is	65.25	nm
NULL	5	2.45	0.008916	0.510844	; theoret. rng at	6000	ft	is	61.75	nm
LOBE	5	2.21	0.010122	0.579938	; theoret. rng at	6000	ft	is	58.52	nm
NULL	6	2.01	0.011322	0.648697	; theoret. rng at	6000	ft	is	55.55	nm
LOBE	6	1.84	0.012517	0.717200	; theoret. rng at	6000	ft	is	52.80	nm
NULL	7	1.69	0.013710	0.785500	; theoret. rng at	6000	ft	is	50.27	nm
LOBE	7	1.57	0.014899	0.853638	; theoret. rng at	6000	ft	is	47.92	nm
NULL	8	1.46	0.016086	0.921643	; theoret. rng at	6000	ft	is	45.75	nm
LOBE	8	1.37	0.017271	0.989537	; theoret. rng at	6000	ft	is	43.73	nm
NULL	9	1.29	0.018454	1.057339	; theoret. rng at	6000	ft	is	41.86	nm
LOBE	9	1.21	0.019636	1.125061	; theoret. rng at	6000	ft	is	40.13	nm
NULL	10	1.15	0.020817	1.192715	; theoret. rng at	6000	ft	is	38.51	nm
LOBE	10	1.09	0.021997	1.260311	; theoret. rng at	6000	ft	is	37.00	nm
NULL	11	1.04	0.023175	1.327855	; theoret. rng at	6000	ft	is	35.59	nm

Lobing Study

Site Name: NPS, CA

Focal Point Elevation: 158   ft
Reflective Surface Elevation: 1.00   ft
Radar Frequency: 1305.0 MHz
K-Factor: 1.350
Average Screening Angle: -2.0000 degrees

The 1st null forms immediately above the horizon
and intersects 11000 ft at 145.08 nm

		Reflective	G a m m a	
Lobe No.		Dist NM	Radians	Degrees
LOBE	1	8.93	-0.000259	-0.014828 ; theoret. rng at 11000 ft is 129.87 nm
NULL	2	6.71	0.001339	0.076713 ; theoret. rng at 11000 ft is 122.61 nm
LOBE	2	5.32	0.002742	0.157094 ; theoret. rng at 11000 ft is 116.58 nm
NULL	3	4.38	0.004062	0.232759 ; theoret. rng at 11000 ft is 111.20 nm
LOBE	3	3.69	0.005340	0.305960 ; theoret. rng at 11000 ft is 106.26 nm
NULL	4	3.19	0.006592	0.377712 ; theoret. rng at 11000 ft is 101.67 nm
LOBE	4	2.79	0.007829	0.448544 ; theoret. rng at 11000 ft is 97.38 nm
NULL	5	2.49	0.009054	0.518753 ; theoret. rng at 11000 ft is 93.35 nm
LOBE	5	2.24	0.010272	0.588524 ; theoret. rng at 11000 ft is 89.56 nm
NULL	6	2.03	0.011484	0.657972 ; theoret. rng at 11000 ft is 85.99 nm
LOBE	6	1.86	0.012692	0.727174 ; theoret. rng at 11000 ft is 82.62 nm
NULL	7	1.71	0.013896	0.796187 ; theoret. rng at 11000 ft is 79.45 nm
LOBE	7	1.59	0.015098	0.865048 ; theoret. rng at 11000 ft is 76.46 nm
NULL	8	1.48	0.016298	0.933787 ; theoret. rng at 11000 ft is 73.63 nm
LOBE	8	1.38	0.017496	1.002424 ; theoret. rng at 11000 ft is 70.97 nm
NULL	9	1.30	0.018692	1.070976 ; theoret. rng at 11000 ft is 68.45 nm
LOBE	9	1.23	0.019887	1.139457 ; theoret. rng at 11000 ft is 66.07 nm
NULL	10	1.16	0.021081	1.207877 ; theoret. rng at 11000 ft is 63.82 nm
LOBE	10	1.10	0.022275	1.276244 ; theoret. rng at 11000 ft is 61.69 nm
NULL	11	1.05	0.023467	1.344565 ; theoret. rng at 11000 ft is 59.68 nm

Lobing Study

Site Name: NPS, CA

Focal Point Elevation: 158   ft
Reflective Surface Elevation: 1.00   ft
Radar Frequency: 1305.0 MHz
K-Factor: 1.350
Average Screening Angle: -2.0000 degrees

The 1st null forms immediately above the horizon
and intersects 21000 ft at 194.55 nm

		Reflective	G a m m a										
Lobe No.		Dist NM	Radians	Degrees									
LOBE	1	8.99	-0.000222	-0.012734	;	theoret.	rng	at	21000	ft	is	179.43	nm
NULL	2	6.77	0.001388	0.079527	;	theoret.	rng	at	21000	ft	is	172.07	nm
LOBE	2	5.37	0.002800	0.160418	;	theoret.	rng	at	21000	ft	is	165.88	nm
NULL	3	4.42	0.004128	0.236508	;	theoret.	rng	at	21000	ft	is	160.27	nm
LOBE	3	3.73	0.005412	0.310092	;	theoret.	rng	at	21000	ft	is	155.05	nm
NULL	4	3.21	0.006671	0.382211	;	theoret.	rng	at	21000	ft	is	150.11	nm
LOBE	4	2.82	0.007913	0.453402	;	theoret.	rng	at	21000	ft	is	145.43	nm
NULL	5	2.51	0.009145	0.523970	;	theoret.	rng	at	21000	ft	is	140.95	nm
LOBE	5	2.25	0.010369	0.594102	;	theoret.	rng	at	21000	ft	is	136.67	nm
NULL	6	2.05	0.011588	0.663916	;	theoret.	rng	at	21000	ft	is	132.57	nm
LOBE	6	1.87	0.012802	0.733491	;	theoret.	rng	at	21000	ft	is	128.63	nm
NULL	7	1.72	0.014013	0.802881	;	theoret.	rng	at	21000	ft	is	124.86	nm
LOBE	7	1.60	0.015221	0.872126	;	theoret.	rng	at	21000	ft	is	121.25	nm
NULL	8	1.49	0.016428	0.941254	;	theoret.	rng	at	21000	ft	is	117.78	nm
LOBE	8	1.39	0.017633	1.010287	;	theoret.	rng	at	21000	ft	is	114.46	nm
NULL	9	1.31	0.018836	1.079241	;	theoret.	rng	at	21000	ft	is	111.26	nm
LOBE	9	1.24	0.020039	1.148128	;	theoret.	rng	at	21000	ft	is	108.20	nm
NULL	10	1.17	0.021240	1.216959	;	theoret.	rng	at	21000	ft	is	105.27	nm
LOBE	10	1.11	0.022440	1.285742	;	theoret.	rng	at	21000	ft	is	102.45	nm
NULL	11	1.05	0.023640	1.354483	;	theoret.	rng	at	21000	ft	is	99.74	nm

Lobing Study

Site Name: NPS, CA

Focal Point Elevation: 158   ft
Reflective Surface Elevation: 1.00   ft
Radar Frequency: 1305.0 MHz
K-Factor: 1.350
Average Screening Angle: -2.0000 degrees

The 1st null forms immediately above the horizon
and intersects 26000 ft at 214.73 nm

| | | Reflective | G a m m a | |
Lobe No.	Dist NM	Radians	Degrees	
LOBE 1	9.00	-0.000213	-0.012180	; theoret. rng at 26000 ft is 199.64 nm
NULL 2	6.78	0.001401	0.080257	; theoret. rng at 26000 ft is 192.25 nm
LOBE 2	5.38	0.002815	0.161268	; theoret. rng at 26000 ft is 186.02 nm
NULL 3	4.43	0.004144	0.237452	; theoret. rng at 26000 ft is 180.35 nm
LOBE 3	3.74	0.005430	0.311120	; theoret. rng at 26000 ft is 175.05 nm
NULL 4	3.22	0.006690	0.383315	; theoret. rng at 26000 ft is 170.02 nm
LOBE 4	2.82	0.007934	0.454581	; theoret. rng at 26000 ft is 165.22 nm
NULL 5	2.51	0.009167	0.525223	; theoret. rng at 26000 ft is 160.62 nm
LOBE 5	2.26	0.010392	0.595429	; theoret. rng at 26000 ft is 156.20 nm
NULL 6	2.05	0.011612	0.665316	; theoret. rng at 26000 ft is 151.95 nm
LOBE 6	1.88	0.012828	0.734965	; theoret. rng at 26000 ft is 147.86 nm
NULL 7	1.73	0.014040	0.804431	; theoret. rng at 26000 ft is 143.92 nm
LOBE 7	1.60	0.015250	0.873753	; theoret. rng at 26000 ft is 140.12 nm
NULL 8	1.49	0.016458	0.942959	; theoret. rng at 26000 ft is 136.46 nm
LOBE 8	1.40	0.017664	1.012071	; theoret. rng at 26000 ft is 132.94 nm
NULL 9	1.31	0.018869	1.081105	; theoret. rng at 26000 ft is 129.54 nm
LOBE 9	1.24	0.020073	1.150074	; theoret. rng at 26000 ft is 126.27 nm
NULL 10	1.17	0.021275	1.218987	; theoret. rng at 26000 ft is 123.12 nm
LOBE 10	1.11	0.022477	1.287853	; theoret. rng at 26000 ft is 120.08 nm
NULL 11	1.06	0.023678	1.356678	; theoret. rng at 26000 ft is 117.15 nm

****
    UNCLASSIFIED   24 Jan. 1994
****

79

Lobing Study

Site Name: NPS, CA

Focal Point Elevation:	158	ft
Reflective Surface Elevation:	1.00	ft
Radar Frequency:	1305.0	MHz
K-Factor:	1.350	
Average Screening Angle:	-2.0000	degrees

The 1st null forms immediately above the horizon
and intersects 31000 ft at 233.05 nm

		Reflective	G a m m a								
Lobe No.		Dist NM	Radians	Degrees							
LOBE	1	9.01	-0.000205	-0.011768	; theoret. rng at	31000	ft is	217.97	nm
NULL	2	6.79	0.001410	0.080798	; theoret. rng at	31000	ft is	210.57	nm
LOBE	2	5.39	0.002826	0.161894	; theoret. rng at	31000	ft is	204.30	nm
NULL	3	4.43	0.004156	0.238144	; theoret. rng at	31000	ft is	198.59	nm
LOBE	3	3.74	0.005443	0.311869	; theoret. rng at	31000	ft is	193.23	nm
NULL	4	3.23	0.006704	0.384117	; theoret. rng at	31000	ft is	188.13	nm
LOBE	4	2.83	0.007949	0.455433	; theoret. rng at	31000	ft is	183.25	nm
NULL	5	2.51	0.009183	0.526125	; theoret. rng at	31000	ft is	178.56	nm
LOBE	5	2.26	0.010409	0.596379	; theoret. rng at	31000	ft is	174.03	nm
NULL	6	2.05	0.011629	0.666316	; theoret. rng at	31000	ft is	169.67	nm
LOBE	6	1.88	0.012846	0.736015	; theoret. rng at	31000	ft is	165.46	nm
NULL	7	1.73	0.014059	0.805531	; theoret. rng at	31000	ft is	161.38	nm
LOBE	7	1.60	0.015270	0.874903	; theoret. rng at	31000	ft is	157.44	nm
NULL	8	1.49	0.016479	0.944161	; theoret. rng at	31000	ft is	153.64	nm
LOBE	8	1.40	0.017686	1.013325	; theoret. rng at	31000	ft is	149.96	nm
NULL	9	1.31	0.018892	1.082412	; theoret. rng at	31000	ft is	146.40	nm
LOBE	9	1.24	0.020096	1.151434	; theoret. rng at	31000	ft is	142.96	nm
NULL	10	1.17	0.021300	1.220401	; theoret. rng at	31000	ft is	139.64	nm
LOBE	10	1.11	0.022503	1.289323	; theoret. rng at	31000	ft is	136.43	nm
NULL	11	1.06	0.023705	1.358204	; theoret. rng at	31000	ft is	133.32	nm

Lobing Study

Site Name: NPS, CA

Focal Point Elevation: 158   ft
Reflective Surface Elevation: 1.00   ft
Radar Frequency: 1305.0 MHz
X-Factor: 1.350
Average Screening Angle: -2.0000 degrees

The 1st null forms immediately above the horizon
and intersects 41000 ft at 265.69 nm

	Reflective	G a m m a	
Lobe No.	Dist NM	Radians	Degrees
LOBE 1	9.03	-0.000195	-0.011183 ; theoret. rng at 41000 ft is 250.64 nm
NULL 2	6.81	0.001423	0.081560 ; theoret. rng at 41000 ft is 243.21 nm
LOBE 2	5.41	0.002841	0.162770 ; theoret. rng at 41000 ft is 236.90 nm
NULL 3	4.44	0.004173	0.239108 ; theoret. rng at 41000 ft is 231.12 nm
LOBE 3	3.75	0.005461	0.312906 ; theoret. rng at 41000 ft is 225.68 nm
NULL 4	3.23	0.006723	0.385222 ; theoret. rng at 41000 ft is 220.48 nm
LOBE 4	2.83	0.007969	0.456601 ; theoret. rng at 41000 ft is 215.48 n
NULL 5	2.52	0.009204	0.527355 ; theoret. rng at 41000 ft is 210.66 nm
LOBE 5	2.26	0.010431	0.597670 ; theoret. rng at 41000 ft is 205.98 nm
NULL 6	2.06	0.011653	0.667668 ; theoret. rng at 41000 ft is 201.45 nm
LOBE 6	1.88	0.012871	0.737428 ; theoret. rng at 41000 ft is 197.06 nm
NULL 7	1.73	0.014085	0.807007 ; theoret. rng at 41000 ft is 192.79 nm
LOBE 7	1.61	0.015297	0.876442 ; theoret. rng at 41000 ft is 188.65 nm
NULL 8	1.50	0.016507	0.945763 ; theoret. rng at 41000 ft is 184.63 nm
LOBE 8	1.40	0.017715	1.014991 ; theoret. rng at 41000 ft is 180.72 nm
NULL 9	1.32	0.018922	1.084143 ; theoret. rng at 41000 ft is 176.93 nm
LOBE 9	1.24	0.020128	1.153232 ; theoret. rng at 41000 ft is 173.24 nm
NULL 10	1.17	0.021333	1.222267 ; theoret. rng at 41000 ft is 169.66 nm
LOBE 10	1.11	0.022537	1.291256 ; theoret. rng at 41000 ft is 166.18 nm
NULL 11	1.06	0.023740	1.360205 ; theoret. rng at 41000 ft is 162.80 nm

Lobing Study

Site Name: NPS, CA

```
Focal Point Elevation:          158    ft
Reflective Surface Elevation:  1.00   ft
Radar Frequency:               1305.0 MHz
K-Factor:                      1.350
Average Screening Angle:       -2.0000 degrees
```

The 1st null forms immediately above the horizon
and intersects 46000 ft at 280.51 nm

	Lobe No.	Reflective Dist NM	Gamma Radians	Gamma Degrees						
LOBE	1	9.04	-0.000191	-0.010966	; theoret. rng at	46000 ft is	265.46 nm
NULL	2	6.81	0.001428	0.081842	; theoret. rng at	46000 ft is	258.03 nm
LOBE	2	5.41	0.002846	0.163092	; theoret. rng at	46000 ft is	251.70 nm
NULL	3	4.45	0.004179	0.239461	; theoret. rng at	46000 ft is	245.90 nm
LOBE	3	3.75	0.005468	0.313285	; theoret. rng at	46000 ft is	240.42 nm
NULL	4	3.24	0.006730	0.385623	; theoret. rng at	46000 ft is	235.19 nm
LOBE	4	2.84	0.007977	0.457024	; theoret. rng at	46000 ft is	230.15 nm
NULL	5	2.52	0.009212	0.527798	; theoret. rng at	46000 ft is	225.27 nm
LOBE	5	2.27	0.010439	0.598134	; theoret. rng at	46000 ft is	220.54 nm
NULL	6	2.06	0.011661	0.668153	; theoret. rng at	46000 ft is	215.95 nm
LOBE	6	1.88	0.012879	0.737933	; theoret. rng at	46000 ft is	211.49 nm
NULL	7	1.73	0.014094	0.807532	; theoret. rng at	46000 ft is	207.15 nm
LOBE	7	1.61	0.015306	0.876988	; theoret. rng at	46000 ft is	202.93 nm
NULL	8	1.50	0.016517	0.946330	; theoret. rng at	46000 ft is	198.83 nm
LOBE	8	1.40	0.017725	1.015580	; theoret. rng at	46000 ft is	194.83 nm
NULL	9	1.32	0.018933	1.084753	; theoret. rng at	46000 ft is	190.94 nm
LOBE	9	1.24	0.020139	1.153864	; theoret. rng at	46000 ft is	187.16 nm
NULL	10	1.17	0.021344	1.222920	; theoret. rng at	46000 ft is	183.48 nm
LOBE	10	1.11	0.022548	1.291932	; theoret. rng at	46000 ft is	179.90 nm
NULL	11	1.06	0.023752	1.360904	; theoret. rng at	46000 ft is	176.41 nm

Lobing Study

Site Name: NPS, CA

Focal Point Elevation: 158   ft
Reflective Surface Elevation: 1.00   ft
Radar Frequency: 1305.0 MHz
K-Factor: 1.350
Average Screening Angle: -2.0000 degrees

The 1st null forms immediately above the horizon
and intersects 51000 ft at 294.54 nm

		Reflective		G a m m a								
Lobe No.		Dist NM	Radians	Degrees								
LOBE	1	9.04	-0.000188	-0.010781	; theoret. rng at	51000	ft	is	279.50	nm
NULL	2	6.82	0.001433	0.082080	; theoret. rng at	51000	ft	is	272.06	nm
LOBE	2	5.41	0.002851	0.163365	; theoret. rng at	51000	ft	is	265.72	nm
NULL	3	4.45	0.004185	0.239758	; theoret. rng at	51000	ft	is	259.89	nm
LOBE	3	3.76	0.005473	0.313603	; theoret. rng at	51000	ft	is	254.39	nm
NULL	4	3.24	0.006736	0.385960	; theoret. rng at	51000	ft	is	249.13	nm
LOBE	4	2.84	0.007983	0.457378	; theoret. rng at	51000	ft	is	244.05	nm
NULL	5	2.52	0.009218	0.528169	; theoret. rng at	51000	ft	is	239.13	nm
LOBE	5	2.27	0.010446	0.598521	; theoret. rng at	51000	ft	is	234.35	nm
NULL	6	2.06	0.011669	0.668556	; theoret. rng at	51000	ft	is	229.71	nm
LOBE	6	1.88	0.012887	0.738353	; theoret. rng at	51000	ft	is	225.19	nm
NULL	7	1.73	0.014102	0.807968	; theoret. rng at	51000	ft	is	220.79	nm
LOBE	7	1.61	0.015314	0.877440	; theoret. rng at	51000	ft	is	216.50	nm
NULL	8	1.50	0.016525	0.946799	; theoret. rng at	51000	ft	is	212.32	nm
LOBE	8	1.40	0.017734	1.016065	; theoret. rng at	51000	ft	is	208.26	nm
NULL	9	1.32	0.018941	1.085256	; theoret. rng at	51000	ft	is	204.29	nm
LOBE	9	1.24	0.020148	1.154383	; theoret. rng at	51000	ft	is	200.42	nm
NULL	10	1.17	0.021353	1.223458	; theoret. rng at	51000	ft	is	196.66	nm
LOBE	10	1.11	0.022558	1.292487	; theoret. rng at	51000	ft	is	192.99	nm
NULL	11	1.06	0.023762	1.361477	; theoret. rng at	51000	ft	is	189.41	nm

End of lobing study

APPENDIX B

COMPARISON BETWEEN HIGH-SITED AND LOW-SITED RADAR
(FAA ORDER 6340.15, 1983, pg 139)
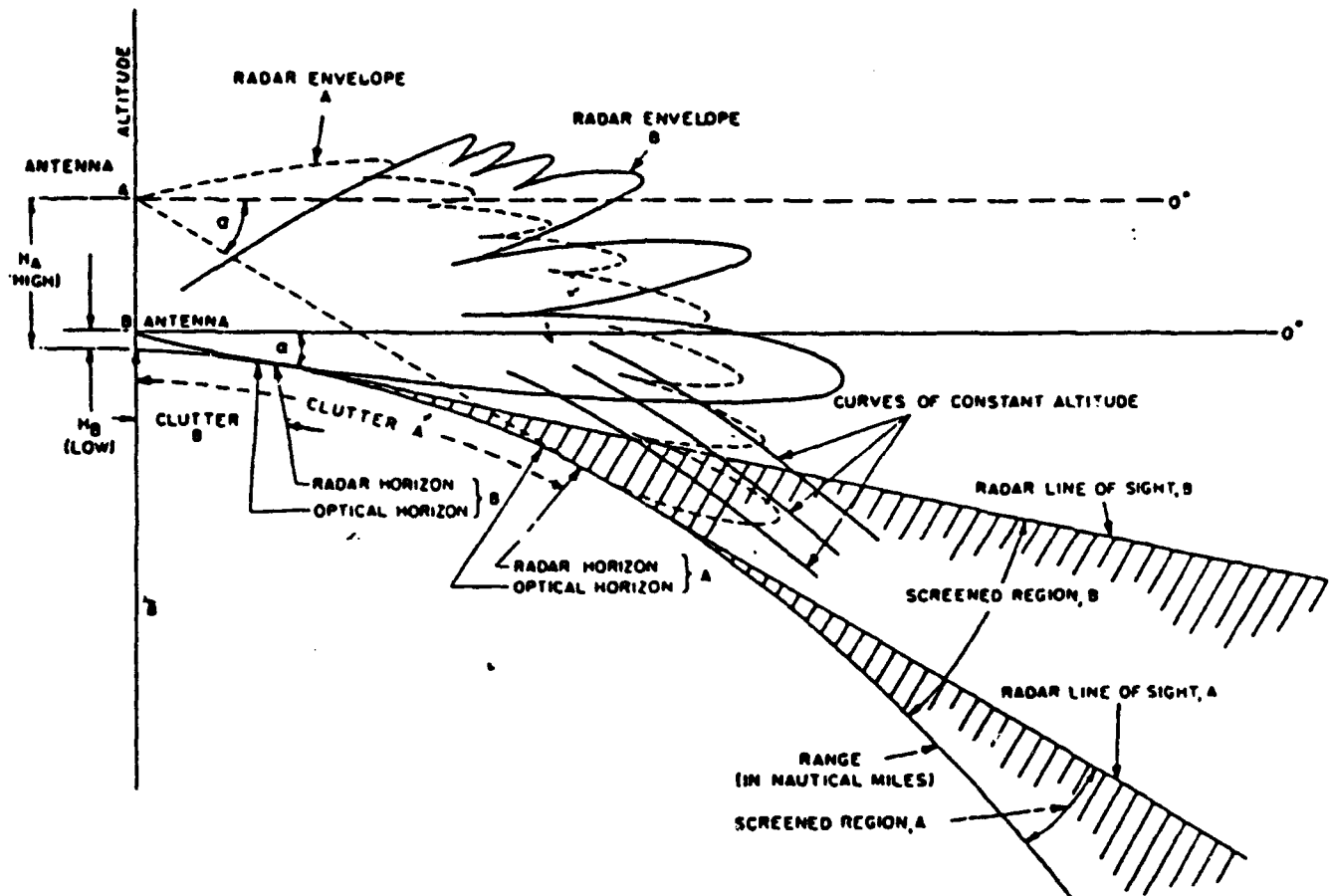
APPENDIX C

RAW NPS RADIOSONDE DATA (7 MAY 1991)
(NPS Meteorology Department, 1994)

```
Start Up Date  7 MAY 91 23:10 GMT

System test passed  -No errors found




Sounding program REV 7.10 with Omega windfinding

Station       :  72364
Location      :  36.60 N 121.90 W    30 m above mean sea level

RS-number     :  073982152

Started at:       7 MAY 91 23:27 GMT
```

Time min s	Hgt/MSL m/MSL	Pressure hPa	Temp degC	RH %	Dewp degC	RI	MRI	Hgt/MSL ft/MSL	Dir deg	Speed kts
0 0	30	1012.5	18.5	68	12.5	332	337	98	320	8.0
0 2	41	1011.2	18.4	68	12.4	332	338	135	320	8.0
0 4	52	1009.9	18.3	69	12.6	332	340	171	305	12.8
0 6	62	1008.7	18.3	69	12.6	332	341	203	305	12.8
0 8	72	1007.5	18.2	70	12.7	332	343	236	304	12.8
0 10	82	1006.3	18.1	70	12.6	331	344	269	304	12.8
0 12	93	1005.1	18.1	70	12.6	331	346	305	304	12.8
0 14	104	1003.8	18.0	71	12.7	331	348	341	304	13.0
0 16	115	1002.5	18.0	71	12.7	331	349	377	304	13.0
0 18	126	1001.2	17.9	72	12.8	331	351	413	304	13.0
0 20	137	1000.0	17.8	72	12.7	331	352	449	304	13.0
0 22	146	998.9	17.7	72	12.6	330	353	479	304	13.0
0 24	155	997.8	17.6	73	12.8	330	355	509	303	13.2
0 26	165	996.7	17.6	73	12.8	330	356	541	303	13.2
0 28	175	995.5	17.5	74	12.9	330	358	574	303	13.4
0 30	185	994.4	17.5	75	13.0	331	360	607	303	13.4
0 32	195	993.2	17.4	75	13.0	330	361	640	303	13.4
0 34	205	992.0	17.3	76	13.1	331	363	673	302	13.4
0 36	215	990.8	17.3	76	13.1	330	364	705	302	13.4
0 38	226	989.6	17.2	77	13.2	331	366	741	302	13.6
0 40	237	988.3	17.1	78	13.2	331	368	778	302	13.6
0 42	247	987.2	17.0	78	13.2	330	369	810	302	13.6
0 44	257	986.0	16.9	79	13.3	330	371	843	302	13.6
0 46	267	984.8	16.9	79	13.3	330	372	876	302	13.6
0 48	277	983.7	16.8	80	13.4	330	374	909	301	13.8
0 50	287	982.5	16.8	80	13.3	330	375	942	301	13.8
0 52	296	981.5	16.7	80	13.3	329	376	971	301	13.8
0 54	305	980.4	16.6	81	13.4	330	378	1001	301	14.0
0 56	314	979.4	16.6	81	13.4	329	379	1030	301	14.0
0 58	323	978.5	16.5	81	13.3	329	380	1060	300	14.0
1 0	331	977.5	16.5	81	13.2	329	381	1086	300	14.0
1 2	337	976.8	16.5	81	13.3	328	381	1106	300	14.0
1 4	342	976.2	16.4	82	13.4	329	383	1122	298	14.6
1 6	348	975.5	16.4	82	13.4	329	383	1142	298	14.6
1 8	354	974.8	16.3	83	13.5	329	385	1161	298	14.6
1 10	360	974.2	16.3	83	13.4	329	385	1181	298	14.6
1 12	366	973.5	16.3	83	13.5	329	386	1201	298	14.6
1 14	372	972.8	16.2	84	13.5	329	387	1220	298	14.6
1 16	378	972.2	16.2	84	13.5	329	388	1240	298	14.6
1 18	383	971.5	16.1	84	13.4	328	388	1257	298	14.6
1 20	389	970.9	16.1	84	13.4	328	389	1276	298	14.6
1 22	394	970.3	16.1	84	13.4	328	390	1293	298	14.6
1 24	399	969.7	16.0	84	13.3	328	390	1309	299	14.6
1 26	405	969.1	16.0	84	13.3	327	391	1329	299	14.6
1 28	410	968.4	15.9	84	13.2	327	391	1345	299	14.6
1 30	416	967.8	15.9	84	13.2	327	392	1365	299	14.6
1 32	422	967.1	15.9	84	13.2	327	393	1385	299	14.6
1 34	428	966.5	15.8	85	13.3	327	394	1404	299	14.4
1 36	433	965.9	15.8	84	13.2	326	394	1421	299	14.4
1 38	436	965.6	15.7	81	12.5	323	392	1430	299	14.2
1 40	439	965.2	15.7	79	12.1	322	390	1440	299	14.2
1 42	441	964.9	15.7	76	11.5	319	388	1447	299	14.2
1 44	444	964.6	15.7	73	10.9	317	386	1457	298	14.0
1 46	448	964.2	15.7	70	10.3	314	385	1470	298	14.0
1 48	453	963.6	15.6	67	9.6	311	383	1486	298	13.8
1 50	458	963.1	15.6	64	8.8	309	381	1503	298	13.8
1 52	464	962.4	15.6	62	8.4	307	380	1522	298	13.8

1	54	469	961.7	15.6	59	7.7	305	378	1539	298	13.4
1	56	476	960.9	15.6	57	7.2	303	378	1562	298	13.4
1	58	485	960.0	15.7	55	6.8	301	377	1591	298	13.2
2	0	493	959.1	15.7	53	6.2	299	377	1617	298	13.2
2	2	502	958.0	15.7	53	6.2	299	378	1647	298	13.2
2	4	511	957.0	15.6	52	5.8	298	378	1677	298	13.0
2	6	520	956.0	15.6	52	5.8	298	379	1706	298	13.0
2	8	529	955.0	15.5	52	5.8	297	380	1736	298	12.6
2	10	538	953.9	15.5	52	5.7	297	381	1765	298	12.6
2	12	546	953.0	15.4	52	5.7	297	382	1791	298	12.6
2	14	555	952.1	15.3	52	5.6	296	383	1821	298	12.2
2	16	563	951.2	15.2	52	5.5	296	384	1847	298	12.2
2	18	570	950.4	15.1	52	5.4	295	385	1870	298	11.9
2	20	578	949.5	15.1	52	-5.3	295	386	1896	298	11.9
2	22	584	948.8	15.2	51	5.2	294	386	1916	298	11.9
2	24	591	948.0	15.3	50	5.0	294	386	1939	299	11.7
2	26	598	947.3	15.3	50	5.0	293	387	1962	299	11.7
2	28	605	946.4	15.3	50	5.0	293	388	1985	301	11.3
2	30	613	945.6	15.3	50	5.0	293	389	2011	301	11.3
2	32	618	945.0	15.3	50	5.0	293	390	2028	301	11.3
2	34	623	944.5	15.3	50	5.0	293	390	2044	302	10.7
2	36	628	943.8	15.3	50	5.0	292	391	2060	302	10.7
2	38	635	943.1	15.2	50	4.9	292	392	2083	304	10.3
2	40	642	942.4	15.2	50	4.9	292	393	2106	304	10.3
2	42	650	941.5	15.1	50	4.8	292	394	2133	304	10.3
2	44	657	940.7	15.0	51	5.0	292	395	2156	306	10.1
2	46	665	939.8	14.9	51	4.9	292	396	2182	306	10.1
2	48	674	938.8	14.8	51	4.8	291	397	2211	309	9.7
2	50	683	937.8	14.7	51	4.7	291	398	2241	309	9.7
2	52	694	936.6	14.6	51	4.6	290	399	2277	309	9.7
2	54	705	935.4	14.5	51	4.5	290	401	2313	311	9.3
2	56	715	934.2	14.5	51	4.5	290	402	2346	311	9.3
2	58	726	933.0	14.4	52	4.7	290	404	2382	314	8.9
3	0	737	931.8	14.4	52	4.7	290	405	2418	314	8.9
3	2	748	930.7	14.3	52	4.6	289	407	2454	314	8.9
3	4	759	929.5	14.2	52	4.5	289	408	2490	316	8.7
3	6	769	928.3	14.3	52	4.6	288	409	2523	316	8.7
3	8	780	927.1	14.4	51	4.5	288	410	2559	319	8.4
3	10	791	925.9	14.6	51	4.6	287	412	2595	319	8.4
3	12	801	924.8	14.7	51	4.7	287	413	2628	319	8.4
3	14	812	923.6	14.8	50	4.5	286	414	2664	320	8.2
3	16	822	922.5	15.0	50	4.7	286	415	2697	320	8.2
3	18	831	921.5	15.1	49	4.5	285	416	2726	324	7.8
3	20	840	920.5	15.2	48	4.3	284	416	2756	324	7.8
3	22	849	919.5	15.3	48	4.4	284	418	2785	324	7.8
3	24	858	918.6	15.4	47	4.2	283	418	2815	323	7.4
3	26	868	917.6	15.5	47	4.3	283	420	2848	323	7.4
3	28	877	916.6	15.6	46	4.1	282	420	2877	327	7.0
3	30	886	915.6	15.7	46	4.1	282	421	2907	327	7.0
3	32	889	915.2	15.8	46	4.3	282	422	2917	327	7.0
3	34	892	914.9	15.9	45	4.1	281	422	2927	331	6.8
3	36	896	914.5	15.9	45	4.1	281	422	2940	331	6.8
3	38	899	914.2	16.0	44	3.8	281	422	2949	335	6.4
3	40	902	913.8	16.0	44	3.8	281	422	2959	335	6.4
3	42	906	913.4	16.0	44	3.8	280	423	2972	335	6.4
3	44	911	912.9	16.1	44	3.9	280	423	2989	334	6.0
3	46	915	912.5	16.1	44	3.9	280	424	3002	334	6.0
3	48	919	912.0	16.2	43	3.7	279	424	3015	338	5.8
3	50	923	911.6	16.3	43	3.7	279	424	3028	338	5.8
3	52	928	911.1	16.4	43	3.9	279	425	3045	338	5.8

3 54	933	910.5	16.5	43	4.0	279	426	3061	342	5.4
3 56	938	910.0	16.5	43	4.0	279	427	3077	342	5.4
3 58	943	909.5	16.6	42	3.7	278	426	3094	346	5.2
4 0	948	908.9	16.7	41	3.4	278	426	3110	346	5.2
` 2	953	908.4	16.7	41	3.5	277	427	3127	346	5.2
4 4	958	907.9	16.8	41	3.5	277	428	3143	350	5.1
` 6	962	907.4	16.8	41	3.5	277	428	3156	350	5.1
` 3	967	906.9	16.8	41	3.5	277	429	3173	355	4.7
4 10	971	906.5	16.8	41	3.5	277	429	3186	355	4.7
4 12	974	906.1	16.8	41	3.5	277	430	3196	355	4.7
` 14	977	905.8	16.8	42	3.9	278	431	3205	355	4.5
4 16	981	905.4	16.8	42	3.9	278	432	3219	355	4.5
4 18	984	905.1	16.8	42	3.9	277	432	3228	360	4.3
4 20	987	904.7	16.8	42	3.8	277	432	3238	360	4.3
` 22	992	904.2	16.8	41	3.5	276	432	3255	360	4.3
4 24	997	903.7	16.8	40	3.2	275	432	3271	1	4.3
4 26	1003	903.1	16.8	40	3.2	275	433	3291	1	4.3
4 28	1008	902.5	16.8	39	2.8	274	433	3307	5	4.1
` 30	1014	901.8	16.8	39	2.8	274	433	3327	5	4.1
4 32	1018	901.5	16.8	39	2.8	274	434	3340	5	4.1
4 34	1021	901.1	16.8	39	2.8	274	434	3350	7	3.9
4 36	1025	900.7	16.8	39	2.8	274	435	3363	7	3.9
4 38	1029	900.3	16.9	39	2.9	274	435	3376	10	3.9
4 40	1033	899.9	16.9	39	2.9	274	436	3389	10	3.9
4 42	1037	899.4	16.9	39	2.9	274	436	3402	10	3.9
4 44	1042	899.0	16.8	39	2.8	273	437	3419	13	3.7
4 46	1046	898.6	16.8	39	2.8	273	437	3432	13	3.7
4 48	1049	898.2	16.7	39	2.8	273	438	3442	15	3.7
4 50	1052	897.9	16.7	39	2.7	273	438	3451	15	3.7
` 52	1056	897.5	16.7	39	2.8	273	439	3465	15	3.7
4 54	1060	897.0	16.7	40	3.1	274	440	3478	20	3.7
4 56	1064	896.6	16.7	40	3.1	273	440	3491	20	3.7
4 58	1067	896.3	16.6	40	3.0	273	441	3501	20	3.9
5 0	1071	895.9	16.6	40	3.0	273	441	3514	20	3.9
5 5	1081	894.8	16.5	40	2.9	273	442	3547	19	4.1
5 10	1095	893.3	16.4	40	2.8	272	444	3593	18	4.1
5 15	1108	892.0	16.3	41	3.1	273	447	3635	16	4.7
5 20	1118	890.9	16.3	41	3.1	272	448	3668	15	4.9
5 25	1131	889.6	16.3	42	3.4	273	450	3711	13	5.1
5 30	1143	888.3	16.1	42	3.2	272	452	3750	11	5.4
5 35	1154	887.2	16.0	42	3.1	272	453	3786	9	5.6
5 40	1164	886.1	16.0	43	3.5	272	455	3819	7	6.0
5 45	1176	884.8	15.9	42	3.0	271	456	3858	6	6.2
5 50	1189	883.5	15.8	42	2.9	271	457	3901	4	6.6
5 55	1199	882.5	15.8	41	2.6	270	458	3934	3	6.6
6 0	1210	881.4	15.9	41	2.7	269	459	3970	360	7.0
6 5	1222	880.1	15.8	41	2.6	269	461	4009	358	7.2
6 10	1234	878.8	15.8	41	2.6	269	462	4049	355	7.6
6 15	1245	877.7	15.7	41	2.5	268	464	4085	353	8.0
6 20	1257	876.4	15.7	40	2.2	267	464	4124	350	8.4
6 25	1268	875.4	15.8	39	1.9	266	465	4160	348	8.6
6 30	1280	874.1	15.7	38	1.5	265	466	4199	345	8.9
6 35	1292	872.8	15.7	38	1.5	264	467	4239	342	9.1
6 40	1303	871.8	15.7	38	1.5	264	469	4275	340	9.5
6 45	1315	870.5	15.6	38	1.4	264	470	4314	337	9.7
6 50	1325	869.4	15.6	38	1.4	263	471	4347	335	9.9
6 55	1338	868.1	15.6	39	1.7	264	474	4390	333	10.5
7 0	1350	866.9	15.6	39	1.7	264	475	4429	331	10.5
7 5	1365	865.4	15.6	36	0.6	261	475	4478	330	10.7
7 10	1377	864.1	15.6	35	0.2	260	476	4518	328	10.9

7	15	1388	863.1	15.6	34	-0.2	259	477	4554	326	11.3
7	20	1400	861.8	15.6	33	-0.6	257	477	4593	324	11.3
7	25	1412	860.5	15.6	33	-0.6	257	479	4633	323	11.5
7	30	1427	859.1	15.5	33	-0.7	257	481	4682	321	11.5
	35	1437	858.0	15.4	33	-0.8	256	482	4715	320	11.5
7	40	1448	857.0	15.4	33	-0.8	256	433	4751	318	11.7
7	45	1460	855.7	5.4	31	-1.6	254	483	4790	317	11.7
7	50	1472	854.5	.4	29	-2.5	252	483	4829	316	11.7
7	55	1485	853.2	15.4	27	-3.5	250	484	4872	314	11.7
8	0	1501	851.6	15.4	26	-4.0	249	485	4925	313	11.7
8	5	1514	850.3	15.4	26	-4.0	249	487	4967	312	11.7
8	10	1526	849.1	15.4	26	-4.0	249	488	5007	310	11.7
8	15	1541	847.6	15.4	26	-4.0	248	490	5056	309	11.5
8	20	1553	846.4	15.3	27	-3.6	249	492	5095	308	11.5
8	25	1563	845.3	15.3	29	-2.6	250	495	5128	307	11.5
8	30	1576	844.1	15.3	31	-1.7	251	498	5171	305	11.5
8	35	1590	842.7	15.2	31	-1.8	251	500	5217	304	11.3
8	40	1603	841.4	15.1	32	-1.4	251	503	5259	303	11.3
8	45	1613	840.4	15.0	34	-0.7	252	505	5292	302	11.3
8	50	1625	839.2	14.9	35	-0.4	252	508	5331	301	11.1
8	55	1638	837.9	14.9		?.0	253	510	5374	300	11.3
9	0	1650	836.7	14.8	5.	.3	253	512	5413	299	11.1
9	5	1660	835.7	14.8	41	1.7	256	517	5446	298	10.9
9	10	1671	834.7	14.7	42	2 0	256	519	5482	297	10.7
9	15	1685	833.3	14.6	42	1.9	256	520	5528	296	10.5
9	20	1698	832.0	14.6	42	1.9	255	522	5571	295	10.3
9	25	1708	831.0	14.6	42	1.9	255	523	5604	293	10.1
9	30	1722	829.6	14.5	42	1.8	255	525	5650	292	9.9
9	35	1731	828.8	14.4	43	2.0	255	527	5679	291	9.9
9	40	1741	827.8	14.3	44	2.2	255	529	5712	290	9.7
9	45	1755	826.4	14.2	44	2.1	255	531	5753	289	9.5
9	50	1768	825.2	14.1	44	2.1	255	532	5803	288	9.3
9	55	1780	824.0	14.0	44	2.0	254	534	5840	286	9.1
10	0	1794	822.5	13.9	44	1.9	254	535	5885	285	8.9
10	10	1817	820.3	13.7	45	2.0	254	539	5961	282	8.6
10	20	1840	818.1	13.6	45	1.9	253	542	6037	280	8.4
10	30	1866	815.5	13.4	46	2.0	253	546	6122	277	8.2
10	40	1887	813.6	13.3	46	1.9	252	548	6191	276	8.0
10	50	1912	811.2	13.0	46	1.7	251	551	6273	273	7.8
11	0	1934	809.0	12.9	47	1.9	251	555	6345	270	7.6
11	10	1953	807.2	12.7	47	1.7	250	557	6407	267	7.4
11	20	1979	804.7	12.4	47	1.4	249	560	6493	264	7.4
11	30	2004	802.3	12.3	47	1.3	249	563	6575	262	7.4
11	40	2026	800.2	12.2	46	0.9	247	565	6647	260	7.4
11	50	2051	797.8	12.1	45	0.5	246	568	6729	258	7.4
12	0	2073	795.7	12.0	45	0.5	245	571	6801	256	7.4
12	10	2098	793.4	11.8	45	0.3	244	574	6883	254	7.6
12	20	2120	791.2	11.7	45	0.2	244	577	6955	254	7.6
12	30	2145	788.9	11.5	45	0.0	243	580	7037	253	7.8
12	40	2165	787.0	11.3	45	-0.2	242	582	7103	252	8.0
12	50	2190	784.7	11.1	45	-0.4	241	585	7185	252	8.2
13	0	2210	782.8	11.0	46	-0.2	241	588	7251	252	8.4
13	10	2234	780.5	10.8	46	-0.3	241	591	7329	253	8.7
13	20	2257	778.4	10.7	47	-0.1	240	595	7405	254	8.9
3	30	2281	776.1	10.6	47	-0.2	240	598	7484	254	9.1
3	40	2302	774.2	10.5	46	-0.6	239	600	7552	255	9.5
13	50	2322	772.3	10.3	46	-0.8	238	602	7618	256	9.9
14	0	2346	770.1	10.1	46	-1.0	237	605	7697	258	10.1
14	10	2371	767.8	9.9	46	-1.2	236	609	7779	259	10.5
14	20	2393	765.8	9.8	45	-1.6	235	611	7851	260	10.7

14	30	2417	763.5	9.8	44	-1.9	234	613	7930	261	11.
14	40	2438	761.7	9.7	45	-1.6	234	617	7999	263	11.
14	50	2460	759.6	9.6	42	-2.7	232	618	8071	263	11.
15	0	2482	757.6	9.7	34	-5.4	227	616	8143	264	11.
15	10	2504	755.5	9.8	27	-8.3	222	615	8215	265	12.
15	20	2529	753.3	9.8	23	-10.3	219	616	8297	266	12.
15	30	2551	751.3	9.7	22	-11.0	218	619	8369	266	12.
15	40	2575	749.1	9.6	24	-10.0	219	623	8448	267	12.
15	50	2598	747.1	9.4	27	-8.6	220	628	8524	267	13.
16	0	2620	745.1	9.2	30	-7.5	221	632	8596	268	13..
16	10	2646	742.7	9.0	32	-6.8	221	637	8681	268	13..
16	20	2670	740.6	8.7	32	-7.1	221	640	8760	268	13..
16	30	2691	738.8	8.6	31	-7.6	220	642	8829	269	13..
16	40	2717	736.4	8.5	30	-8.1	218	645	8914	269	13..
16	50	2741	734.3	8.4	28	-9.0	217	647	8993	270	13.
17	0	2765	732.1	8.1	28	-9.3	216	650	9072	272	13.
17	10	2787	730.2	8.0	27	-9.9	215	653	9144	272	13.
17	20	2807	728.4	7.8	27	-10.0	215	655	9209	273	13.
17	30	2838	725.7	7.5	27	-10.3	214	659	9311	274	14.
17	40	2858	723.9	7.4	26	-10.8	213	661	9377	276	14.
17	50	2880	722.0	7.4	20	-14.1	209	662	9449	277	14.
18	0	2900	720.2	7.4	17	-16.1	207	663	9514	279	14..
18	10	2920	718.5	7.3	17	-16.2	207	665	9580	280	14..
18	20	2944	716.4	7.3	13	-19.3	204	667	9659	282	15..
18	30	2966	714.5	7.4	11	-21.2	203	669	9731	283	15.
18	40	2986	712.7	7.4	10	-22.3	202	671	9797	284	15.
18	50	3012	710.5	7.3	10	-22.4	201	674	9882	285	15.
19	0	3036	708.4	7.1	8	-25.0	200	677	9961	286	16.
19	10	3056	706.7	7.1	11	-21.4	201	681	10026	286	16.
9	20	3082	704.4	7.0	19	-15.1	204	688	10112	287	16..
19	30	3112	701.8	6.7	27	-11.0	207	696	10210	287	16..
19	40	3136	699.8	6.4	33	-8.7	209	702	10289	286	16..
19	50	3158	697.9	6.3	33	-8.8	209	704	10361	286	17..
20	0	3180	696.0	6.1	29	-10.6	206	706	10433	286	17.
20	10	3208	693.7	5.9	29	-10.8	206	709	10525	285	17.
20	20	3232	691.6	5.6	29	-11.0	205	712	10604	284	17.
20	30	3258	689.4	5.4	29	-11.2	204	716	10689	283	17..
20	40	3284	687.3	5.3	28	-11.7	203	719	10774	282	17..
20	50	3310	685.1	5.1	28	-11.9	203	722	10860	282	17.
21	0	3340	682.6	4.8	28	-12.2	202	726	10958	281	17.
21	10	3362	680.7	4.7	28	-12.3	202	729	11030	281	17.
21	20	3392	678.3	4.4	27	-13.0	200	733	11129	281	17.
21	30	3415	676.3	4.3	25	-14.0	199	735	11204	281	17..
21	40	3443	674.0	4.2	18	-18.0	196	736	11296	281	17..
21	50	3471	671.7	4.1	23	-15.2	197	742	11388	280	17..
22	0	3499	669.4	4.1	27	-13.2	198	747	11480	280	17.
22	10	3525	667.3	4.0	29	-12.4	198	752	11565	280	17.
22	20	3552	665.0	3.9	28	-13.0	197	755	11654	279	17.
22	30	3574	663.2	3.8	28	-13.0	197	758	11726	279	17.
22	40	3600	661.1	3.5	29	-12.9	196	762	11811	279	17.
22	50	3628	658.8	3.3	30	-12.6	196	766	11903	279	17.
23	0	3653	656.8	3.1	31	-12.4	196	769	11985	278	17.
23	10	3675	655.0	3.0	31	-12.5	195	772	12057	277	17..
23	20	3703	652.8	2.8	30	-13.1	194	776	12149	277	17.
23	30	3732	650.4	2.7	30	-13.2	194	780	12244	276	18.
23	40	3752	648.8	2.8	31	-12.7	194	783	12310	274	18..
23	50	3778	646.7	2.7	32	-12.4	193	787	12395	273	18..
24	0	3805	644.5	2.6	32	-12.4	193	790	12484	272	18..
24	10	3829	642.6	2.5	31	-12.9	192	793	12562	271	19..
24	20	3855	640.6	2.3	29	-13.9	191	796	12648	270	19..

24 30	3882	638.4	2.2	30	-13.6	190	800	12736	269	19.6
24 40	3906	636.5	2.0	37	-11.2	192	805	12815	268	20.0
24 50	3932	634.5	1.9	37	-11.3	192	809	12900	267	20.2
25 0	3959	632.4	2.1	30	-13.7	189	810	12989	265	20.6
25 10	3985	630.4	2.1	28	-14.5	187	813	13074	265	21.0
25 20	4012	628.2	1.8	28	-14.8	187	817	13163	264	21.4
25 30	4036	626.4	1.7	26	-15.8	186	819	13241	263	21.6
25 40	4061	624.4	1.7	23	-17.2	184	822	13323	262	22.0
25 50	4087	622.4	1.6	23	-17.3	184	825	13409	261	22.4
26 0	4111	620.6	1.5	23	-17.4	183	828	13488	260	22.5
26 10	4140	618.3	1.4	24	-17.0	183	833	13583	260	22.9
26 20	4166	616.4	1.2	24	-17.2	182	836	13668	259	23.1
26 30	4191	614.4	1.1	23	-17.8	181	839	13750	258	23.3
26 40	4217	612.5	0.9	23	-17.9	181	843	13835	257	23.5
26 50	4240	610.7	0.7	23	-18.1	180	846	13911	257	23.7
27 0	4266	608.7	0.4	24	-17.8	180	850	13996	255	23.9
27 10	4289	607.0	0.2	24	-18.0	180	853	14072	254	24.1
27 20	4314	605.0	0.1	25	-17.6	179	857	14154	254	24.1
27 30	4340	603.1	0.0	24	-18.2	179	860	14239	253	24.3
27 40	4371	600.8	-0.2	21	-19.9	177	863	14341	252	24.3
27 50	4396	598.9	-0.3	17	-22.4	175	866	14423	250	24.5
28 0	4424	596.8	-0.4	15	-23.9	174	869	14514	249	24.5
28 10	4453	594.6	-0.5	10	-28.5	172	871	14610	248	24.5
28 20	4476	592.9	-0.6	9	-29.7	171	874	14685	246	24.7
28 30	4502	591.0	-0.7	9	-29.8	171	878	14770	245	24.7
28 40	4529	589.0	-0.8	14	-25.0	172	883	14859	243	24.7
28 50	4556	587.0	-1.0	16	-23.7	172	887	14948	242	24.9
29 0	4582	585.1	-1.1	12	-27.0	170	890	15033	241	24.9
29 10	4611	583.0	-1.3	12	-27.1	170	894	15128	240	24.9
9 20	4636	581.1	-1.4	17	-23.4	171	898	15210	239	25.1
29 30	4661	579.3	-1.5	21	-21.0	171	903	15292	238	25.1
29 40	4688	577.3	-1.7	23	-20.1	171	907	15381	237	25.1
29 50	4714	575.5	-1.9	21	-21.4	170	910	15466	236	25.3
30 0	4743	573.4	-2.2	20	-22.2	169	914	15561	236	25.3
30 10	4764	571.9	-2.3	18	-23.5	169	916	15630	236	25.3
30 20	4789	570.0	-2.4	21	-21.8	169	921	15712	235	25.3
30 30	4816	568.1	-2.6	26	-19.5	170	926	15801	235	25.3
30 40	4842	566.3	-2.8	27	-19.2	169	930	15886	234	25.5
30 50	4869	564.4	-3.1	29	-18.7	169	934	15974	234	25.5
31 0	4896	562.4	-3.3	29	-18.8	169	937	16063	234	25.5
31 10	4921	560.7	-3.5	28	-19.4	168	941	16145	234	25.5
31 20	4944	559.0	-3.7	27	-20.0	167	944	16220	233	25.7
31 30	4973	557.0	-3.9	26	-20.6	167	947	16316	233	25.7
31 40	5000	555.1	-4.1	27	-20.4	166	951	16404	232	25.7
31 50	5027	553.2	-4.3	29	-19.7	166	955	16493	232	25.9
32 0	5054	551.3	-4.6	30	-19.6	166	959	16581	231	26.0
32 10	5080	549.4	-4.8	29	-20.1	165	963	16667	231	26.0
32 20	5105	547.7	-5.0	28	-20.7	165	966	16749	230	26.2
32 30	5132	545.8	-5.2	29	-20.5	164	970	16837	230	26.4
32 40	5157	544.1	-5.5	31	-20.0	164	974	16919	229	26.6
32 50	5184	542.2	-5.7	31	-20.2	164	978	17008	229	26.8
33 0	5211	540.4	-5.8	32	-19.9	163	982	17096	229	27.2
33 10	5239	538.4	-6.1	34	-19.4	163	986	17188	229	27.4
33 20	5264	536.7	-6.2	34	-19.5	163	989	17270	228	27.8
33 30	5287	535.1	-6.5	36	-19.1	163	993	17346	228	28.2
3 40	5314	533.3	-6.5	35	-19.5	162	996	17434	228	28.6
33 50	5341	531.5	-6.7	34	-20.0	161	1000	17523	227	29.0
34 0	5367	529.7	-6.7	37	-19.0	161	1004	17608	227	29.4
34 10	5396	527.7	-6.7	36	-19.3	161	1008	17703	227	29.7
34 20	5423	525.9	-6.9	36	-19.5	160	1012	17792	227	30.1

71

34	30	5449	524.1	-7.1	36	-19.7	160	1015	17877	227	30.5
34	40	5478	522.2	-7.2	32	-21.1	158	1018	17972	227	30.9
34	50	5504	520.4	-7.3	26	-23.6	157	1021	18058	227	31.3
~5	0	5531	518.6	-7.2	21	-25.9	155	1024	18146	226	31.7
.	10	5558	516.9	-7.3	22	=25.4	155	1028	18235	226	32.1
₃5	20	5588	514.9	-7.4	24	-24.6	155	1032	18333	227	32.3
35	30	5618	512.9	-7.6	23	-25.2	154	1036	18432	227	32.7
35	40	5641	511.4	-7.8	24	-24.9	154	1039	18507	227	32.9
35	50	5670	509.5	-8.1	25	-24.7	154	1044	18602	227	33.0
36	0	5700	507.5	-8.3	25	-24.9	153	1048	18701	228	33.4
36	10	5725	505.9	-8.4	26	-24.5	153	1052	18783	228	33.6
36	20	5751	504.2	-8.7	26	-24.8	152	1055	18868	229	33.8
36	30	5781	502.2	-8.9	26	-25.0	152	1059	18967	229	33.8
36	40	5804	500.7	-9.1	26	-25.1	151	1063	19042	230	34.0
36	50	5830	499.0	-9.3	25	-25.8	151	1066	19127	230	34.0
37	0	5859	497.2	-9.6	25	-26.0	150	1070	19222	230	34.2
37	10	5887	495.4	-9.7	25	-26.1	150	1074	19314	231	34.2
37	20	5915	493.6	-10.0	24	-26.8	149	1078	19406	232	34.2
37	30	5942	491.9	-10.1	23	-27.4	149	1081	19495	232	34.2
37	40	5968	490.2	-10.3	23	-27.5	148	1085	19580	233	34.2
37	50	5990	488.8	-10.4	22	-28.1	148	1088	19652	233	34.2
38	0	6017	487.1	-10.6	21	-28.8	⌐147	1092	19741	234	34.2
38	10	6045	485.3	-10.8	20	-29.5	146	1095	19833	234	34.2
38	20	6069	483.8	-11.0	19	-30.2	146	1099	19911	235	34.4
38	30	6095	482.1	-11.2	19	-30.4	145	1102	19997	235	34.2
38	40	6120	480.6	-11.4	19	-30.5	145	1106	20079	236	34.2
38	50	6148	478.8	-11.6	19	-30.7	145	1110	20171	236	34.2
39	0	6172	477.3	-11.7	17	-31.9	144	1113	20249	237	34.2
39	10	6196	475.8	-11.9	16	-32.7	143	1116	20328	237	34.2
9	20	6221	474.3	-12.0	14	-34.2	143	1119	20410	238	34.2
.9	30	6251	472.5	-12.2	14	-34.4	142	1124	20509	238	34.4
39	40	6273	471.1	-12.4	15	-33.8	142	1127	20581	238	34.4
39	50	6295	469.7	-12.6	15	-34.0	142	1130	20653	239	34.6
40	0	6325	467.9	-12.9	14	-34.9	141	1134	20751	239	34.6
40	10	6349	466.4	-13.1	14	-35.1	141	1138	20830	240	34.6
40	20	6375	464.8	-13.2	14	-35.2	140	1141	20915	240	34.8
40	30	6398	463.4	-13.5	14	-35.4	140	1145	20991	241	35.0
40	40	6425	461.7	-13.7	14	-35.6	140	1148	21079	241	35.0
40	50	6451	460.2	-13.9	14	-35.8	139	1152	21165	241	35.2
41	0	6477	458.6	-14.2	14	-36.0	139	1156	21250	242	35.4
41	10	6501	457.1	-14.3	14	-36.1	139	1159	21329	242	35.4
41	20	6529	455.5	-14.5	14	-36.3	138	1163	21421	242	35.6
41	30	6559	453.7	-14.7	14	-36.4	138	1168	21519	242	35.6
41	40	6581	452.4	-14.9	14	-36.6	137	1171	21591	242	35.8
41	50	6609	450.7	-15.1	13	-37.5	137	1175	21683	242	35.8
42	0	6634	449.2	-15.2	13	-37.6	136	1178	21765	242	35.8
42	10	6664	447.4	-15.5	13	-37.8	136	1182	21864	242	35.8
42	20	6692	445.8	-15.7	13	-38.0	136	1186	21955	241	36.0
42	30	672₂	444.1	-15.9	13	-38.1	135	1190	22051	241	36.0
42	40	6749	442.4	-16.2	13	-38.4	135	1194	22142	240	36.0
42	50	6778	440.7	-16.4	13	-38.6	134	1199	22238	239	36.0
43	0	6805	439.1	-16.7	13	-38.8	134	1202	22326	239	36.0
43	10	6833	437.5	-16.9	13	-39.0	134	1206	22418	238	36.0
43	20	6862	435.8	-17.1	13	-39.1	133	1211	22513	237	35.8
~3	30	6 ₉3	434.0	-17.3	13	-39.3	133	1215	22615	237	35.8
3	40	6921	432.4	-17.6	14	-38.8	133	1219	22707	236	35.8
43	50	6950	430.7	-17.9	14	-39.1	132	1223	22802	235	35.8
44	0	6977	429.1	-18.1	14	-39.2	132	1227	22890	234	35.8
44	10	7008	427.4	-18.4	14	-39.5	131	1232	22992	233	35.6
44	20	7037	425.7	-18.5	13	-40.3	131	1236	23087	233	35.6

44	30	7068	423.9	-18.7	13	-40.4	130	1240	23189	232	35.4
44	40	7096	422.4	-18.9	13	-40.6	130	1244	23281	232	35.4
44	50	7127	420.6	-19.2	13	-40.9	130	1243	23383	232	35.2
'5	0	7154	419.1	-19.4	13	-41.0	129	1252	23471	231	35.2
5	10	7186	417.3	-19.7	13	-41.3	129	1257	23575	231	35.2
5	20	7217	415.5	-19.9	13	-41.4	128	1261	23673	230	35.2
45	30	7248	413.8	-20.1	13	-41.6	128	1266	23780	230	35.0
45	40	7277	412.2	-20.3	12	-42.5	127	1270	23875	230	35.2
45	50	7308	410.5	-20.6	12	-42.8	127	1274	23976	229	35.2
46	0	7331	409.2	-20.7	12	-42.8	127	1278	24052	229	35.2
46	10	7365	407.3	-21.0	11	-43.9	126	1282	24163	229	35.2
46	20	7394	405.7	-21.2	11	-44.1	126	1287	24259	229	35.2
46	30	7430	403.7	-21.4	11	-44.2	125	1292	24377	229	35.2
46	40	7457	402.2	-21.7	11	-44.5	125	1296	24465	229	35.2
46	50	7482	400.9	-21.9	11	-44.6	125	1299	24547	229	35.2
47	0	7513	399.2	-22.1	12	-44.0	124	1304	24649	229	35.2
47	10	7540	397.8	-22.3	12	-44.2	124	1308	24733	229	35.2
47	20	7567	396.3	-22.6	12	-44.4	123	1311	24826	229	35.4
47	30	7597	394.7	-22.9	12	-44.6	123	1316	24925	230	35.4
47	40	7624	393.2	-23.1	12	-44.8	123	1320	25013	230	35.4
47	50	7652	391.7	-23.4	13	-44.3	122	1324	25105	231	35.4
48	0	7679	390.3	-23.7	13	-44.6	122	1328	25194	231	35.4
48	10	7706	388.8	-23.9	13	-44.7	122	1332	25282	232	35.4
48	20	7733	387.4	-24.2	13	-45.0	121	1336	25371	232	35.4
48	30	7759	386.0	-24.4	14	-44.5	121	1339	25456	233	35.6
48	40	7786	384.6	-24.5	13	-45.2	121	1343	25545	234	35.6
48	50	7813	383.2	-24.7	12	-46.1	120	1347	25633	234	35.6
49	0	7839	381.8	-24.9	12	-46.3	120	1351	25719	235	35.6
49	10	7868	380.3	-25.2	12	-46.5	120	1355	25814	234	35.8
9	20	7894	378.9	-25.4	12	-46.7	119	1359	25899	235	36.0
9	30	7919	377.6	-25.6	12	-46.9	119	1362	25981	235	36.0
49	40	7942	376.4	-25.9	18	-43.4	119	1366	26056	235	36.0
49	50	7970	374.9	-26.0	32	-37.9	119	1370	26143	235	36.2
50	0	7995	373.7	-26.1	45	-34.6	119	1375	26230	235	36.2
50	10	8020	372.4	-26.4	47	-34.4	119	1378	26312	235	36.3
50	20	8043	371.2	-26.6	48	-34.4	119	1382	26388	234	36.3
50	30	8069	369.8	-26.9	49	-34.5	119	1385	26473	233	36.5
50	40	8092	368.7	-27.1	50	-34.4	118	1389	26549	232	36.5
50	50	8120	367.2	-27.4	51	-34.5	118	1393	26640	232	36.5
51	0	8148	365.8	-27.6	53	-34.3	118	1397	26732	232	36.3
51	10	8171	364.6	-27.8	54	-34.3	117	1400	26808	231	36.5
51	20	8197	363.3	-27.9	55	-34.2	117	1404	26893	231	36.5
51	30	8225	361.9	-28.1	53	-34.8	117	1408	26985	230	36.3
51	40	8252	360.6	-28.4	53	-35.1	116	1412	27073	230	36.3
51	50	8278	359.3	-28.6	52	-35.4	116	1416	27159	230	36.2
52	0	8306	357.9	-28.9	52	-35.7	116	1420	27251	229	36.2
52	10	8330	356.6	-29.1	50	-36.3	115	1423	27329	229	36.2
52	20	8358	355.2	-29.4	44	-37.9	115	1427	27421	229	36.2
52	30	8381	354.1	-29.5	38	-39.4	114	1430	27497	229	36.0
52	40	8412	352.6	-29.6	35	-40.3	113	1434	27598	228	36.2
52	50	8438	351.3	-29.8	34	-40.7	113	1438	27684	228	36.0
53	0	8463	350.1	-30.0	33	-41.2	113	1441	27766	228	36.0
53	10	8490	348.7	-30.2	32	-41.7	112	1445	27854	228	36.0
53	20	8516	347.4	-30.4	29	-42.8	112	1449	27940	228	35.8
53	30	8539	346.3	-30.6	28	-43.3	112	1452	28015	228	35.8
3	40	8570	344.8	-30.8	28	-43.5	111	1457	28117	228	35.8
53	50	8596	343.6	-31.1	29	-43.4	111	1461	28202	228	35.8
54	0	8624	342.2	-31.3	30	-43.3	111	1465	28294	228	35.8
54	10	8653	340.8	-31.6	30	-43.6	110	1469	28389	228	35.6
54	20	8681	339.5	-31.8	31	-43.4	110	1473	28481	227	35.6

54	30	8707	338.2	-32.1	31	-43.7	110	1477	28566	227	35.6
54	40	8734	336.9	-32.4	31	-44.0	109	1481	28655	227	35.6
54	50	8764	335.5	-32.6	31	-44.1	109	1485	28753	227	35.4
55	0	8791	334.2	-32.9	32	-44.1	109	1489	28842	227	35.4
5	10	8820	332.8	-33.2	33	-44.1	108	1493	28937	227	35.4
55	20	8846	331.6	-33.4	34	-44.0	108	1497	29022	228	35.2
55	30	8873	330.3	-33.6	31	-45.0	108	1501	29111	228	35.2
55	40	8897	329.2	-33.7	27	-46.4	107	1504	29190	228	35.2
55	50	8926	327.8	-33.9	25	-47.3	107	1508	29285	229	35.2
56	0	8952	326.6	-34.1	24	-47.8	107	1512	29370	229	35.2
56	10	8981	325.3	-34.3	24	-48.0	106	1516	29465	229	35.2
56	20	9007	324.1	-34.5	25	-47.8	106	1520	29551	230	35.4
56	30	9037	322.7	-34.8	26	-47.7	106	1524	29649	230	35.6
56	40	9065	321.4	-35.0	28	-47.2	105	1528	29741	231	35.8
56	50	9092	320.2	-35.3	32	-46.3	105	1533	29829	232	35.8
57	0	9117	319.0	-35.5	34	-45.9	105	1536	29911	232	36.0
57	10	9146	317.7	-35.7	37	-45.3	105	1540	30007	234	36.2
57	20	9173	316.4	-35.9	38	-45.3	104	1544	30095	234	36.3
57	30	9202	315.1	-36.1	40	-45.0	104	1549	30190	235	36.5
57	40	9229	313.9	-36.4	41	-45.0	104	1553	30279	235	36.7
57	50	9256	312.7	-36.6	42	-45.0	103	1557	30367	236	37.1
58	0	9285	311.4	-37.0	45	-44.7	103	1561	30463	237	37.3
58	10	9314	310.1	-37.2	44	-45.1	103	1565	30558	238	37.5
58	20	9342	308.8	-37.3	42	-45.6	102	1569	30650	238	37.9
58	30	9371	307.5	-37.5	40	-46.3	102	1573	30745	239	38.1
58	40	9398	306.3	-37.8	39	-46.8	102	1577	30833	240	38.3
58	50	9423	305.2	-38.0	37	-47.4	101	1581	30915	241	38.5
59	0	9450	304.0	-38.1	33	-48.5	101	1585	31004	241	38.7
59	10	9482	302.6	-38.3	27	-50.5	100	1589	31109	243	38.7
9	20	9511	301.3	-38.4	21	-52.8	100	1593	31204	243	38.9
59	30	9537	300.2	-38.5	18	-54.2	100	1597	31289	244	38.9
59	40	9566	298.9	-38.7	16	-55.3	99	1601	31385	244	39.1
59	50	9593	297.8	-38.9	15	-56.0	99	1605	31473	245	39.1
60	0	9619	296.6	-39.1	14	-56.8	99	1609	31558	245	39.3
60	10	9645	295.5	-39.2	14	-56.9	98	1612	31644	246	39.3
60	20	9671	294.4	-39.5	16	-56.0	98	1616	31729	246	39.5
60	30	9698	293.2	-39.7	16	-56.2	98	1620	31818	246	39.5
60	40	9726	292.0	-39.9	17	-55.8	97	1624	31909	246	39.7
60	50	9751	290.9	-40.1	17	-56.0	97	1628	31991	246	39.7
61	0	9780	289.7	-40.4	18	-55.8	97	1632	32087	246	39.7
61	10	9805	288.7	-40.6	22	-54.3	97	1636	32169	246	39.7
61	20	9833	287.5	-40.8	27	-52.7	96	1640	32260	246	39.7
61	30	9863	286.2	-41.0	29	-52.3	96	1644	32359	246	39.7
61	40	9889	285.1	-41.3	30	-52.3	96	1648	32444	246	39.7
61	50	9917	283.9	-41.5	31	-52.2	95	1652	32536	246	39.7
62	0	9946	282.7	-41.8	32	-52.2	95	1657	32631	246	39.5
62	10	9970	281.7	-42.0	34	-51.8	95	1660	32710	245	39.5
62	20	9997	280.6	-42.3	35	-51.8	95	1664	32799	245	39.5
62	30	10023	279.5	-42.5	37	-51.5	94	1668	32884	245	39.3
62	40	10050	278.4	-42.6	38	-51.4	94	1672	32972	245	39.1
62	50	10074	277.4	-42.8	37	-51.8	94	1675	33051	245	39.1
63	0	10104	276.2	-43.0	36	-52.2	93	1680	33150	245	38.9
63	10	10130	275.1	-43.1	34	-52.8	93	1684	33235	244	38.9
63	20	10156	274.0	-43.3	32	-53.5	93	1687	33320	244	38.9
63	30	10184	272.9	-43.5	31	-54.0	92	1691	33412	244	38.9
3	40	10211	271.8	-43.7	31	-54.2	92	1695	33501	244	38.9
63	50	10237	270.8	-44.0	30	-54.7	92	1699	33586	244	39.1
64	0	10263	269.7	-44.2	30	-54.9	92	1703	33671	244	39.1
64	10	10289	268.7	-44.5	30	-55.2	91	1707	33757	244	39.1
64	20	10315	267.6	-44.8	31	-55.1	91	1711	33842	244	39.3

74

64	30	10340	266.7	-44.9	31	-55.2	91	1714	33924	244	39.3
64	40	10368	265.5	-45.2	31	-55.5	91	1718	34016	245	39.5
64	50	10392	264.6	-45.3	32	-55.3	90	1722	34094	245	39.5
65	0	10421	263.4	-45.7	31	-56.0	90	1726	34190	245	39.7
5	10	10446	262.5	-45.9	32	-55.9	90	1730	34272	245	39.7
65	20	10473	261.4	-46.2	32	-56.2	90	1734	34360	245	39.7
65	30	10498	260.4	-46.4	33	-56.1	89	1738	34442	245	39.8
65	40	10525	259.3	-46.6	33	-56.3	89	1741	34531	244	39.7
65	50	10551	258.3	-47.0	32	-56.7	89	1745	34616	244	39.7
66	0	10579	257.3	-47.0	32	-56.9	88	1749	34708	245	39.7
66	10	10603	256.3	-47.3	32	-57.1	88	1753	34787	245	39.7
66	20	10630	255.2	-47.5	32	-57.3	88	1757	34875	245	39.7
66	30	10654	254.3	-47.7	31	-57.8	88	1760	34954	244	39.7
66	40	10683	253.2	-48.0	31	-58.0	87	1765	35049	244	39.7
66	50	10711	252.2	-48.1	31	-58.1	87	1769	35141	244	39.7
67	0	10736	251.2	-48.3	30	-58.6	87	1772	35223	244	39.8
67	10	10762	250.2	-48.5	30	-58.8	87	1776	35308	244	39.8
67	20	10791	249.1	-48.8	29	-59.3	86	1780	35404	244	39.8
67	30	10817	248.1	-48.9	28	-59.7	86	1784	35489	245	39.8
67	40	10844	247.1	-49.1	27	-60.1	86	1788	35577	245	40.0
67	50	10871	246.1	-49.3	26	-60.6	85	1792	35666	245	40.2
68	0	10902	244.9	-49.6	25	-61.2	85	1797	35768	245	40.4
68	10	10925	244.0	-49.7	25	-61.3	85	1800	35843	245	40.6
68	20	10956	242.9	-49.8	24	-61.7	85	1805	35945	245	41.0
68	30	10983	241.9	-50.0	23	-62.2	84	1809	36033	245	41.2
68	40	11010	240.9	-50.3	23	-62.5	84	1813	36122	245	41.6
68	50	11037	239.9	-50.6	23	-62.7	84	1817	36211	244	42.0
69	0	11066	238.8	-50.8	23	-62.9	83	1821	36306	244	42.2
69	10	11090	238.0	-50.9	23	-63.0	83	1824	36385	244	42.6
9	20	11118	236.9	-51.1	22	-63.5	83	1828	36476	244	42.8
69	30	11144	236.0	-51.4	22	-63.8	83	1832	36562	244	43.2
69	40	11172	235.0	-51.6	22	-64.0	82	1836	36654	243	43.3
69	50	11201	233.9	-51.8	22	-64.1	82	1841	36749	243	43.5
70	0	11231	232.9	-52.0	21	-64.7	82	1845	36847	243	43.7
70	10	11254	232.0	-52.1	21	-64.8	82	1848	36923	243	43.9
70	20	11284	230.9	-52.4	21	-65.0	81	1853	37021	242	44.1
70	30	11311	230.0	-52.6	20	-65.6	81	1857	37110	242	44.3
70	40	11339	229.0	-52.8	19	-66.1	81	1861	37201	242	44.3
70	50	11368	228.0	-53.0	19	-66.3	80	1865	37297	242	44.5
71	0	11396	227.0	-53.2	18	-66.9	80	1869	37388	242	44.5
71	10	11426	225.9	-53.4	17	-67.5	80	1874	37487	242	44.7
71	20	11453	225.0	-53.7	17	-67.7	80	1878	37575	242	44.7
71	30	11481	224.0	-53.9	17	-67.9	79	1882	37667	242	44.9
71	40	11507	223.1	-54.1	16	-68.5	79	1886	37753	242	44.9
71	50	11536	222.1	-54.3	16	-68.7	79	1890	37848	242	45.1
72	0	11565	221.1	-54.6	16	-69.0	79	1894	37943	243	45.1
72	10	11592	220.1	-54.6	16	-69.0	78	1898	38031	243	45.3
72	20	11622	219.1	-55.0	16	-69.3	78	1903	38130	243	45.3
72	30	11648	218.2	-55.1	16	-69.4	78	1906	38215	243	45.5
72	40	11676	217.3	-55.3	15	-70.0	77	1911	38307	244	45.7
72	50	11703	216.4	-55.4	15	-70.1	77	1915	38396	244	45.7
73	0	11729	215.5	-55.5	15	-70.2	77	1918	38481	245	45.9
73	10	11759	214.5	-55.8	15	-70.5	77	1923	38579	245	46.1
73	20	11785	213.6	-56.0	15	-70.6	76	1927	38665	246	46.1
73	30	11816	212.5	-56.2	16	-70.3	76	1931	38766	247	46.3
3	40	11844	211.6	-56.3	16	-70.4	76	1935	38858	247	46.3
73	50	11870	210.7	-56.5	16	-70.6	76	1939	38944	248	46.5
74	0	11898	209.8	-56.8	16	-70.9	75	1943	39035	249	46.7
74	10	11924	208.9	-56.9	16	-71.0	75	1947	39121	250	46.7
74	20	11951	208.1	-57.1	17	-70.7	75	1951	39209	251	46.8

74	30	11978	207.2	-57.4	17	-71.0	75	1955	39298	252	47.0
74	40	12006	206.3	-57.7	17	-71.2	74	1959	39390	253	47.0
74	50	12035	205.3	-57.9	17	-71.4	74	1964	39485	254	47.2
75	0	12060	204.5	-58.1	17	-71.6	74	1967	39557	255	47.4
5	10	12089	203.6	-58.2	18	-71.2	74	1972	39662	255	47.4
5	20	12115	202.7	-58.3	18	-71.3	73	1975	39747	256	47.6
75	30	12144	201.8	-58.5	18	-71.5	73	1980	39843	256	47.6
75	40	12167	201.0	-58.7	18	-71.7	73	1983	39913	256	47.6
75	50	12197	200.1	-59.0	18	-71.9	73	1987	40016	256	47.6
76	0	12226	199.2	-59.2	19	-71.7	72	1992	40112	257	47.8
76	10	12253	198.3	-59.4	19	-71.9	72	1996	40200	257	47.6
76	20	12282	197.4	-59.7	19	-72.2	72	2000	40295	257	47.6
76	30	12314	196.4	-59.8	19	-72.3	71	2005	40400	257	47.6
76	40	12340	195.6	-59.9	19	-72.4	71	2009	40486	256	47.6
76	50	12369	194.7	-60.0	19	-72.4	71	2013	40581	256	47.4
77	0	12398	193.8	-60.2	19	-72.6	71	2017	40676	255	47.2
77	10	12428	192.8	-60.4	18	-73.2	70	2022	40774	256	47.2
77	20	12459	191.9	-60.6	18	-73.3	70	2026	40876	256	47.0
77	30	12488	191.0	-60.8	18	-73.5	70	2030	40971	256	47.0
77	40	12520	190.0	-60.8	18	-73.5	69	2035	41076	255	47.0
77	50	12551	189.0	-60.8	17	-73.9	69	2040	41178	255	46.8
78	0	12583	188.1	-61.0	17	-74.1	69	2044	41283	254	46.7
78	10	12614	187.2	-61.0	17	-74.1	68	2049	41385	254	46.7
78	20	12642	186.3	-61.0	16	-74.5	68	2053	41476	253	46.5
78	30	12671	185.4	-61.1	16	-74.6	68	2057	41572	252	46.7
78	40	12703	184.5	-61.2	15	-75.1	68	2062	41677	252	46.7
78	50	12735	183.5	-61.5	15	-75.4	67	2067	41781	251	46.7
79	0	12765	182.6	-61.7	15	-75.5	67	2071	41880	251	46.7
79	10	12794	181.8	-61.8	14	-76.1	67	2075	41975	250	46.5
9	20	12824	180.9	-61.9	14	-76.2	66	2080	42073	250	46.7
9	30	12856	180.0	-61.8	14	-76.1	66	2084	42178	249	46.8
79	40	12884	179.2	-62.1	13	-76.9	66	2089	42270	249	47.0
79	50	12915	178.3	-62.2	13	-76.9	66	2093	42372	249	47.0
80	0	12946	177.4	-62.3	12	-77.6	65	2098	42474	249	47.2
80	10	12975	176.5	-62.5	12	-77.7	65	2102	42569	249	47.4
80	20	13005	175.7	-62.7	12	-77.9	65	2107	42667	249	47.4
80	30	13034	174.9	-62.8	11	-78.5	65	2111	42762	249	47.6
80	40	13061	174.1	-62.9	11	-78.6	64	2115	42851	249	47.6
80	50	13089	173.3	-63.2	11	-78.9	64	2119	42943	250	47.8
81	0	13115	172.6	-63.3	10	-79.6	64	2123	43028	250	47.8
81	10	13146	171.7	-63.3	10	-79.6	64	2127	43130	250	47.6
81	20	13173	170.9	-63.3	10	-79.6	63	2131	43219	250	47.4
81	30	13202	170.2	-63.5	10	-79.8	63	2136	43314	249	47.2
81	40	13229	169.4	-63.9	10	-80.0	63	2140	43402	248	47.0
81	50	13257	168.6	-63.9	10	-80.1	63	2144	43494	248	46.8
82	0	13284	167.9	-64.0	10	-80.2	62	2148	43583	248	46.7
82	10	13312	167.1	-64.1	10	-80.3	62	2152	43675	247	46.3
82	20	13338	166.4	-64.0	10	-80.2	62	2156	43760	246	46.1
82	30	13369	165.6	-64.0	10	-80.2	61	2160	43862	246	45.7
82	40	13395	164.9	-63.8	10	-80.0	61	2164	43947	245	45.3
82	50	13423	164.1	-63.4	10	-79.7	61	2168	44039	245	44.7
83	0	13453	163.3	-62.9	10	-79.3	60	2172	44137	244	44.3
83	10	13482	162.6	-62.4	10	-78.8	60	2177	44232	244	43.7
83	20	13509	161.8	-62.2	9	-79.3	60	2180	44321	243	43.3
3	30	13540	161.0	-62.1	9	-79.3	59	2185	44423	243	42.8
3	40	13568	160.3	-62.2	8	-80.1	59	2189	44514	243	42.2
83	50	13598	159.5	-62.2	8	-80.1	59	2194	44613	243	41.6
84	0	13626	158.8	-62.4	8	-80.3	58	2198	44705	243	41.0
84	10	13654	158.1	-62.6	8	-80.4	58	2202	44797	243	40.6
84	20	13684	157.3	-62.8	7	-81.4	58	2206	44895	242	40.0

|										
34	30	13711	156.6	-62.7	7	-81.4	58	2210	44984	242	39.5
34	40	13742	155.8	-62.8	7	-81.4	57	2215	45085	242	38.9
34	50	13772	155.1	-62.9	7	-81.5	57	2219	45184	241	38.5
35	0	13804	154.3	-63.1	6	-82.7	57	2224	45289	241	38.1
5	10	13831	153.6	-63.1	6	-82.7	57	2228	45377	240	37.9
5	20	13862	152.8	-62.8	6	-82.4	56	2233	45479	240	37.5
35	30	13893	152.1	-62.7	6	-82.3	56	2237	45581	239	37.3
35	40	13923	151.3	-62.4	6	-82.1	56	2242	45679	239	37.1
35	50	13951	150.6	-62.4	6	-82.1	55	2246	45771	238	36.9
36	0	13980	149.9	-62.4	5	-83.2	55	2250	45866	237	36.9
36	10	14010	149.2	-62.5	5	-83.3	55	2255	45965	237	36.9
36	20	14037	148.6	-62.6	5	-83.4	55	2259	46053	236	36.9
36	30	14067	147.8	-62.7	5	-83.5	55	2263	46152	236	36.9
36	40	14094	147.2	-62.6	5	-83.4	54	2267	46240	235	37.1
36	50	14124	146.5	-62.5	5	-83.3	54	2271	46339	235	37.3
37	0	14150	145.9	-62.5	5	-83.3	54	2275	46424	234	37.5
37	10	14182	145.1	-62.8	4	-84.9	54	2280	46529	234	37.7
37	20	14212	144.4	-62.8	4	-84.9	53	2285	46627	234	37.9
37	30	14246	143.6	-63.1	4	-85.1	53	2290	46739	233	37.9
37	40	14270	143.0	-63.1	4	-85.1	53	2293	46818	233	38.1
37	50	14302	142.3	-63.0	4	-85.1	53	2298	46923	233	38.1
38	0	14330	141.7	-62.8	4	-84.9	52	2302	47014	233	38.1
38	10	14362	140.9	-62.8	4	-84.9	52	2307	47119	233	38.1
38	20	14390	140.3	-62.7	4	-84.8	52	2311	47211	233	37.9
38	30	14422	139.6	-62.9	3	-86.7	52	2316	47316	233	37.7
38	40	14449	138.9	-63.2	3	-86.9	51	2320	47405	234	37.3
38	50	14479	138.3	-63.4	3	-87.1	51	2324	47503	235	36.9
89	0	14506	137.7	-63.2	3	-86.9	51	2328	47592	235	36.3
89	10	14535	137.0	-63.1	3	-86.9	51	2333	47687	236	35.8
9	20	14563	136.4	-63.0	3	-86.8	50	2337	47779	237	35.4
9	30	14590	135.8	-62.9	3	-86.7	50	2341	47867	237	34.8
89	40	14619	135.2	-62.8	3	-86.6	50	2345	47963	238	34.2
89	50	14646	134.6	-62.9	3	-86.7	50	2349	48051	239	33.6

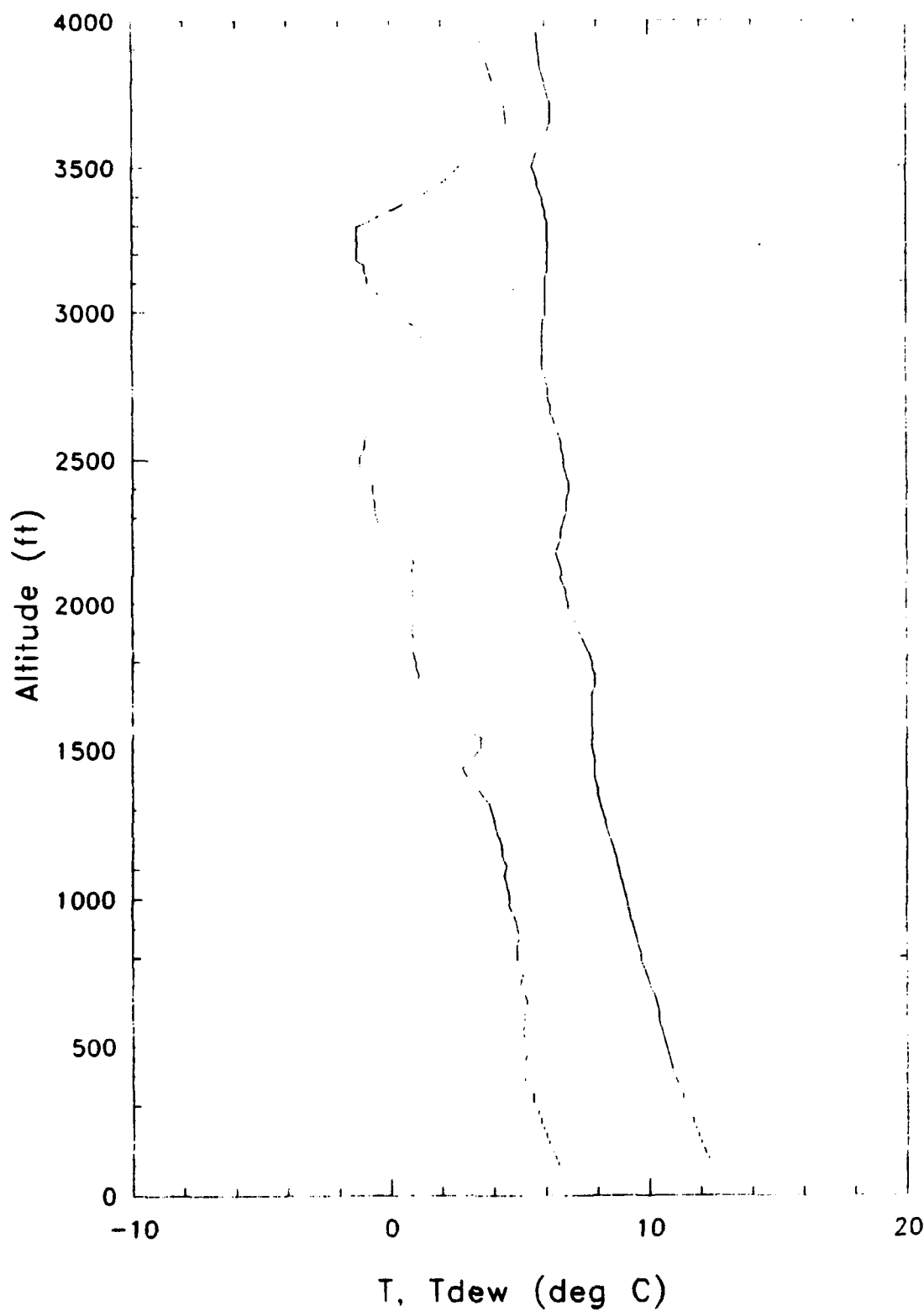**RAW NPS RADIOSONDE DATA PLOTS (7-10 MAY 1991)**

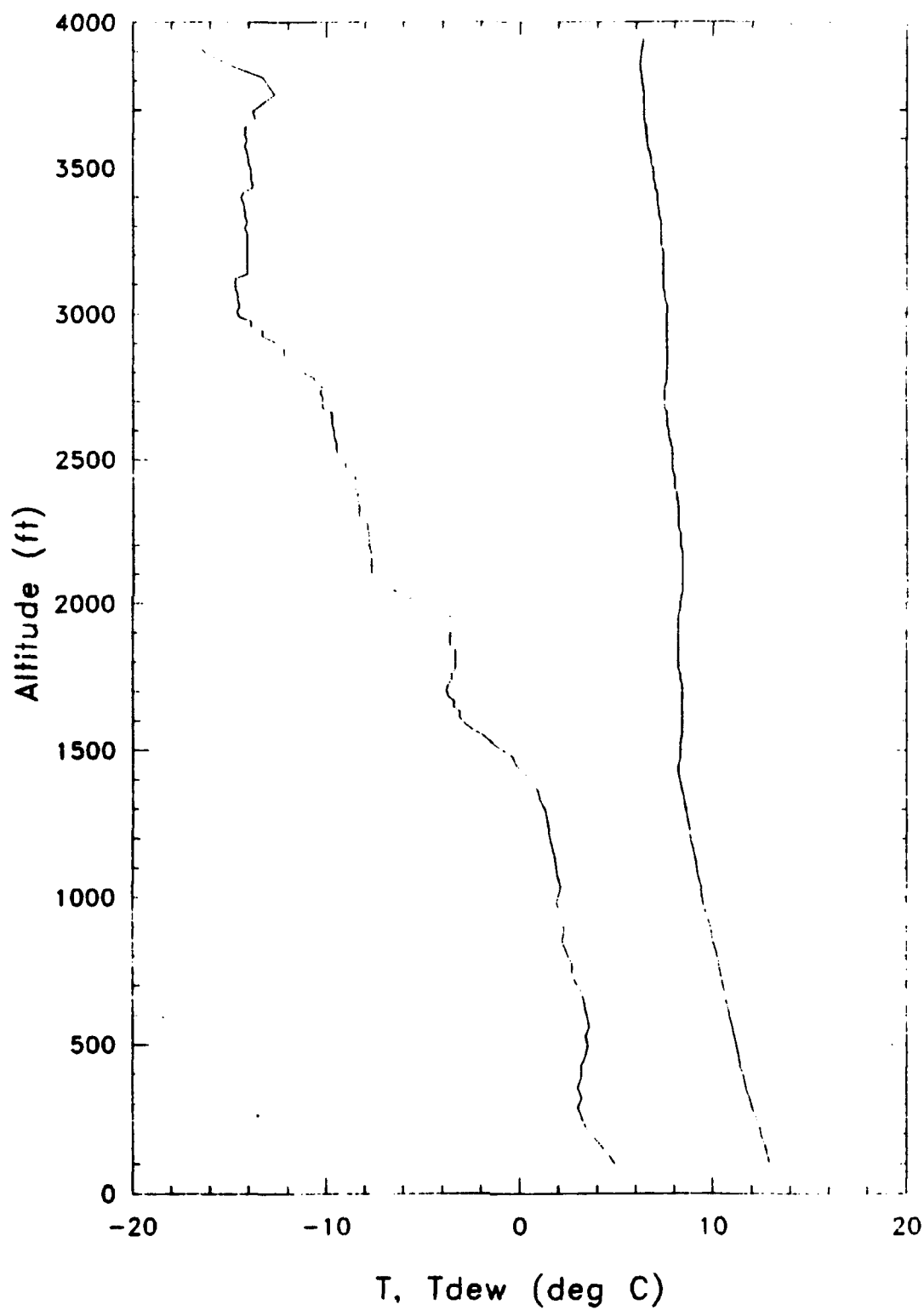Stn 72364   36.60 N 121.90 W   7 MAY 91 23:27 GMT
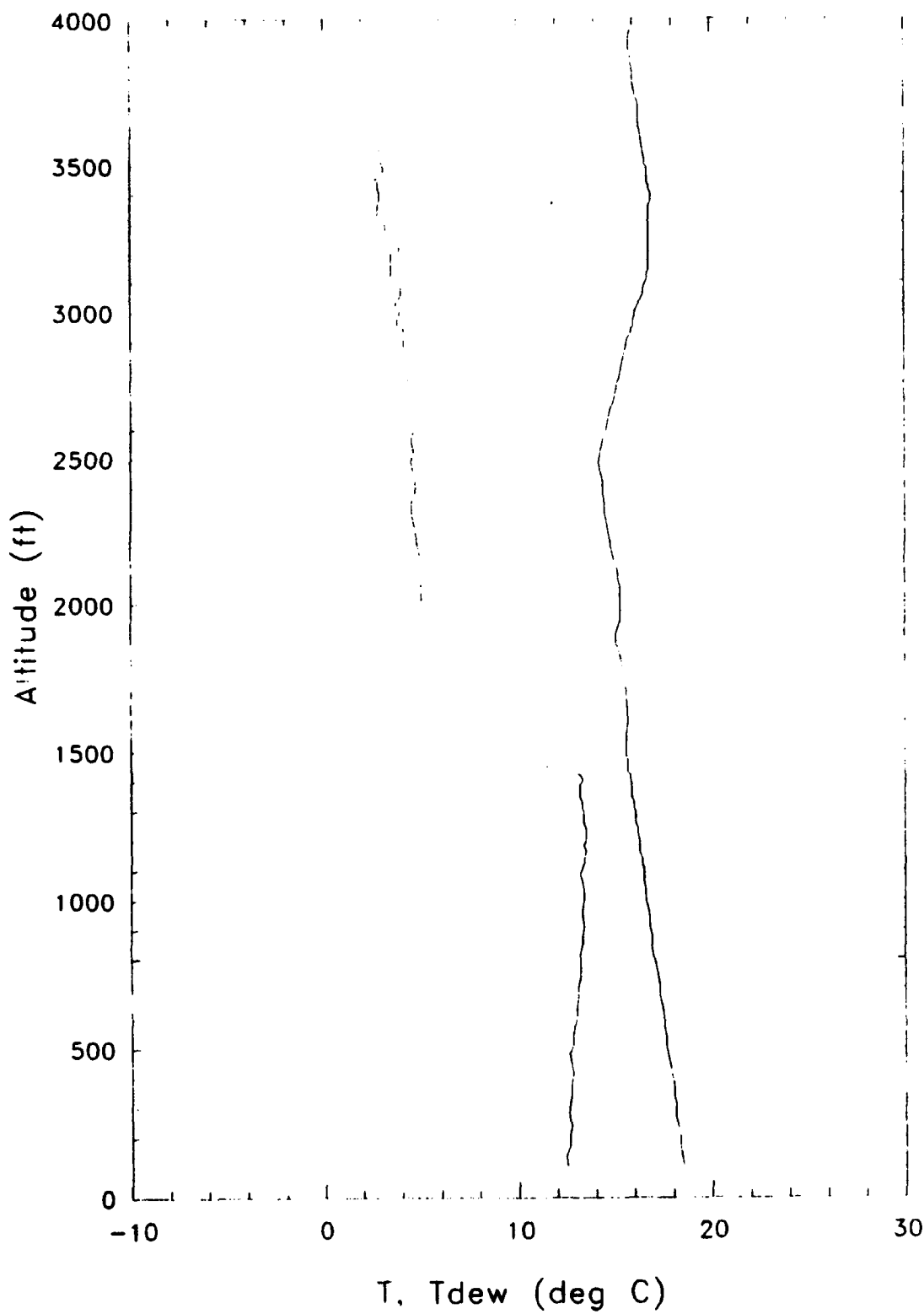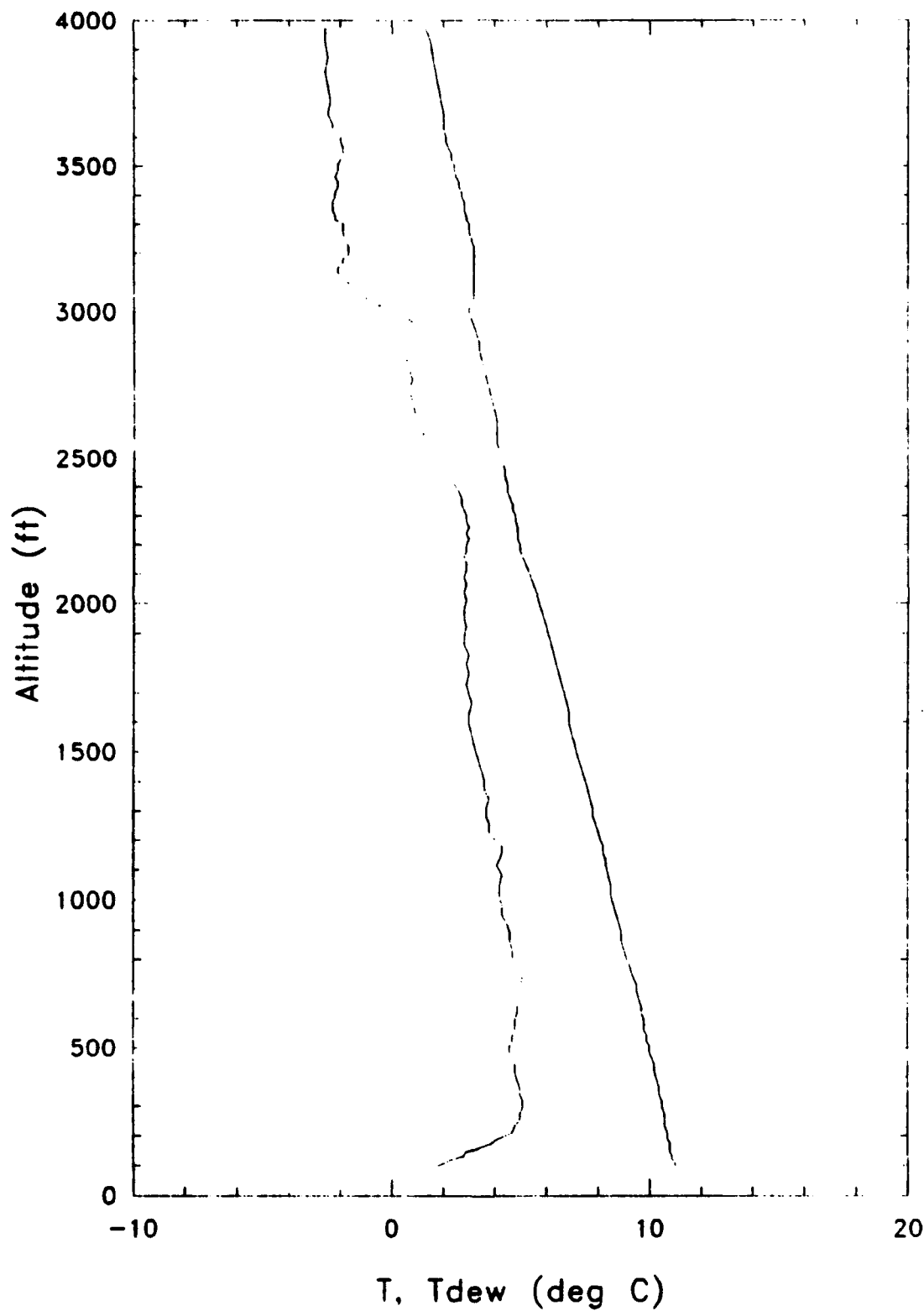
Stn 72364   36.60 N 121.90 W   8 MAY 91 11:46 GMT
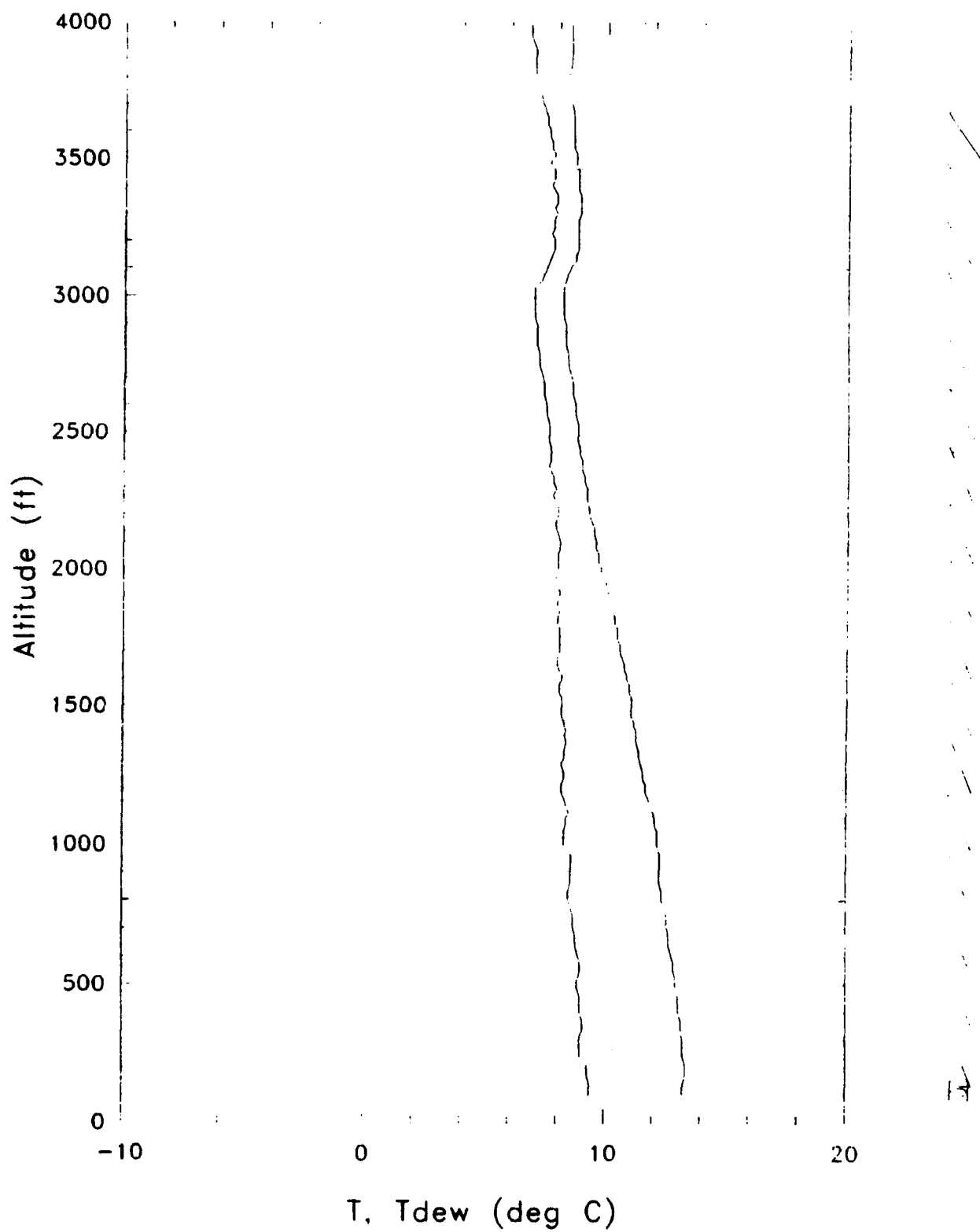
Stn 72364   36.60 N 121.90 W   8 MAY 91 17:35 GMT
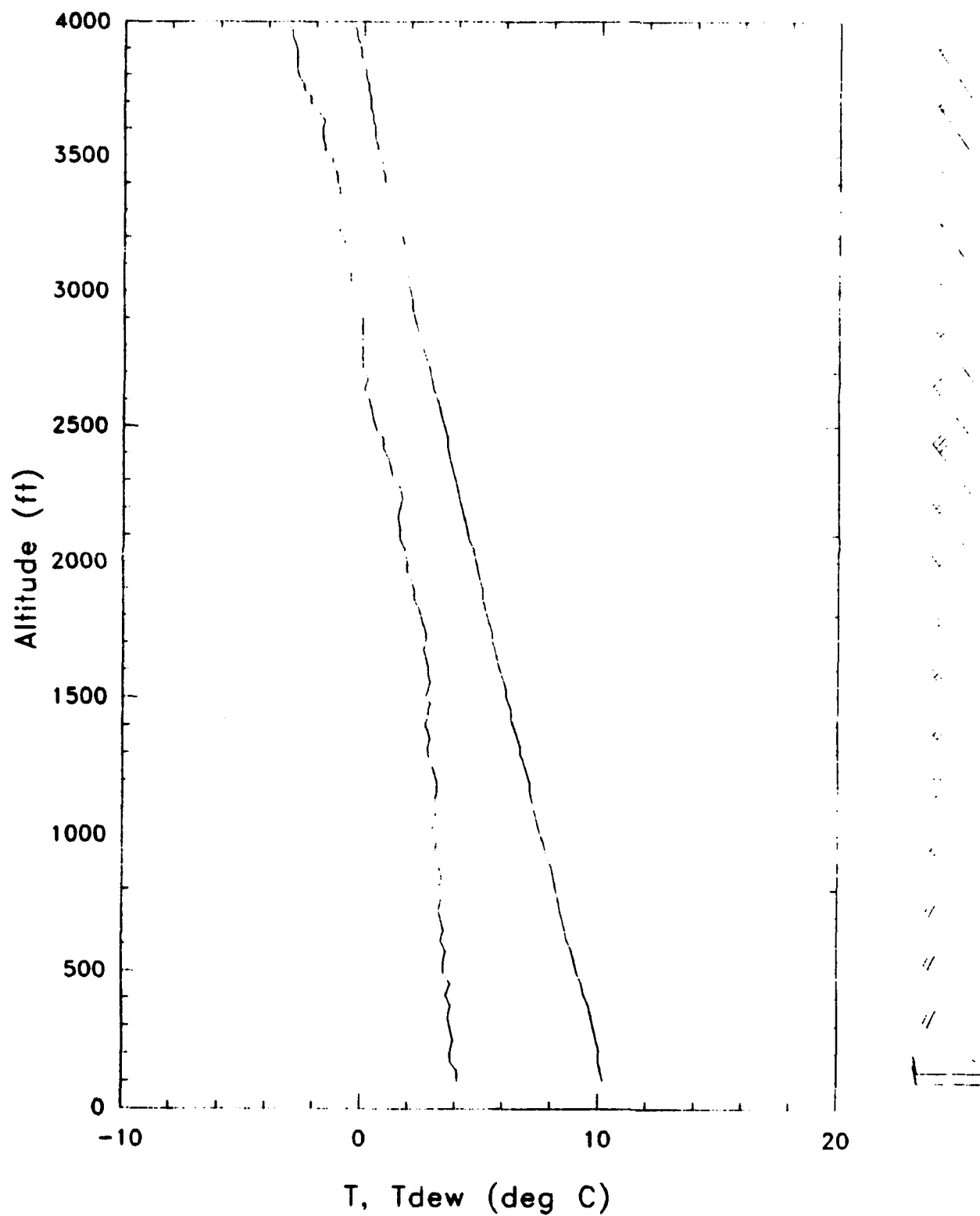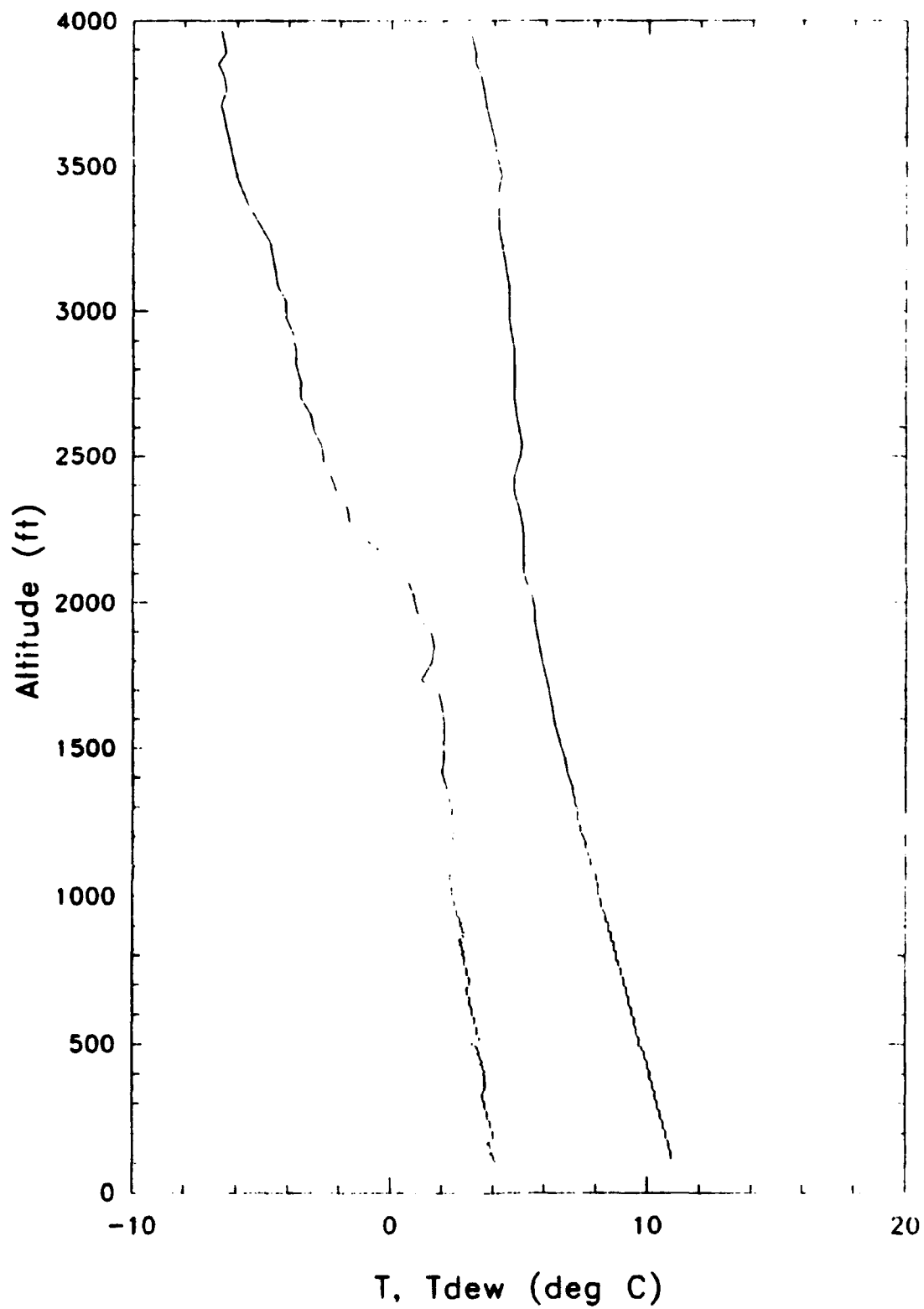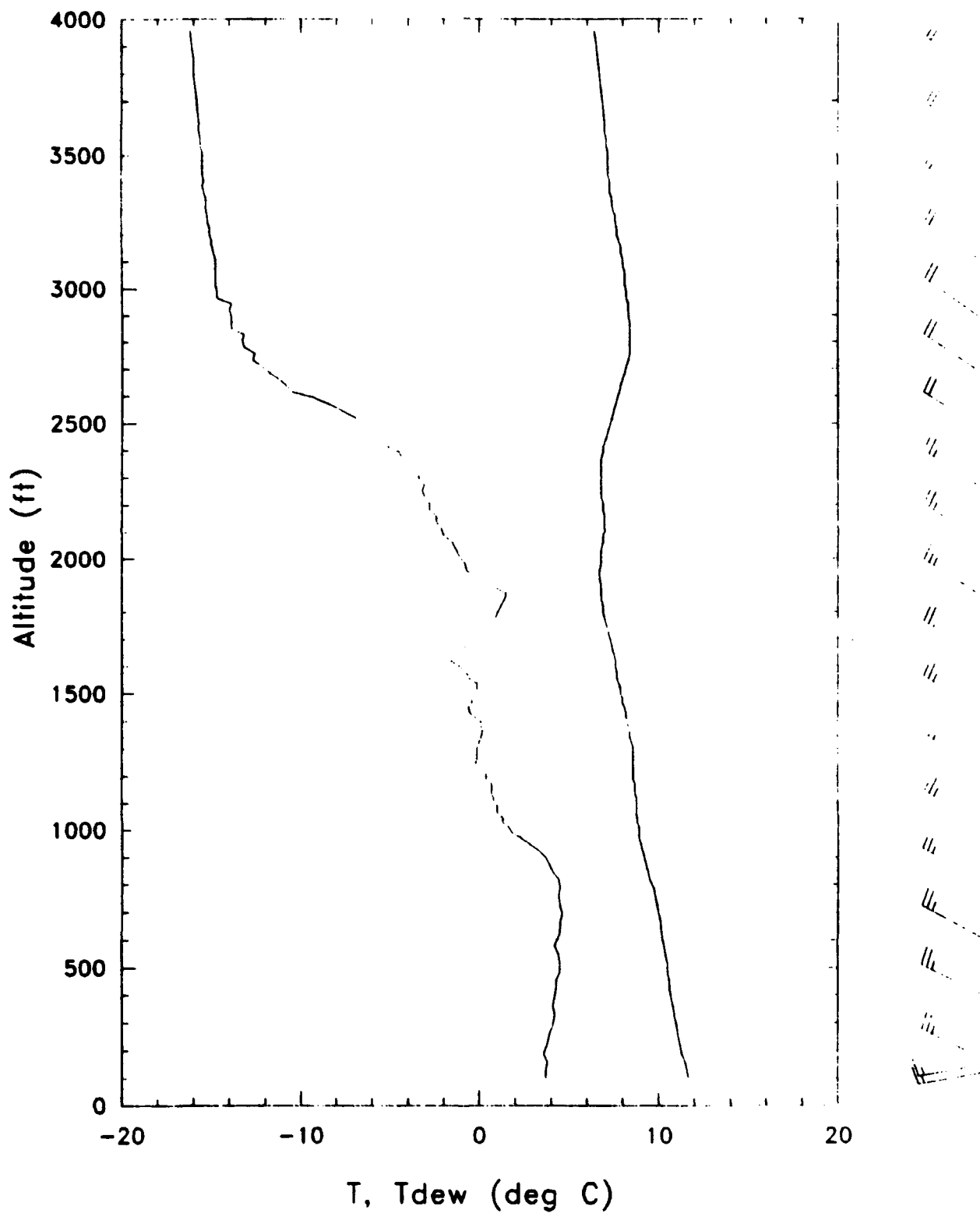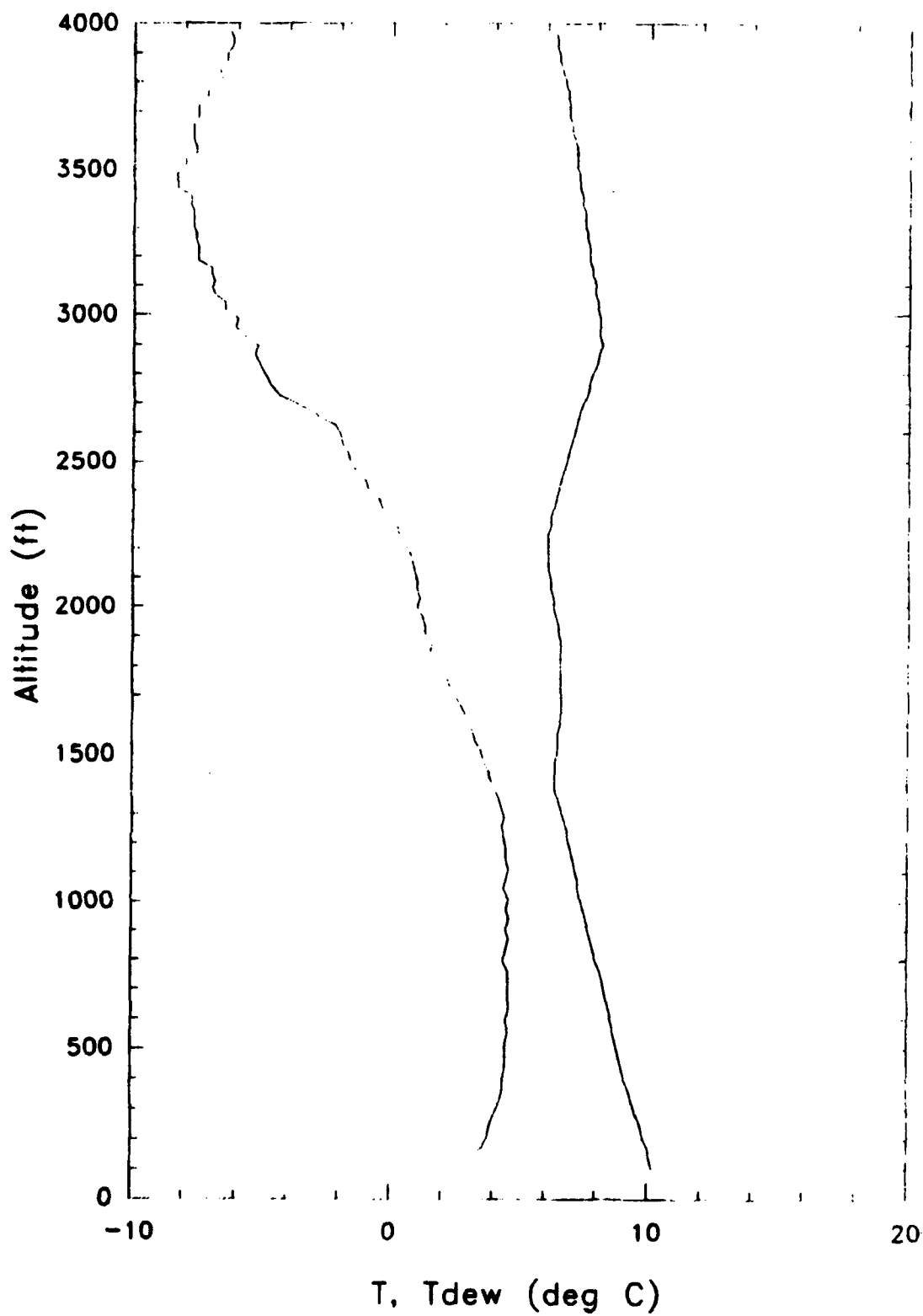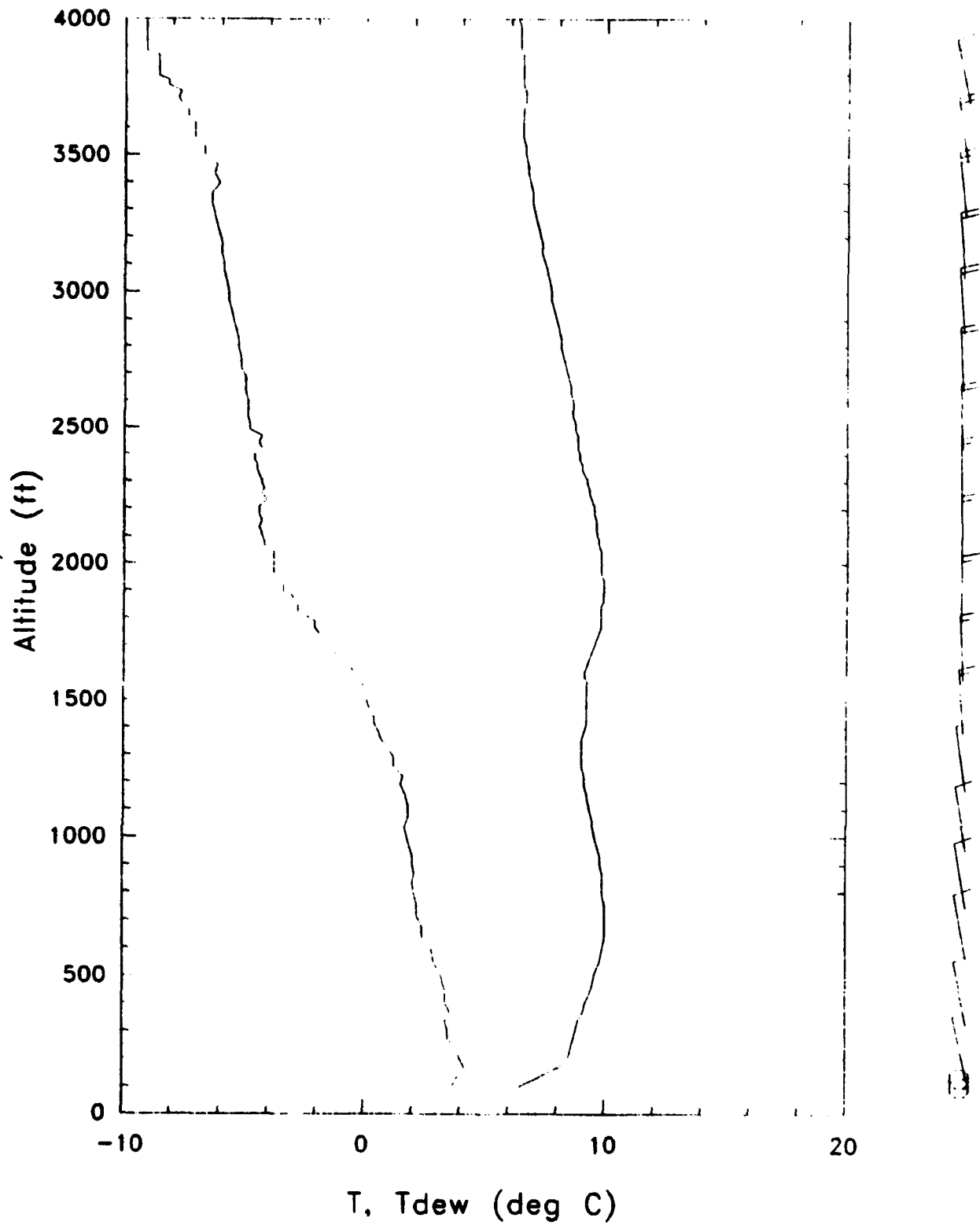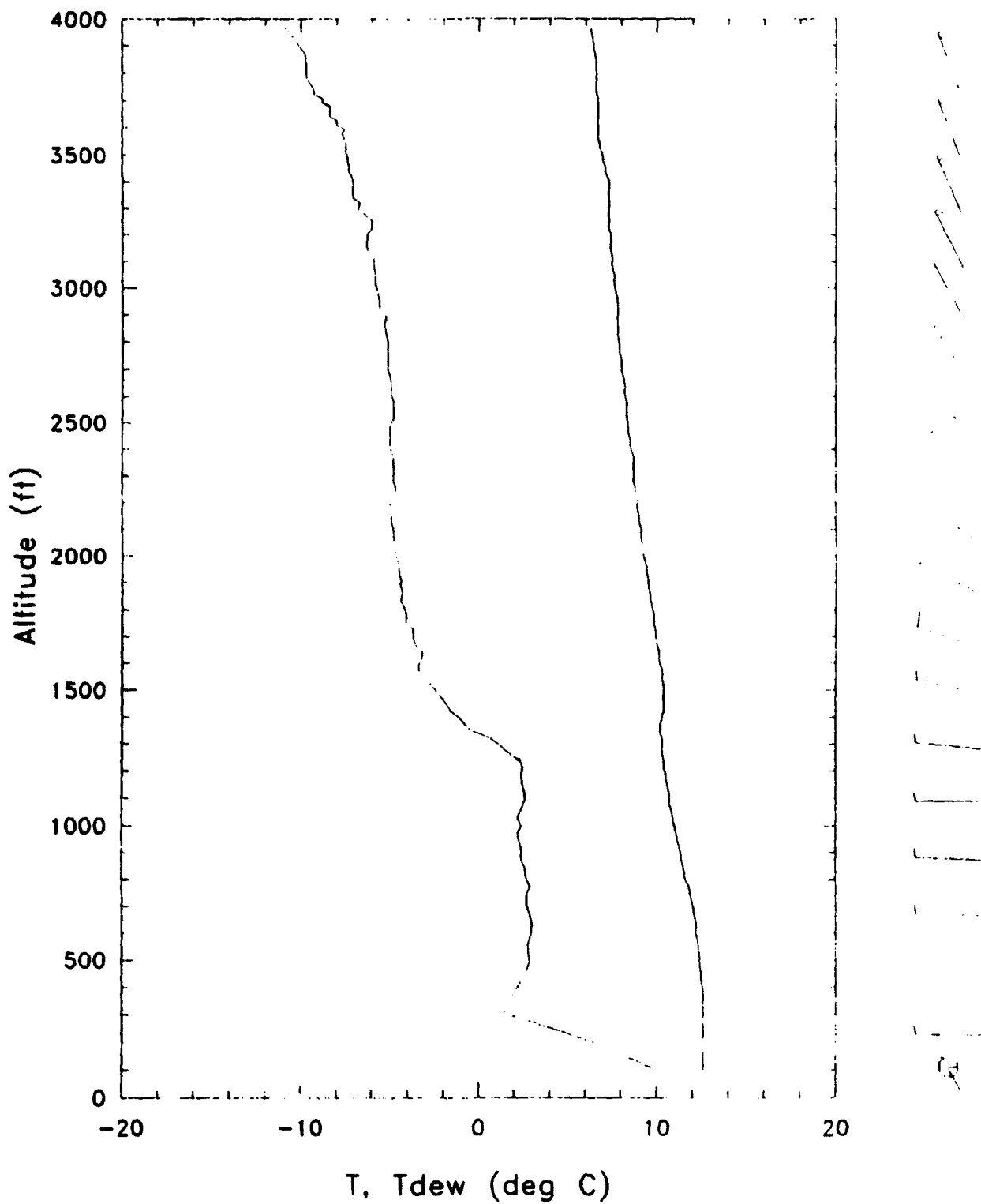
Stn 72364   36.60 N 121.90 W   8 MAY 91 23:28 GMT

T, Tdew (deg C)

Stn 72364   36.60 N 121.90 W   9 MAY 91 11:44 GMT

T, Tdew (deg C)

104

Stn 72364   36.60 N 121.90 W   9 MAY 91 23:26 GMT

T, Tdew (deg C)

105

Stn 72364   36.60 N 121.90 W   10 MAY 91   5:26 GMT

107

Stn 72364   36.60 N 121.90 W   10 MAY 91 12:12 GMT
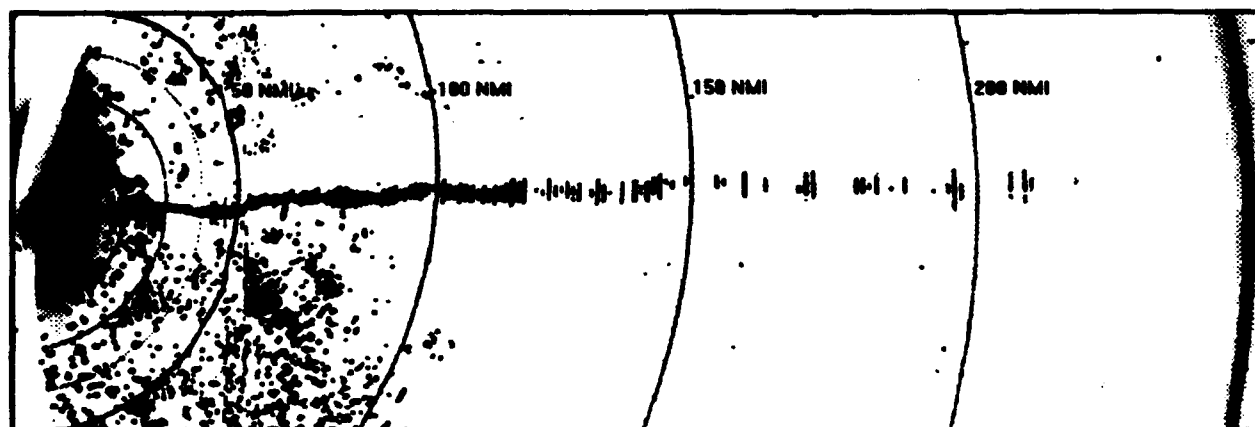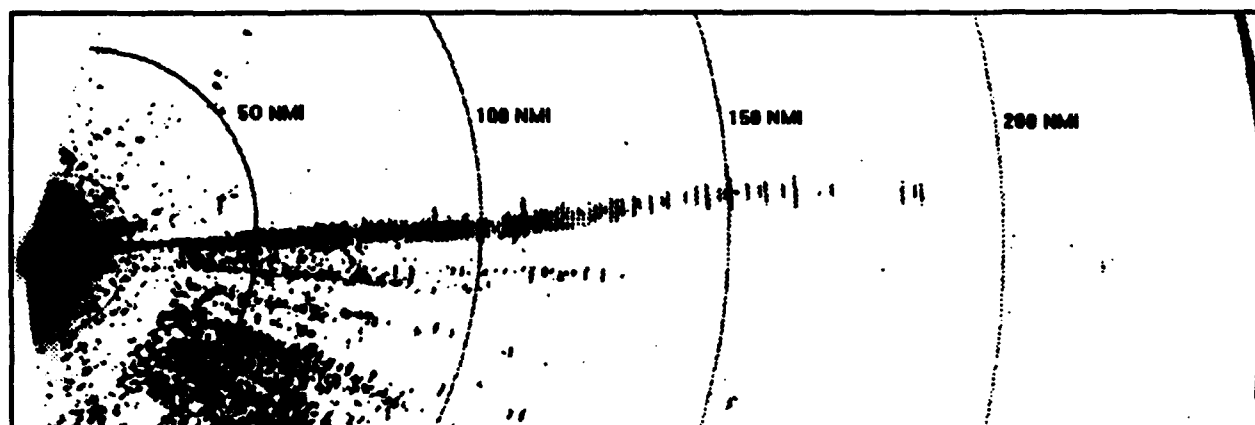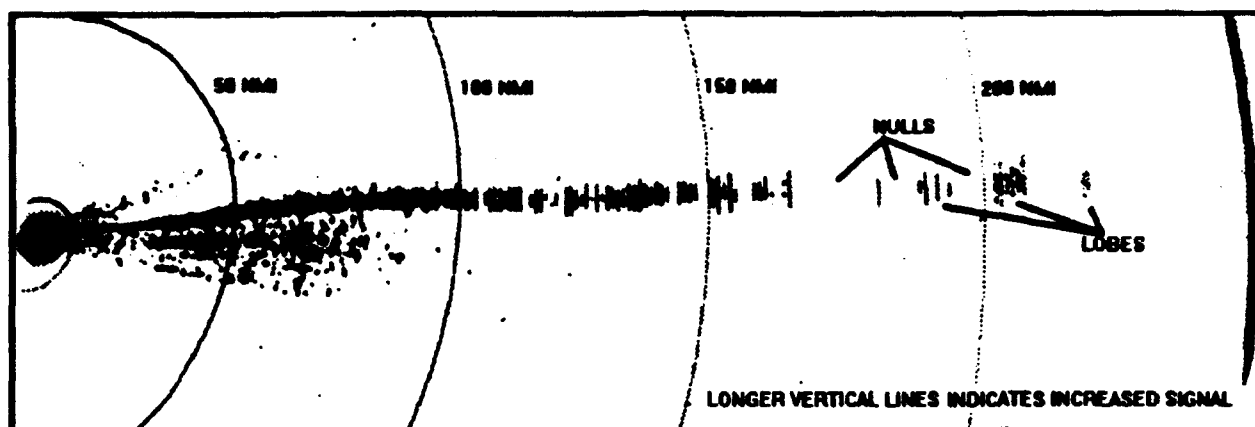
107

Stn 72364   36.60 N 121.90 W   10 MAY 91 17:46 GMT

102

APPENDIX E

PHOTOGRAPHS OF RADAR SCOPE ILLUSTRATING LOBING

These photographs were taken over a two day period at Hurlburt AFB. The photos are taken with the shutter held open while an aircraft was inbound to a radar site. This allows each radar hit or miss (for each radar sweep) to be seen. The radar site is located on the left side of the figure and the aircraft is inbound trying to maintain a consistent heading. Each radar hit is depicted by a vertical line. The longer the vertical line the stronger the radar signal. The figures illustrate the significant effects of the environment on radar detection. Shown by the figures are large gaps/holes in detection and areas of enhanced detection. The figures illustrate the actual day-to-day variability in radar system performance that can be modeled using the tools and procedures discussed in this thesis.

NULLS

LOBES

LONGER VERTICAL LINES INDICATES INCREASED SIGNAL

50 NMI   100 NMI   150 NMI   200 NMI

50 NMI   100 NMI   150 NMI   200 NMI

110

INITIAL DISTRIBUTION LIST

1. Defense Technical Information Center   2
    Cameron Station
    Alexandria, VA 22304-6145

2. Library, Code 52   2
    Naval Postgraduate School
    Monterey, CA 93943-5002

3. Lt Colonel Tom White   1
    AFWIC/SA
    102 Hall Blvd
    Suite 341
    San Antonio, TX 78243-7020

4. Mr. Ross Seely   1
    Department of Electrical and Computer Engineering
    Naval Postgraduate School
    Monterey, CA 93943-5121

5. Professor Frederic Levien, Code EC/LV   2
    Naval Postgraduate School
    Monterey, CA 93943-5121

6. Professor Dan C. Boger, Code SM/BO   1
    Naval Postgraduate School
    Monterey, CA 93943-5193

7. Captain Stan Grant   2
    Route 1 Box 85
    Rothville, MO 64676

8. Mr Jack Ridgway   1
    AFWIC/SA
    102 Hall Blvd
    Suite 341
    San Antonio, TX 78243-7020